

Development of Machine-Augmented Composites for Infrastructure Applications

Final Report

30 December 2003

Prepared by

G. F. HAWKINS,¹ M. J. O'BRIEN,¹ R. J. ZALDIVAR,¹
H. F. VON BREMEN,² and J. N. SCHURR¹
¹Space Materials Laboratory
Laboratory Operations

²University of Southern California
Los Angeles, CA

Prepared for

STATE OF CALIFORNIA
DEPARTMENT OF TRANSPORTATION
Sacramento, CA 94273

Contract No. 59A088

Engineering and Technology Group

LABORATORY OPERATIONS

The Aerospace Corporation functions as an “architect-engineer” for national security programs, specializing in advanced military space systems. The Corporation's Laboratory Operations supports the effective and timely development and operation of national security systems through scientific research and the application of advanced technology. Vital to the success of the Corporation is the technical staff's wide-ranging expertise and its ability to stay abreast of new technological developments and program support issues associated with rapidly evolving space systems. Contributing capabilities are provided by these individual organizations:

Electronics and Photonics Laboratory: Microelectronics, VLSI reliability, failure analysis, solid-state device physics, compound semiconductors, radiation effects, infrared and CCD detector devices, data storage and display technologies; lasers and electro-optics, solid-state laser design, micro-optics, optical communications, and fiber-optic sensors; atomic frequency standards, applied laser spectroscopy, laser chemistry, atmospheric propagation and beam control, LIDAR/LADAR remote sensing; solar cell and array testing and evaluation, battery electrochemistry, battery testing and evaluation.

Space Materials Laboratory: Evaluation and characterizations of new materials and processing techniques: metals, alloys, ceramics, polymers, thin films, and composites; development of advanced deposition processes; nondestructive evaluation, component failure analysis and reliability; structural mechanics, fracture mechanics, and stress corrosion; analysis and evaluation of materials at cryogenic and elevated temperatures; launch vehicle fluid mechanics, heat transfer and flight dynamics; aerothermodynamics; chemical and electric propulsion; environmental chemistry; combustion processes; space environment effects on materials, hardening and vulnerability assessment; contamination, thermal and structural control; lubrication and surface phenomena. Microelectromechanical systems (MEMS) for space applications; laser micromachining; laser-surface physical and chemical interactions; micropropulsion; micro- and nanosatellite mission analysis; intelligent microinstruments for monitoring space and launch system environments.

Space Science Applications Laboratory: Magnetospheric, auroral and cosmic-ray physics, wave-particle interactions, magnetospheric plasma waves; atmospheric and ionospheric physics, density and composition of the upper atmosphere, remote sensing using atmospheric radiation; solar physics, infrared astronomy, infrared signature analysis; infrared surveillance, imaging and remote sensing; multispectral and hyperspectral sensor development; data analysis and algorithm development; applications of multispectral and hyperspectral imagery to defense, civil space, commercial, and environmental missions; effects of solar activity, magnetic storms and nuclear explosions on the Earth's atmosphere, ionosphere and magnetosphere; effects of electromagnetic and particulate radiations on space systems; space instrumentation, design, fabrication and test; environmental chemistry, trace detection; atmospheric chemical reactions, atmospheric optics, light scattering, state-specific chemical reactions, and radiative signatures of missile plumes.

STATE OF CALIFORNIA DEPARTMENT OF TRANSPORTATION
TECHNICAL REPORT DOCUMENTATION PAGE
 TR0003 (REV. 10/98)

1. REPORT NUMBER FHWA/CA/XX-yy/##	2. GOVERNMENT ASSOCIATION NUMBER	3. RECIPIENT'S CATALOG NUMBER
4. TITLE AND SUBTITLE Development of Machine-Augmented Composites for Infrastructure Applications Final Report	5. REPORT DATE 30 December 2003	
	6. PERFORMING ORGANIZATION CODE	
7. AUTHOR(S) G. F. Hawkins, M. J. O'Brien, R. J. Zaldivar, H. F. Von Bremen, and J. N. Schurr	8. PERFORMING ORGANIZATION REPORT NO. ATR-2004(7796)-1	
9. PERFORMING ORGANIZATION NAME AND ADDRESS The Aerospace Corporation Laboratory Operations El Segundo, CA 90245-4691	10. WORK UNIT NUMBER	
	11. CONTRACT OR GRANT NUMBER 59A088	
12. SPONSORING AGENCY AND ADDRESS California Department of Transportation Division of Research and Innovation, MS-83 1227 O Street Sacramento CA 95814	13. TYPE OF REPORT AND PERIOD COVERED	
	14. SPONSORING AGENCY CODE	

15. SUPPLEMENTAL NOTES

16. ABSTRACT

Machine-Augmented Composites Materials (MACterials) are composites that contain many, small, embedded simple machines. Due to the presence of these embedded machines, these composites have properties that cannot be obtained by other means. During this program, we have developed a comprehensive understanding of machine-augmented composite materials to learn how they can be used in infrastructure applications. Manufacturing methods were developed to embed machines of various sizes in a matrix material. Experiments with embedded Z-shaped machines showed how the material converts compressive displacements into shear displacements with an efficiency ranging from 0.5/1 to 2/1, depending on the geometry of the machines. Experiments were conducted measuring the force conversion efficiency with much the same results. This material may have applications in cable stays and in pre-stressing composites in retrofit situations.

We also developed both analytical and finite-element models to allow us to design materials with custom properties using embedded machines. These models were validated with experimental tests. Using the validated models, we designed machines that contained a viscous fluid for use in a material that could be used as a vibration damper. The results also predicted that there would be an optimum viscosity for obtaining efficient damping. Experiments were performed to verify this finding. In addition, we optimized the design of the fluid-filled machine using an hourglass shape. Calculations show that this shape is much more efficient at moving fluids under small displacements. Samples of a material that could be used to damp vibrations during earthquakes were successfully tested.

The goals of this task -- developing the analytical tools and manufacturing methods for using machine-augmented composite materials in infrastructure applications -- have been successfully achieved.

17. KEY WORDS Damping, Composites, Machines, Smart materials	18. DISTRIBUTION STATEMENT No restrictions. This document is available to the public through the National Technical Information Service, Springfield, VA 22161	
19. SECURITY CLASSIFICATION (of this report) Unclassified	20. NUMBER OF PAGES 100	21. PRICE

DEVELOPMENT OF MACHINE-AUGMENTED COMPOSITES FOR INFRASTRUCTURE APPLICATIONS

FINAL REPORT

Prepared

G. F. Hawkins
Office of Innovative Materials
Space Materials Laboratory

M. J. O'Brien
Materials Science Department

R. J. Zaldivar
Materials Science Department

J. N. Schurr
Materials Processing & Evaluation Department

Approved

P. D. Fleischauer, Principal Director
Space Materials Laboratory
Laboratory Operations

Abstract

Machine-Augmented Composites Materials (MACterials) are composites that contain many, small, embedded simple machines. Due to the presence of these embedded machines, these composites have properties that cannot be obtained by other means. During this program, we have developed a comprehensive understanding of machine-augmented composite materials to learn how they can be used in infrastructure applications. Manufacturing methods were developed to embed machines of various sizes in a matrix material. Experiments with embedded Z-shaped machines showed how the material converts compressive displacements into shear displacements with an efficiency ranging from 0.5/1 to 2/1, depending on the geometry of the machines. Experiments were conducted measuring the force conversion efficiency with much the same results. This material may have applications in cable stays and in pre-stressing composites in retrofit situations.

We also developed both analytical and finite-element models to allow us to design materials with custom properties using embedded machines. These models were validated with experimental tests. Using the validated models, we designed machines that contained a viscous fluid for use in a material that could be used as a vibration damper. The results also predicted that there would be an optimum viscosity for obtaining efficient damping. Experiments were performed to verify this finding. In addition, we optimized the design of the fluid-filled machine using an hourglass shape. Calculations show that this shape is much more efficient at moving fluids under small displacements. Samples of a material that could be used to damp vibrations during earthquakes were successfully tested.

The goals of this task -- developing the analytical tools and manufacturing methods for using machine-augmented composite materials in infrastructure applications -- have been successfully achieved.

Acknowledgments

The authors would like to acknowledge the support of the following individuals:

- Li-Hong Sheng (Caltrans) for program guidance throughout this effort
- Paul C. Lu for his assistance and thoughts in lab experiments
- Kenneth J. Park for his assistance in the document editing process
- Dhruv N. Patel for his support to our mechanical loading experiments
- Ching-Yao (Tony) Tang for his research on the fluid-filled damping efforts
- James T. Yamasaki for his ability to fabricate the instruments required to test our innovative materials

Contents

1.	Introduction	1
2.	MACterial Development	3
3.	Testing and Analysis of Z-Machines	5
4.	Developing Design Tools	8
4.1	Finite-Element Analysis	9
4.2	Theory of Beam on Elastic Foundation	10
5.	Machine Augmented Composites For Fluid-Filled Damping	12
5.1	Z-shaped Machines For Fluid-Filled Damping.....	13
5.2	Hourglass-Shaped Fluid-Filled Dampers.....	14
6.	Application of Force Conversion.....	17
7.	Summary.....	19
	Appendix A—The Fabrication and Mechanical Behavior of Z-Shaped Machine-Augmented Composites	21
	Appendix B—The Load-Load Characteristics of Z-Shaped Machines.....	33
	Appendix C—Theoretical and Finite Element Modeling of the Z-MACs.....	51
	Appendix D—Damping Capabilities of Fluid-Filled Machine-Augmented Composites	73
	Appendix E—Potential Infrastructure Applications of Machine Augmented Composites.....	91

Figures

1.	Schematic of simple stress-conversion machine.	3
2.	Scanning electron micrograph of the prototype simple Z- machine.....	3
4.	Composite containing graphite fibers and one ply of machines.....	3

5. 15-mm Z-machines produced through rapid prototyping (left) and 1-mm Z-machines produced by extrusion (right).	4
6. Experimental set-up used to measure shear displacement as a function of compressive force and displacement.	5
7. The effect of inclination angle on the compressive-to-shear displacement behavior of a MAC (15-mm Z-machines).	6
8. Typical plot for a compressive displacement to lateral displacement experiment using a 15-mm Z-type machine for machines with matrix and machines without matrix....	6
9. Experimental setup used to measure lateral forces as a function of shear load.	7
10. Stress conversion behavior of an unreinforced polyurethane resin versus a machine augmented prototype composite utilizing the same polyurethane material as the matrix. ...	7
11. Undeformed mesh of the physical model developed using TrueGrid.	9
12. Undeformed state of the experimental specimen (Figure 12a) and the finite-element model undeformed mesh (Figure 12b).....	9
13. Experimental and FEA compressive versus shear displacements for MACs with polyurethane matrix material and 15-mm cross-section machines for various machine inclination angles	10
14. Physical problem modeled as a beam-on-elastic foundation.....	11
15. Experimental, FEA and beam-on-elastic-foundation solution of the deformed state of the sidewall of a 15-mm cross-section four-machine MAC with matrix material and a 60° inclination angle.....	11
16. Damping capability of various Z-machines.	14
17. Fluid-filled damping machine.....	14
18. Finite-element grid of hourglass-machines with the analytical expression for fluids.	15
19. MACterial application for the prestressing of composite strips for the strengthening of concrete structures.....	17

1. Introduction

Machine Augmented Composite Materials (MACterials) are based on the concept that unique material properties can be obtained through making a composite material by embedding many small simple machines within a matrix. A traditional carbon-fiber composite material is composed of fibers embedded in a matrix material. The embedded fibers are stiff and strong. Consequently, the composite material is also stiff and strong. In MACterials, many small simple machines are buried in a matrix material. These small simple machines modify the forces applied to them. Consequently, the MACterial composite (with embedded small simple machines) modifies the forces applied to it.

In this task, we have developed the technology to embed many small “viscous dampers” in a matrix material. The dampers absorb much of the strain energy induced in the MACterial. When the MACterial is used in a bridge, it would potentially absorb a portion of the energy imparted on the structure by an earthquake, thereby reducing the probability of bridge collapse.

Developing this new material requires an understanding of the physics that controls the response of the material to external forces. After an understanding of the physics of the material has been established, a set of basic equations and computer analysis design tools must then be determined to design the material for this particular damping application. With this knowledge, we would be able to optimize the geometry of the machines embedded within the material in order to increase the effectiveness of the MACterial as a damping material.

The following sections describe how we uncovered the physics of and design tools for the damping material of interest to Caltrans. We began by manufacturing samples containing many small Z-shaped machines. We then measured the tensile stress/strain to shear stress/strain conversion properties of these samples. With this experimental data, knowledge of the behavior of a beam on an elastic foundation, and the development of a finite-element analysis model of our machines, we were able to develop tools that have allowed us to optimize the design of our MACterials to fit required needs of various applications, foremost of which has been in creating a damping material. The most advanced design consists of embedded hourglass-shaped machines filled with fluids to improve damping. Theoretical calculations have shown that this hourglass shape is much more efficient at moving fluids under small displacements, where the movement of fluids has been correlated with a high level of damping.

Appendices A through E have been included in this report, providing a more detailed description of the MACterials being developed for fluid-filled damping.

This page intentionally blank.

2. MACterial Development (Detailed Discussion in Appendix A)

We needed to first uncover the basic concepts governing the MACterial containing many simple machines before we attempted to understand the MACterial containing the relatively complicated viscous dampers. We started with the machine shown in Figure 1. This machine is essentially a four-bar linkage that uses compliant hinges. As shown in the figure, when compressive forces are applied to the top and bottom, the angled sidewalls cause the machine to distort in shear. Conversely, when shear stresses are imposed on this machine, the sidewalls distort, forcing the upper and lower faces apart. In this way, this “Z-machine” converts tensile forces into shear forces and vice versa.

We made this “Z” profile into a small machine as shown in Figure 2. A number of these machines were laid down side by side to form a ply, and these plies were stacked on top of each other. The stack was infiltrated with a polyurethane resin to form the composite. The completed MACterial is shown in Figure 3. The processing steps used to incorporate these Z-machine segments into a composite were patterned after current composite practices. As a result, the production of these MACterials can be easily incorporated into standard composite manufacturing techniques. In this way, the costs of producing MACterials should be similar to the costs of producing traditional composites. In addition, if the end item needs to be stiffer or stronger, plies of fibers can be added during production of the composite. Figure 4 shows a composite that contains graphite fibers as well as a ply of machines.

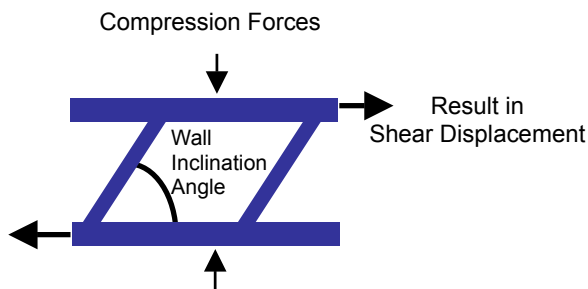


Figure 1. Schematic of simple stress-conversion machine.

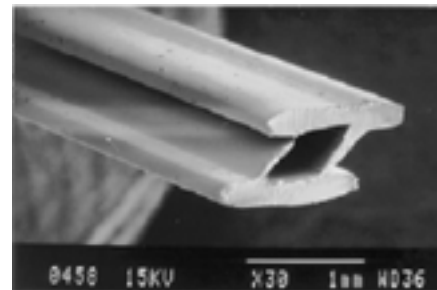


Figure 2. Scanning electron micrograph of the prototype simple Z-machine.

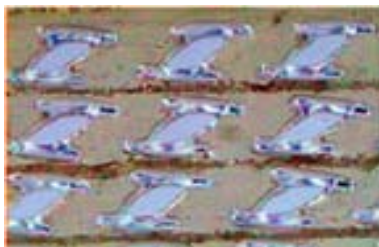


Figure 3. Optical micrograph of three plies of stress-conversion MACterial.



Figure 4. Composite containing graphite fibers and one ply of machines.

The two methods developed for producing Z-machines are through extrusion and through rapid prototyping. The extruded machines are approximately 1-mm in cross-section and can be extruded out of a number of different material systems. The size of these machines can be varied, depending on the desired application. However, we found that the quickest and least expensive way to make machines for the study was through rapid prototyping, by which we drew a schematic of the machine using a 3-D CAD program and produced the machine using a 3-D printer (stereolithography machine). This yielded a full-size plastic part with a 15-mm cross-section, suitable for experimentation. The parts were not very strong, but were adequate to experimentally test the low strain properties of the material and validate the analysis. Figure 5 shows an image of a Z-machine produced through rapid prototyping compared to one produced by extrusion. A full discussion of the manufacturing process is given in Appendix A.

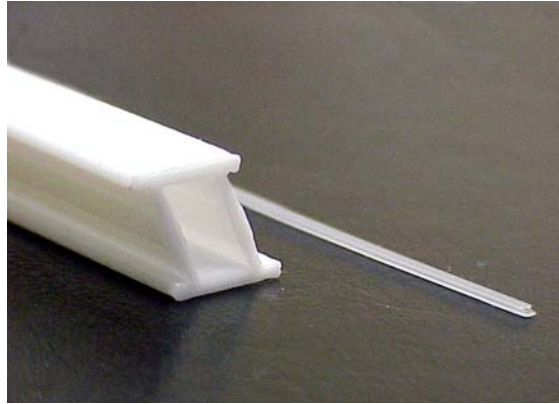


Figure 5. 15-mm Z-machines produced through rapid prototyping (left) and 1-mm Z-machines produced by extrusion (right).

3. Testing and Analysis of Z-Machines (Detailed Discussion in Appendices A & B)

The first series of experiments we performed on the MACterial examined the MACterial's shear displacement characteristics when subjected to compressive displacement. An example of these experiments is shown in Figure 6 and is described in greater detail in Machine-Augmented Composites by G. Hawkins, et al. AIAA 2002-1240. In this particular test using the 1-mm extruded machines, two 10-ply samples were stacked on top of each other and placed in a mechanical testing machine. An aluminum "L" shaped plate was placed between the samples. The samples were arranged such that when compressed, they both moved the plate in the same direction. The movement of the plate was detected by an LVDT and recorded.

Using the same testing method on the 15-mm rapid prototype machines (using two 1-ply samples), we measured the compressive displacement and compared it to the shear displacement of the MACterial. Figure 7 shows the results of one of these mechanical experiments. As can be seen from the figure, in these samples, the shear displacement can be larger or smaller than the compressive displacement depending on the angle of the walls. The geometry of the machines controls their response. An interesting difference between MACterials and typical composites is shown in Figure 8. When the fiber matrix ratio is changed in a typical composite, the material properties vary as a function of the ratio between the amount of fiber to the amount of matrix material. This is called the "rule of mixtures." In Figure 8, displacement-displacement data is shown from two samples. One of the samples contains approximately 50% machines and 50% matrix. The other sample contains 100% machines and 0% matrix. The data for the two samples lies on top of each other. This shows that this property in MACterials does not follow the rules of mixtures but is dependent on the geometry of the embedded machines. This test is described in greater detail in Machine-Augmented Composites by G. Hawkins, et al. AIAA 2002-1240.

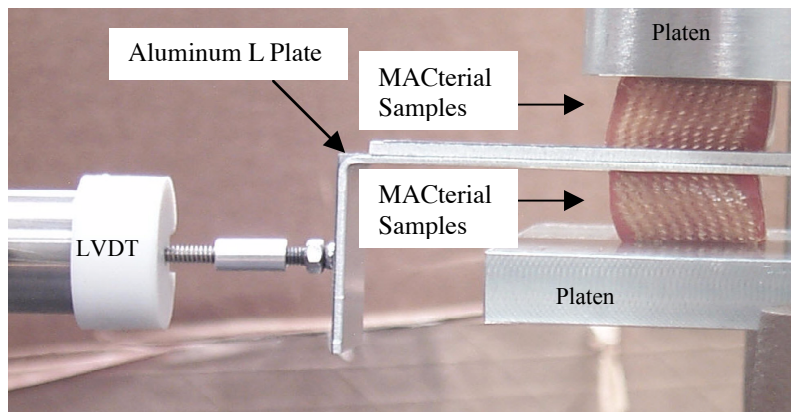


Figure 6. Experimental set-up used to measure shear displacement as a function of compressive force and displacement.

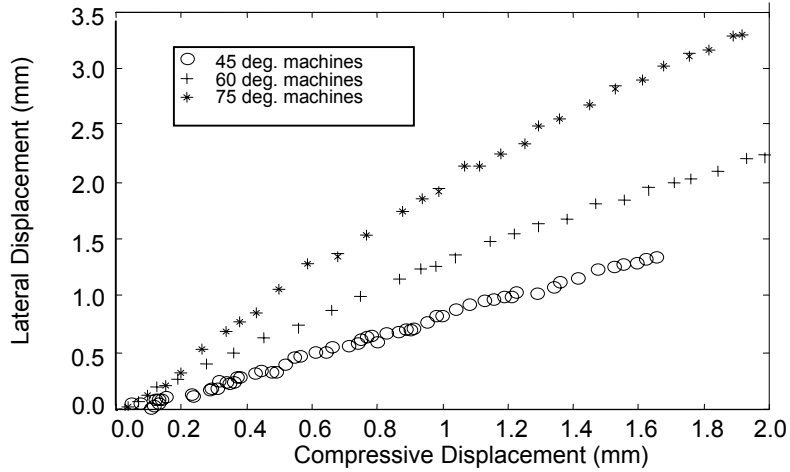


Figure 7. The effect of wall inclination angle on the compressive-to-shear displacement behavior of a MAC (15-mm Z-machines).

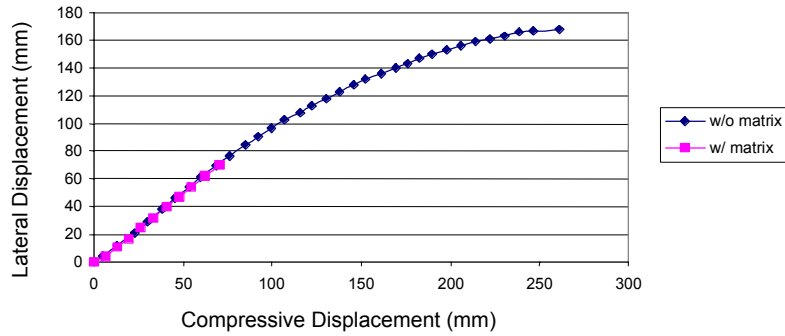


Figure 8. Typical plot for a compressive displacement to lateral displacement experiment using a 15-mm Z-type machine for machines with matrix and machines without matrix.

Up until this point, we have discussed the displacement characteristics of MACterials. In addition, machines are also able to convert forces. The second series of experiments we performed on the MACterials examined the MACterial’s force conversion characteristics when subjected to compressive forces. To test the force conversion properties of this material, we developed the “load-load” testing device shown in Figure 9. A full discussion of the load-load testing is given in Appendix B. The test is similar to a double-lap shear test. The device was mounted in a universal testing (UTS) machine that pulled from the top and bottom. The top two arms were mounted such that they are capable of swinging laterally like a pendulum. As shown in the figure, a load cell detected any forces that were forcing the two arms laterally. Two samples were mounted at the bottom of the device such that they were loaded in shear when the UTS machine pulled in tension. These MACterial samples converted shear forces into lateral compressive forces. These lateral compressive forces then attempted to push the arms apart. The lateral forces were measured with the load cell.

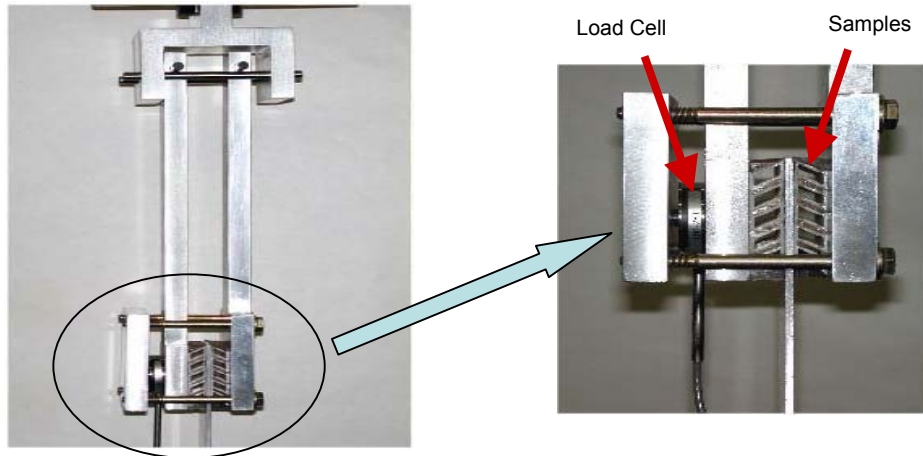


Figure 9. Experimental setup used to measure lateral forces as a function of shear load.

Figure 10 shows the data taken with this load-load device. Data from a sample made from the polyurethane matrix material alone shows that traditional materials without Z-machines do not convert shear forces into compressive forces. The data for the MACterial shows how it converts the forces in approximately a one-to-one ratio. This ability to convert an applied force to a lateral force is a function of the geometry of the machines and can be varied by the material designer.

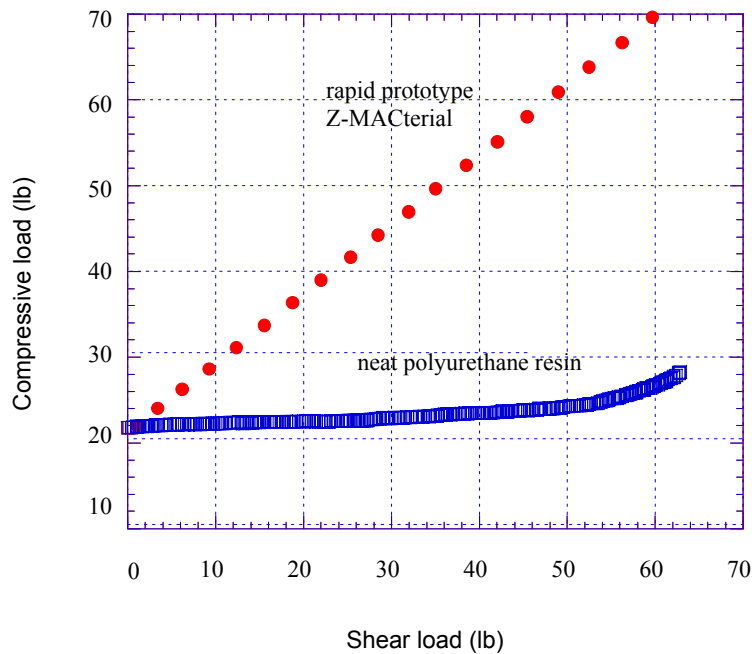


Figure 10. Stress conversion behavior of an unreinforced polyurethane resin versus a machine augmented prototype composite utilizing the same polyurethane material as the matrix.

This page intentionally blank.

4. Developing Design Tools (Detailed Discussion in Appendix C)

As mentioned at the beginning of this section, in order to design MACterials, we needed to develop design tools. Two types of tools have been developed during this program: a Finite-Element Analysis (FEA) and the use of the Theory of a Beam on an Elastic Foundation. First, we will discuss the finite-element analysis tool (for a full discussion see Appendix C).

4.1 Finite-Element Analysis

A commercial finite-element code, ABAQUS, was used during this program. The code was fully nonlinear, and the large deformation strain formulation allowed the nonlinear response present in the MACterials. The grid was developed using a commercial program, TrueGrid, and is shown in Figure 11.

Figure 12 shows a comparison of the shape of the machines under compressive forces as predicted by the FEA model and as observed in experimentation. Depicted are the Z-machines during and after the

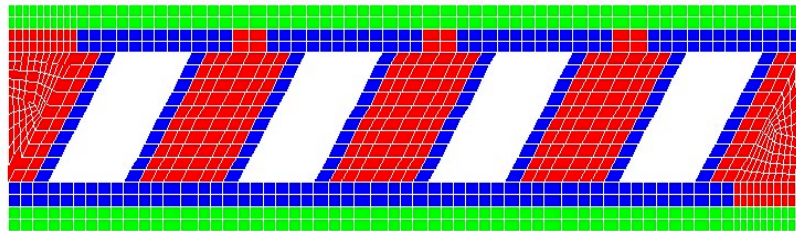


Figure 11. Undeformed mesh of the physical model developed using TrueGrid.

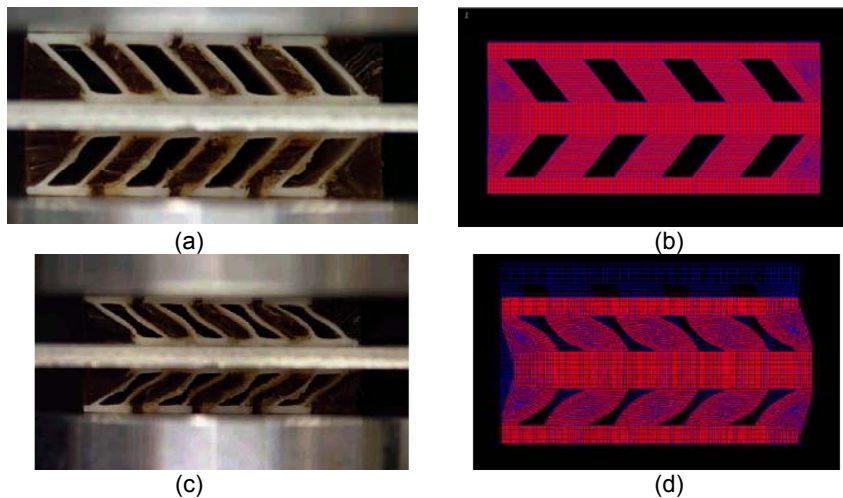


Figure 12. Undeformed state of the experimental specimen (Figure 12a) and the finite-element model undeformed mesh (Figure 12b). Deformed state of the experimental specimen (Figure 12c) and the deformed finite-element model mesh at 10% vertical strain (Figure 12d).

application of compressive forces, as well as the theoretical outputs from a finite-element analysis of the experiment. The two figures compare quite well, demonstrating the qualitative similarity of our Finite-Element Analysis.

Figure 13 shows experimental and finite-element results of a study of the displacement-displacement response of machines with varying wall inclination angle. This data validates our theoretical work with what we have observed experimentally.

4.2 Theory of Beam on Elastic Foundation

An analytical design tool was developed based on the theory of a beam on an elastic foundation model. As shown in Figure 14, the sidewall is supported by the compliant matrix material. This is similar to a beam on an elastic foundation, which is a classic civil engineering problem solved in the 19th century. The equation and its solutions for this case are discussed in detail in Appendix C.

Figure 15 shows the experimental, FEA, and beam-on-elastic-foundation deformation response of a MACterial (rapid prototype, 60° inclination angle) placed under compressive load. The theoretical deformation pattern obtained from the theory of beam on elastic foundation captures very closely the actual deformation pattern obtained from the experiments and is in very close agreement with the FEA results.

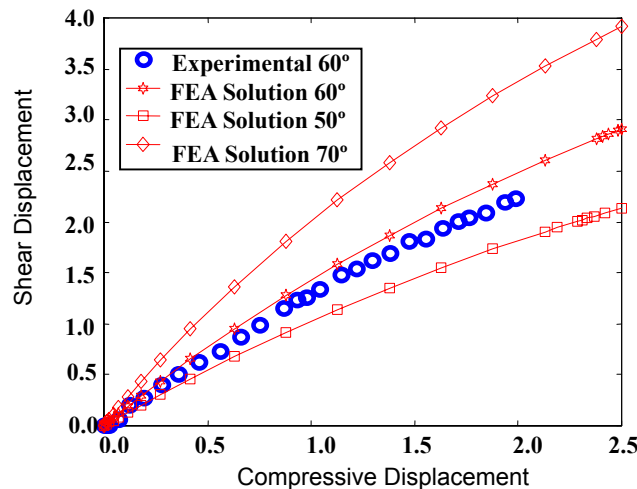


Figure 13. Experimental and FEA compressive versus shear displacements for MACs with polyurethane matrix material and 15-mm cross-section machines for various wall inclination angles. The experimental results are from machines with a 60° inclination angle, and the FEA solutions are for machines with 50°, 60°, and 70° inclination angles.

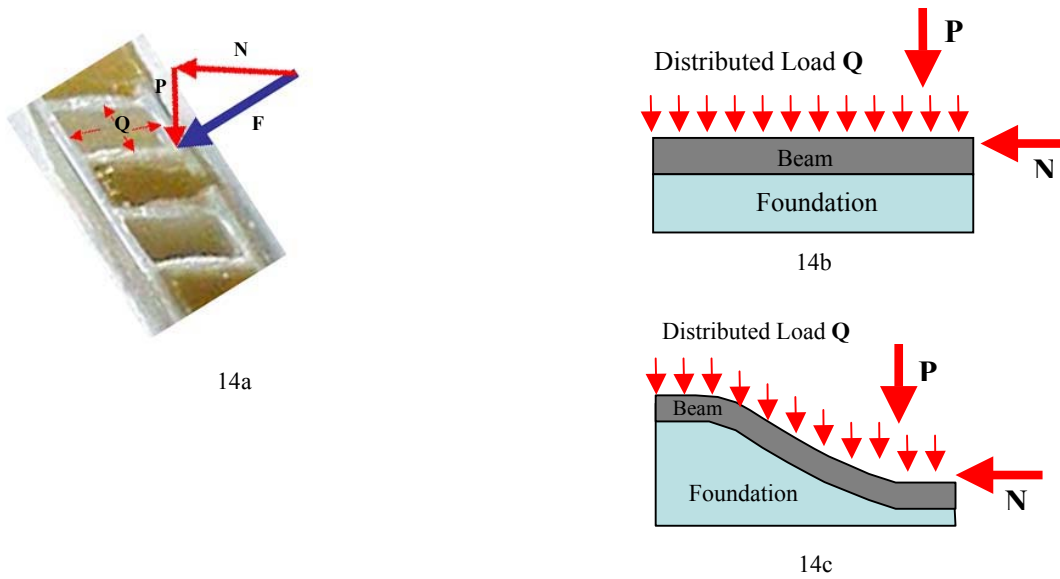


Figure 14. Physical problem modeled as a beam-on-elastic foundation. The sidewall (beam) is supported by the compliant matrix material (foundation). The applied force (F) on the material consists of 2 components perpendicular (P) and parallel (N) to the sidewall. Any internal pressure inside the machines is represented by a distributed load (Q). Figure 14b is a model of the undeformed beam on foundation. Figure 14c is a model of the deformed beam on foundation.

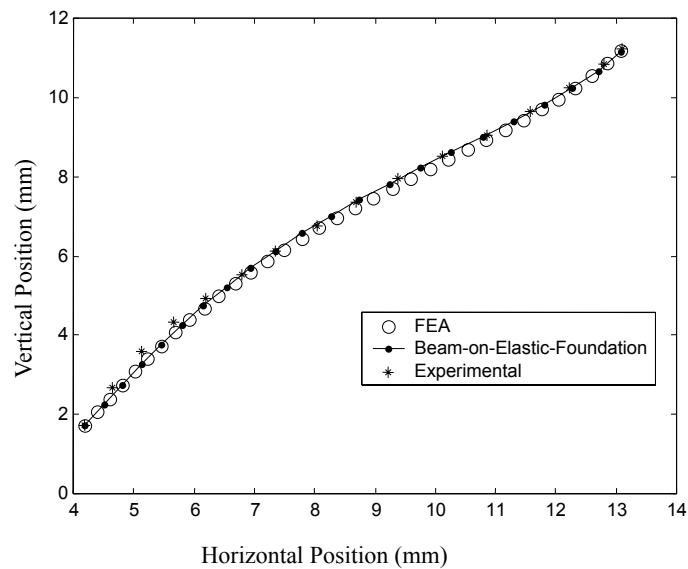


Figure 15. Experimental, FEA and beam-on-elastic-foundation solution of the deformed state of the sidewall of a 15-mm cross-section four-machine MAC with matrix material and a 60° inclination angle.

This page intentionally blank.

5. Machine Augmented Composites For Fluid-Filled Damping (Detailed Discussion in Appendix D)

The main purpose for embedding fluid-filled machines in a matrix is to dissipate the energy of vibrations. Any compression of the fluid-filled Z-shaped machines causes the top and bottom layers of the machines to collapse closer to each other. This motion decreases the internal area, which causes the fluid inside the machine cells to flow. The greater the dissipation rate (i.e., the greater the fraction of fluid being displaced), the better the material is for damping. We began our tests using Z-shaped machines, which was our initial design. After developing design tools that were used to optimize the shape of our machines, we reached the conclusion that an hourglass-shaped machine would be the most effective shape for damping.

5.1 Z-shaped Machines For Fluid-Filled Damping

Various measurements of tan delta ($\tan \delta$) were taken that allowed us to capture damping capabilities and characterize damping behavior of the Z-machines. Dynamic Mechanical Analyses were done using EnduraTEC ELeCTroForce[®] ELF[®] 3200 material testing system to determine the $\tan \delta$ values as functions of frequency of the Z-machines.

We tested samples that included the following: machines without matrix, machines with matrix, machines with matrix filled with water, machines with matrix filled with 13,000-centipoise silicone oil, and machines with matrix filled with 30,000-centipoise silicone oil.

Prior to the test, we specified the dimensions of our specimen and configured the settings inside the DMA control software. We ran 10 conditions, which ranged from 1 Hz to 100 Hz. The dimensions of the specimens were approximately 40 mm in length, 25 mm in width, and 1.5 mm in thickness. Using Fast-Fourier Transform analysis, the DMA software determined the fundamental frequency of data collected for each test condition and calculated the viscoelastic properties of the specimen. The analysis software calculates the $\tan \delta$, which is a measure of the damping of the material.

Figure 16 shows the curve of $\tan \delta$ vs. frequency for various cases of Z-machines and compares them with the $\tan \delta$ of pure polyurethane rubber, which is the material used as matrix inside the machines. As seen by the low $\tan \delta$ values, Z-machines alone provide little damping. However, with rubber matrix impregnated between the machines, $\tan \delta$ value increases significantly, and the machines, especially fluid-filled ones, become fairly good dampers.

One of the most intriguing characteristics we have discovered from the DMA testing of Z-machines is that lower viscosity fluids provide higher damping capabilities. This is counterintuitive, especially when most theoretical descriptions suggest otherwise. The data indicates that embedding water-filled machines inside materials can significantly increase energy dissipation. As seen in the data, damping decreases as frequency increases.

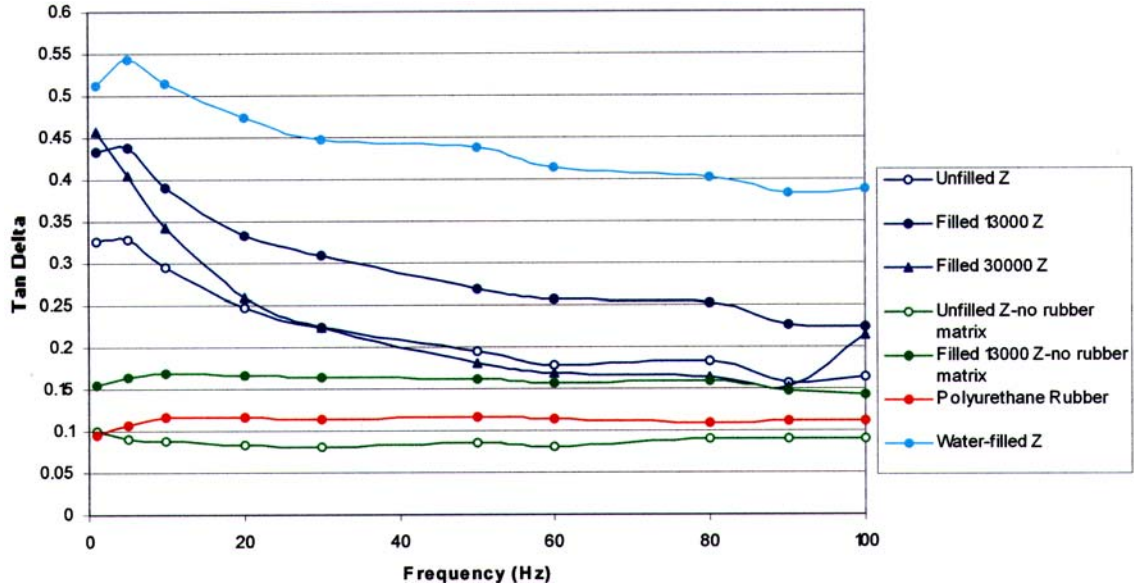


Figure 16. Measurements of the damping as a function of the frequency.

5.2 Hourglass-Shaped Fluid-Filled Dampers

With this understanding of how machines behave when embedded in a matrix material, we were able to design and test a fluid-filled damping machine. A cross section of the machine is shown in Figure 17. When this machine is put into compression, the walls buckle towards each other and reduce the enclosed area. The pressure increased in a fluid contained in that enclosed area. In an extruded machine made with this cross section, the pressure increase will cause the fluid to flow to a lower pressure area. In our design, we intentionally put bubbles in the fluid to provide a region for the fluid to flow.

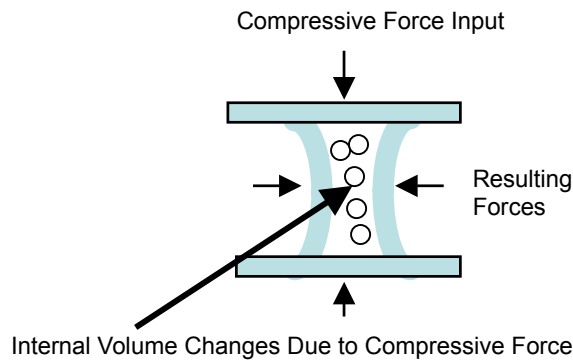


Figure 17. Fluid-filled damping machine. When put into compression, the walls buckle towards each other and reduce the enclosed area.

This fluid-filled machine design was modeled using the finite-element model for the solid portion and an analytical expression for the fluid. The finite-element grid and the analytical expression are shown in Figure 18 (more details are given in Appendix D).

As shown in Figure 16, the highest damping obtained in this study was $\tan \delta = 0.55$, which corresponds to 43% energy dissipation per cycle. This is significantly larger than the energy dissipation of 35% obtained from materials in use today. By optimizing the shape of the machines and the viscosity of the fluid, we anticipate that even higher energy dissipation values can be obtained in fluid-filled dampers.

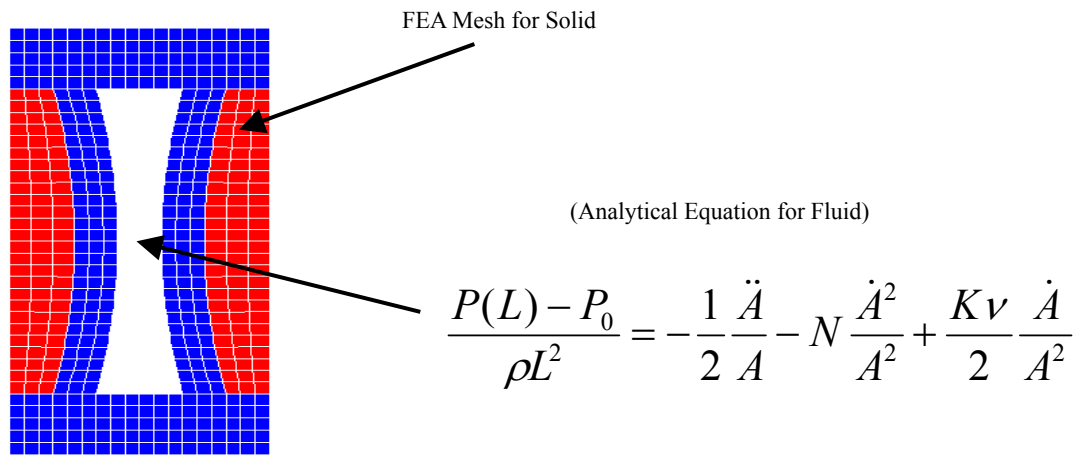


Figure 18. Finite-element grid of hourglass-machines with the analytical expression for fluids.

This page intentionally blank.

6. Application of Force Conversion (Appendix E)

Although we originally studied the Z-machines as a means to understand MACterial behavior, we found a use for this material in infrastructure applications. Traditional composites have been used in recent years to reinforce concrete structures. It has been shown that a stronger concrete structure results if the reinforcing composite is prestressed during its application. To date, it remains a complicated procedure to prestress the composite strips as the adhesive cures in most applications outside of the laboratory. MACterials allow an easy way to prestress composites. As shown schematically in Figure 19, as a composite strip is being adhesively bonded to a concrete beam, anchor plates are placed at either end. The MACterial is located between the composite and the anchor plates, which forces the MACterial into compression as the anchor bolts are tightened. As desired, the stress conversion effect causes the composite to be prestressed as the adhesive cures. A full discussion of this concept is given in Appendix E.

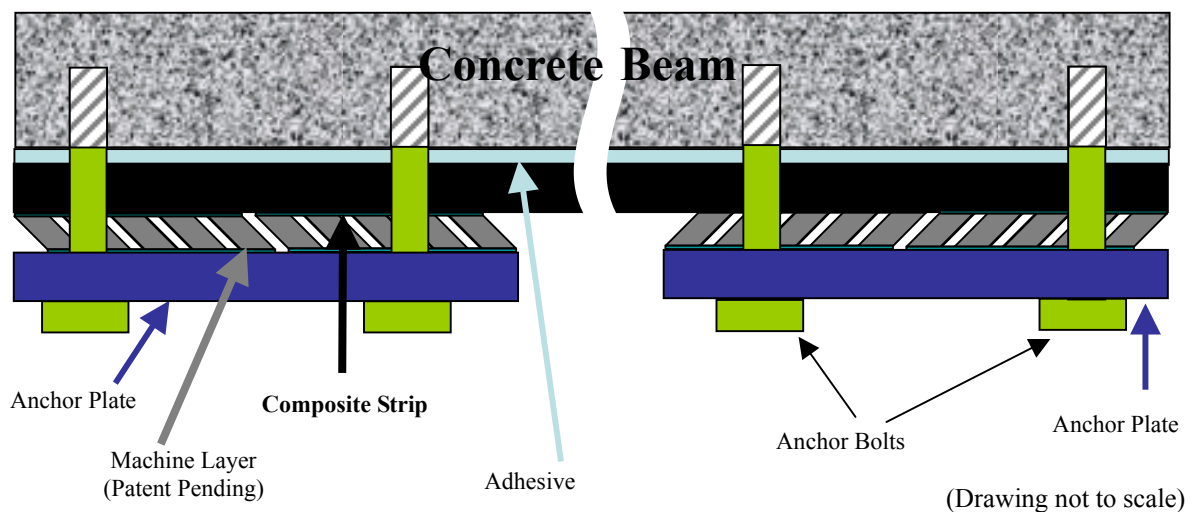


Figure 19. MACterial application for the prestressing of composite strips for the strengthening of concrete structures. The composite strip is stressed in tension when the anchor bolts are tightened. Both the bolts and adhesive hold the composite strip in a prestressed state.

This page intentionally blank.

7. Summary

During the course of this task, we have developed a basic understanding of how Machine Augmented Composite Materials can be used in infrastructure applications. We began by manufacturing samples containing many small Z-shaped machines that convert tensile stresses/strains into shear stresses/strains. Experiments with these samples showed how Machine Augmented Composites convert compressive displacements into shear displacements with an efficiency from 0.5:1 to 2:1, depending on the geometry of the machines. Experiments were also conducted measuring the MACterial's force conversion efficiency with much the same results. An interesting observation was made concerning the "rule of mixtures," which is well established in the composites industry. In MACterials, the rule of mixtures does not apply when considering these stress conversion effects.

The next task involved developing tools that allowed us to design into these MACterials custom-tailored properties, which came from altering the internal geometry, size, and material consistency of the internalized machines. First, we developed an analytical solution for the shape of the machines by comparing the machine's walls to a beam on an elastic foundation. The solutions to the beam on elastic foundation problem have been long established and the solutions have fit our experimental values quite well. We also developed a finite-element analysis model of our machines, allowing us to predict the response of our machines with complicated designs. These results have also compared very well with our observed experimental values.

Using the knowledge and tools developed earlier, we designed and experimented with machines that contained a viscous fluid for use as vibration dampers. We started by injecting fluids of differing viscosities into our Z-machines and measuring the resulting damping properties. Our theoretical models predicted that there would be an optimum viscosity for obtaining efficient damping. Our experiments showed that as we decreased the viscosity, the damping increased. We have not yet obtained the optimal value.

In addition to our work with various fluids, we have also performed work optimizing the design of the fluid-filled machine, which has resulted in an hourglass-shaped machine. Theoretical calculations show that this shape is much more efficient at moving fluids under small displacements, where the movement of fluids is correlated with a high level of damping. Experiments on this design are being continued.

As a side note, during the course of these studies, an issue arose concerning the prestressing of composite reinforcements during their installation on bridges and other structures. We showed both analytically and experimentally that quite high levels of prestress can be obtained by embedding Z-type machines in a composite bondline before application to a structure.

In summary, we have developed the rules, tools, and manufacturing methods for Machine Augmented Composite Materials. We have shown that they can be used in infrastructure applications to prestress composites in retrofit situations and can potentially be used to dampen the vibrational energy caused by earthquakes. These were the goals of this task and they have been successfully achieved.

This page intentionally blank.

Appendix A—The Fabrication and Mechanical Behavior of Z-Shaped Machine-Augmented Composites

Prepared by

RAFAEL J. ZALDIVAR, JAMES T. YAMASAKI,
JULIET N. SCHURR, and GARY F. HAWKINS
Space Materials Laboratory
Laboratory Operations

Abstract

Machine-augmented composites (MACs) are a new class of composite materials that utilize the tailored shape of their reinforcement to create novel properties best suited for an application. The particular geometries of the machines control the composite's internal forces. These machines can be fabricated into numerous shapes and out of many material systems, thereby providing different mechanical responses.

In this first part of two reports, we focus primarily on the manufacturing and testing of a new type of composite material that contains Z machines. These Z machines were designed to provide compression-to-shear stress conversion properties. In order to better understand the stress conversion response of Z machine MACs, we have measured the shear displacement and deformation behavior of these composites as a function of compressive displacement. The effect of machine inclination angle, machine reinforcement volume, and machine size were also experimentally evaluated. Direct correlations between a prototype system and the extruded system MACs were verified. The data collected in this report were then used to develop an analytical framework to better predict machine behavior. The second report will describe the finite-element analysis model of Z machine MACs. A thorough understanding of both our experimental and analytical results will contribute in the design of future machine configurations.

A-1. Introduction

Machine-augmented composites (MAC) are a new class of composite materials that utilize the tailored shape of embedded machines to create unique mechanical properties. Composite materials typically use cylindrical fiber reinforcements, such as carbon, glass, and polymeric fibers, aligned in preferred orientations in order to meet mechanical performance requirements. However, if these reinforcements are tailored into specific machine shapes, other properties can also be obtained from the same structural system leading to a dual-use system. The geometry of the machines can modify the composite's internal forces, creating as many different mechanical properties as there are possibilities for the cross-sectional shapes of machines. Other researchers have experimented with different cross-sectional shapes for fiber reinforcements. However, the majority of this work has been focused on improving the fiber-matrix contact area in order to promote interfacial bonding. In contrast, in describing our MAC materials, we use the term “machine” to describe “an instrument (such as a lever) designed to modify the application of power, force, or motion” by virtue of its geometry.

Figure A-1 shows a schematic of the cross section of a simple stress-conversion machine that converts shear forces into tensile/compressive forces and vice versa. This machine consists of two parallel (horizontal) plates connected through two struts (slanted walls) situated at an angle to the plates (Z-type configuration). Note that if shear forces are applied to the machine as shown, the slanted walls change their angle, forcing the top and bottom plates to move apart. This movement causes compressive forces on any adjacent contacting material. Conversely, if compressive forces are applied to the top and the bottom faces, the machine imposes shear forces on any abutting material. As indicated in the figure, this machine responds to shear forces with a tensile/compressive strain.

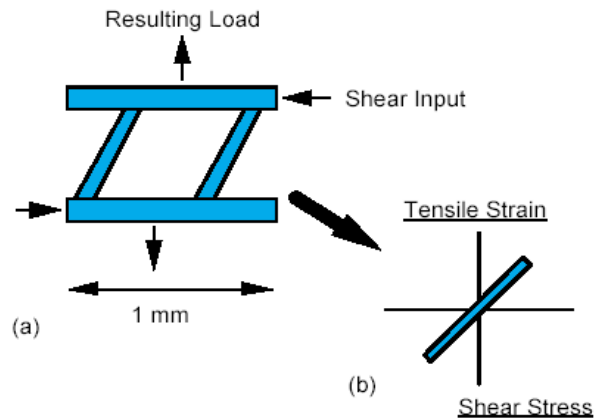
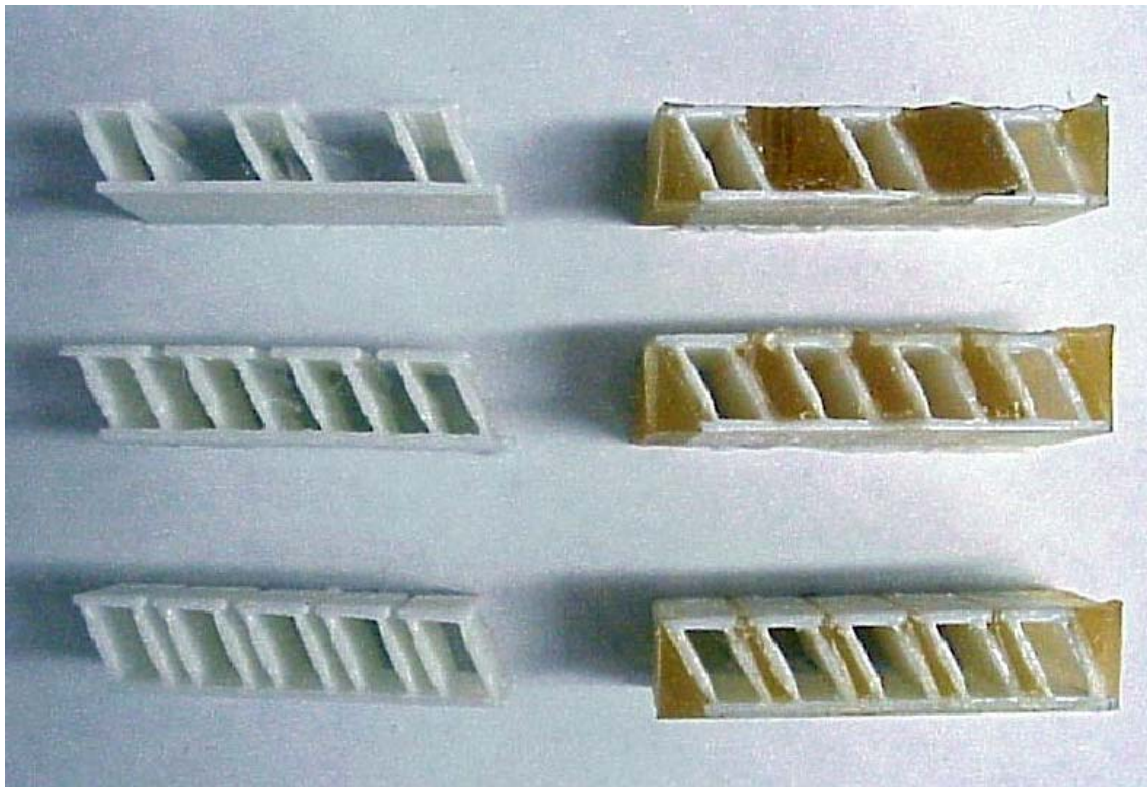


Figure A-1. Schematic of Z-shaped machine. (a) machine action; (b) tensile strain vs shear stress response.

We used this concept to develop a centimeter-scale prototype composite that we can use to experimentally test and theoretically evaluate the stress-conversion properties attributed to this machine. Figure A-2a shows a photograph of this prototype Z machine. Figure A-2b shows the corresponding composite made with these machines. The white material represents the prototype machines, and the yellow material represents the matrix material. Each cell represents one machine as described in Figure A-1. These prototype composites can be rapidly modified by changing the structural parameters of the machines, such as, wall thickness, aspect ratio, wall inclination angle, overall cross-sectional area, and cell unit volume. This allows for a rapid evaluation of proof of concept prior to the extruding of these machine-shaped reinforcements, allowing us to be more cost and time effective.

In this report, we report primarily on the manufacturing techniques and the experiments performed on our Z-type stress conversion composites. Testing was performed on both our centimeter-scale prototype and millimeter-scale extruded machines. The effects of machine inclination angle, machine reinforcement volume, and machine size were experimentally evaluated to better understand the behavior of the system. In addition, the deformation behavior of the machines was experimentally evaluated as a function of load. These data were then compared with our analytical and finite-element micro-mechanical models, which will be discussed in a future report.



(a)

(b)

A-2. Experimental

A-2.1 Fabrication of Prototype Z Machines

All prototype Z machines were produced using a Konners 3D printer. The samples were designed using a Fastran design program and fabricated into the desired shapes. Samples consisting of 3, 4, and 5-celled Z-shaped machines are shown in Figure A-2. Most samples tested had 60° inclination angles unless otherwise stated. The sample dimensions were approximately 45 mm x 50 mm x 10 mm. The cross-sectional dimensions of each Z-shaped machine was approximately 10 x 7 mm. Additional prototype machines with inclination angles of 45° and 75° were also fabricated.

A-2.2 Fabrication of Prototype Machine Augmented Composites (MAC)

In order to evaluate the effect of these Z-shaped prototype machines on composite properties, a polyurethane material was infiltrated into the system as a matrix material between the Z-shaped machines. Smooth-On urethane compound PMC-121/30 (Resin A and Resin B “Dry” formulation) was used as the matrix material. This system was mixed in a 1:1 volume ratio and degassed under vacuum. The prototype machines were placed in Teflon molds and the polyurethane mixture was poured into the spaces between the machines. The open face of each of the volume cells was sealed in order to prevent infiltration into the machine’s hollow center. The infiltrated sample was allowed to cure for 24 h. Excess flash polyurethane resin was removed using a sharp blade.

A-2.3 Fabrication of Nylon Extruded Z Machines

The Z machines are approximately 1.0 mm in cross section and were extruded from nylon stock. Extrusioneering Inc., located in Temecula, CA extruded all of the 1-mm Z machines used in this study. These machines have been extruded out of a number of different material systems. The size of these machines can also be varied, depending on the desired application. Figure A-3 shows the cross section of one of these Z-shaped extruded machines.

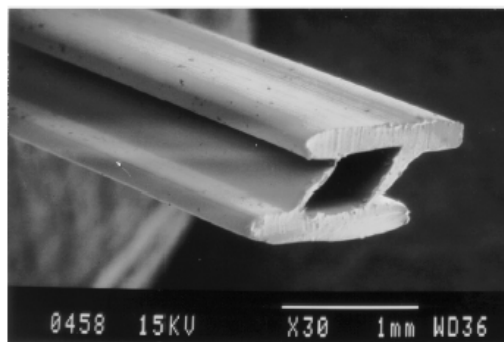


Figure A-3. SEM of extruded nylon machine showing Z-type configuration.

A-2.4 Fabrication of Extruded Z-MAC

The processing steps incorporating these Z-machine segments into a composite were patterned after current composite practices. The extruded Z-machine segments were laid down, side-by-side in a specially designed grooved Teflon mold, and adhesively bonded (3M Super 77 Spray Adhesive) to a polyester scrim cloth (see Figure A-4). This assembly represents one ply of machines. The ends of the machines were sealed with an adhesive (white glue). To produce a composite laminate, the single ply of machines was impregnated with a room-temperature-curing polyurethane resin matrix material (Smooth-On PMC-121/30) and placed in an evacuated bell jar to outgas the polyurethane as it polymerized and hardened. After the polyurethane cured, the sealed sample ends were trimmed off with sharp scissors so that the open machine ends were exposed (see Figure A-5).

A-2.5 Tensile Tests of Constituent Materials

In order to have accurate material constituent properties for our model, tensile testing was performed on (a) the prototype structure material, (b) the polyurethane matrix material, and (c) the nylon extruded machines. All testing was performed using a Universal Instron Testing Machine equipped with a data acquisition interface system. The displacement data were obtained from both the crosshead displacement and an extensometer. The loading rate was 0.005 in./min using a 200-lb load cell.



Figure A-4. Extruded nylon machines aligned on a grooved Teflon mold and bonded to a scrim cloth.

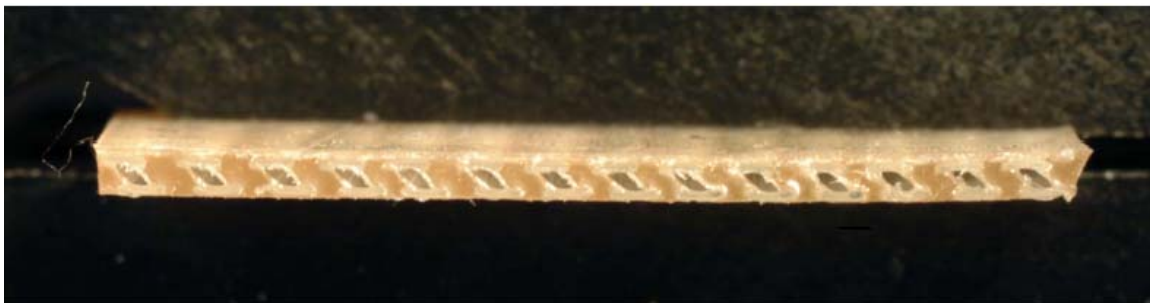


Figure A-5. Extruded nylon Z-machines aligned in a polyurethane resin matrix.

A-2.6 Compressive-Shear Displacement Mechanical Testing of Samples

All compressive-shear displacement tests were performed using a Universal testing machine at a crosshead speed of 0.005 in./min. The test set-up is shown in Figure A-6. When a compressive force is applied, the MAC distorts in shear. Thus, when a MAC sample is placed in a typical mechanical testing machine, the surfaces of the testing machine constrict the MAC movement so it cannot displace in shear. To circumvent this problem, two MAC samples were placed on top of each other, with one sample's orientation reversed with respect to the other. An aluminum plate was placed between the two MAC samples (see Figure A-6).

In this arrangement, neither of the two samples subject the testing machine to shear forces. When the top sample pushes the aluminum plate that is between the samples to the right, the bottom sample also pushes the aluminum plate to the right. The shear displacement is determined by measuring the movement of the aluminum plate. The lateral motion is measured with an LVDT probe shown touching the aluminum plate at the right of the figure. Besides providing a convenient measuring surface, the plate cancels out any symmetrical forces caused by the Poisson effect. Both prototype machine composites and extruded machine composites were tested in the same manner.

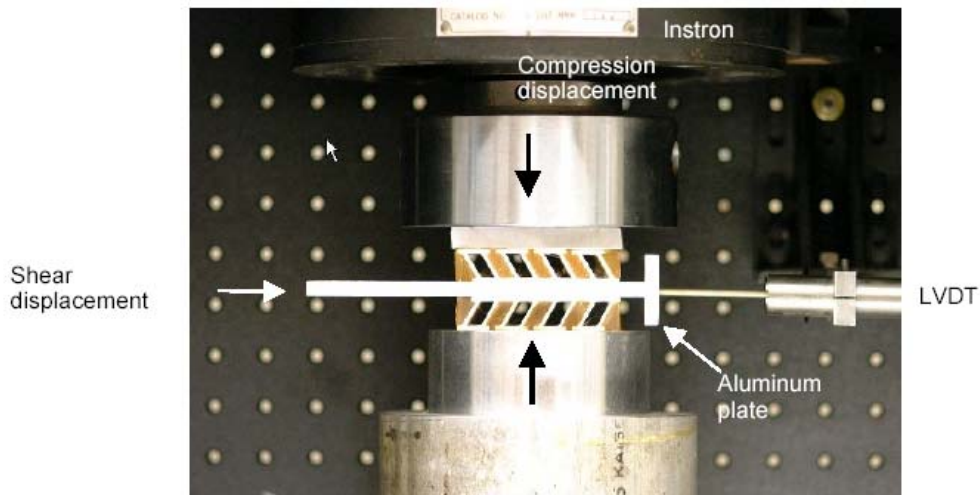


Figure A-6. Photograph showing test set-up for compression-to-shear displacement tests.

A-3. Results and Discussion

As described earlier, our prototype Z-machine structures provide a means for us to rapidly collect experimental data to evaluate how the shape of our machines affect composite mechanical behavior. It also allows us to better fine tune our analytical model. Table A-1 shows the various types of prototype and extruded Z machines fabricated for this study.

As shown, the first three samples are the Z machines alone with no matrix. The samples have either 3, 4, or 5 machine cells per unit area in the structure. All of these samples have a wall inclination angle of 60°. The following three samples are the same machines with infiltrated polyurethane resin as the matrix material. The last three prototype samples were fabricated in order to determine the effect of wall inclination angle on machine mechanical behavior. The cell unit volume was kept constant at 4 cells per unit area while the inclination angle was varied by 15° from 45° to 75°. These last three prototype samples were fabricated with larger (15 mm) machines than the previous prototype machines to mitigate delamination effects seen in some of the 10-mm-size prototype machines. The final sample is a 15-cell extruded composite with 1-mm-size nylon Z-machines. Polyurethane was used as the matrix material.

A-3.1 Deformation Characteristics

Figure A-7 shows the deformation characteristic of an unfilled prototype machine sample subjected to a compressive load. Figure A-8 shows the deformation behavior of the same prototype machine filled with matrix material. As expected for both cases, by applying a compressive load, which causes a compressive displacement, the shape of the machine promotes a shear translation.

In the case of no matrix material (Figure A-7), the machines behave as hinges. As the compressive load is applied, the machines hinge at their junction sites and move in a shear direction. Both the filled and unfilled systems behave similarly under small strains.

Table A-1. Prototype and Extruded Machines and Composites Fabricated for This Study

Z-machine type prototype (p) extruded (e)	Number of cells	Inclination angle (°)	Matrix material	Size (mm)
p	3	60	none	10
p	4	60	none	10
p	5	60	none	10
p	3	60	Polyurethane (low modulus)	10
p	4	60	Polyurethane (low modulus)	10
p	5	60	Polyurethane (low modulus)	10
p	4	45	Polyurethane (low modulus)	15
p	4	60	Polyurethane (low modulus)	15
p	4	75	Polyurethane (low modulus)	15
e	15	60	Polyurethane (low modulus)	1

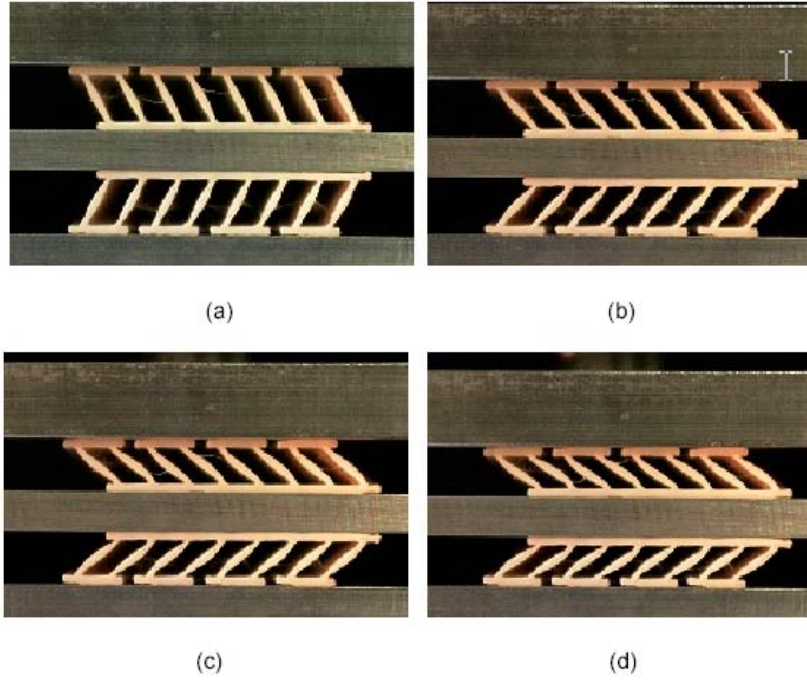


Figure A-7 Deformation characteristics of an unfilled 4-celled machine composite under load.

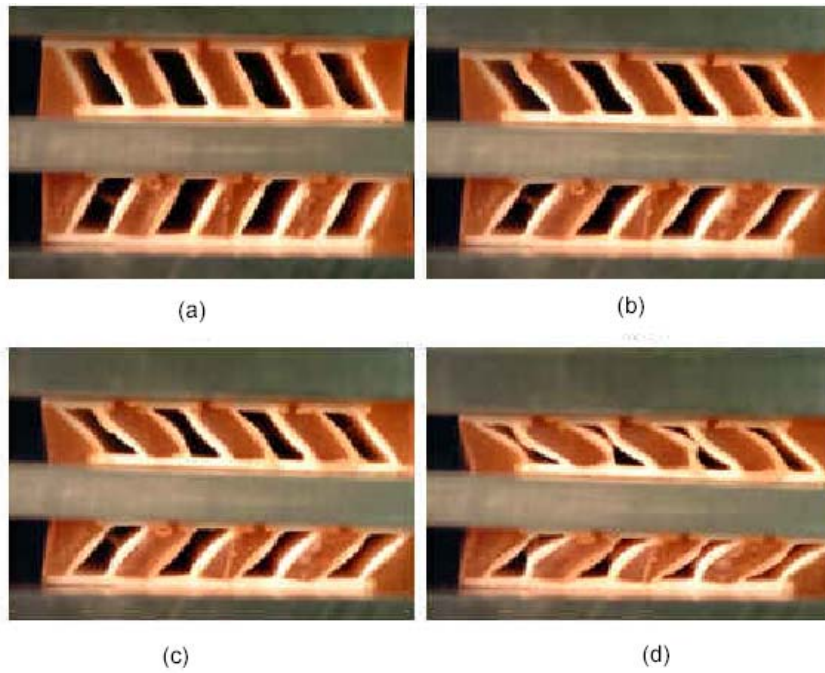


Figure A-8. Deformation characteristics of a filled 4-celled machine composite under load.

The machines appear to convert applied compressive loads to shear loads. However, at the higher strains, the polymer matrix applies a force on the cell walls due to the Poisson effect of the resin and distorts the shape of the cell walls (Figure A-8). The deformation shape of the walls of the filled systems follows more of an s-type deformation than the hinged lever behavior observed for the unfilled system. The effect this has on the compressive-to-shear translation will be subsequently discussed.

A-3.2 Effect of Machine Volume Ratio on MAC Displacement Behavior

In standard fiber-reinforced polymers, the fiber volume ratio influences many of the mechanical properties of the material, such as the modulus, strength, thermal expansion, etc. Calculating these properties involves the well-known rule of mixtures that accounts for the volume ratio of the fibers to matrix material. To investigate this effect, samples with the same overall dimensions were manufactured containing different numbers of machines per unit volume. Samples containing three, four, and five 60° angle prototype machines were manufactured. The samples were then fabricated into composites using a polyurethane matrix. The results of the compression-to-shear displacement tests are shown in Figure A-9.

As shown, the ratio of compression-to-shear translation (strain conversion ratio) is approximately one for all of the different cell machine volumes. Therefore, the material response is dominated by the geometry of the embedded machines and not the machine density. This would indicate that the rule of mixtures does not apply for MACs when considering the compressive-to-shear displacement ratio. Included in Figure A-9 is the data from a sample that had no matrix material. This sample was an unfilled prototype machine as previously shown in Figure A-7.

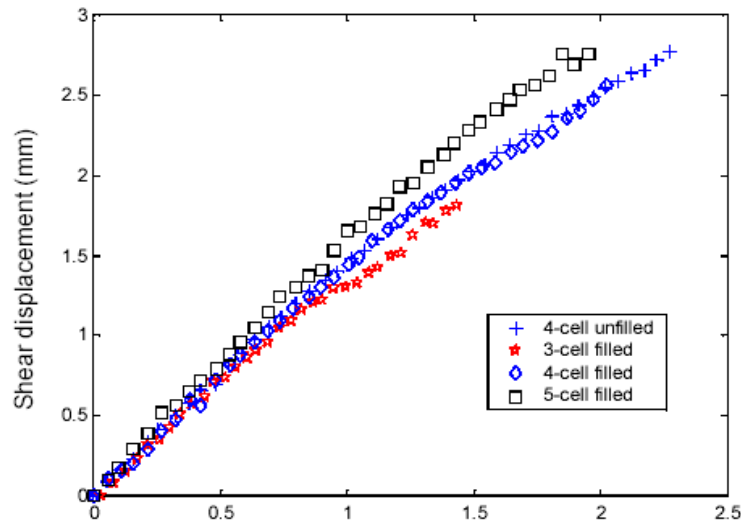


Figure A-9. Shear vs. compressive displacement for rapid prototype machines as a function of machine volume percent (3-, 4-, and 5-celled machine composites).

Interestingly, these data follow the same curve as the matrix filled samples, which would indicate that compressive-to-shear displacement ratio is affected minimally by the matrix material. This indicates that the variation in the deformation behavior between filled and unfilled system is negligible with respect to displacement. However, it should be noted that the load-to-displacement curve for these composites will still remain a function of the matrix material properties.

A-3.3 Effect Due to Changes in Machine Inclination Angle

The most direct effect on the compression/shear conversion ratio is the angle between the sidewalls and the base of the machines. In a four-bar linkage, an angle of 45° yields a one-to-one ratio of compression to shear, and the ratio goes to infinity as the angle increases to 90° . These Z machines do not convert compression to shear as efficiently as a four-bar linkage, but the data follow the same trend as the wall angle is changed. As shown in Figure A-10, for a given compressive strain, the shear displacement increases as the angle is increased (15-mm Z-shaped machines).

A-3.4 Scaling Effects

Single-ply composite samples were fabricated using 1-mm-sized extruded nylon Z-shaped machines with a 60° inclination angle. The samples were then tested to verify that the small extruded MACs behaved similarly to the two larger prototype samples. Figure 11 shows the shear versus compressive displacement for MACs with three different-sized machines. All of the samples contained machines with a 60° inclination angle. For small displacements, there is very good accordance between the two different-sized prototype samples and the extruded samples. The first thing to note is that the ratio of the shear-to-compressive displacement is approximately one to one. If the machine were a perfect four-bar linkage with hinges at the corners, simple geometry shows that the ratio would have been greater than one. The actual value is less than that because the machines act as a flexure, not as a hinge.

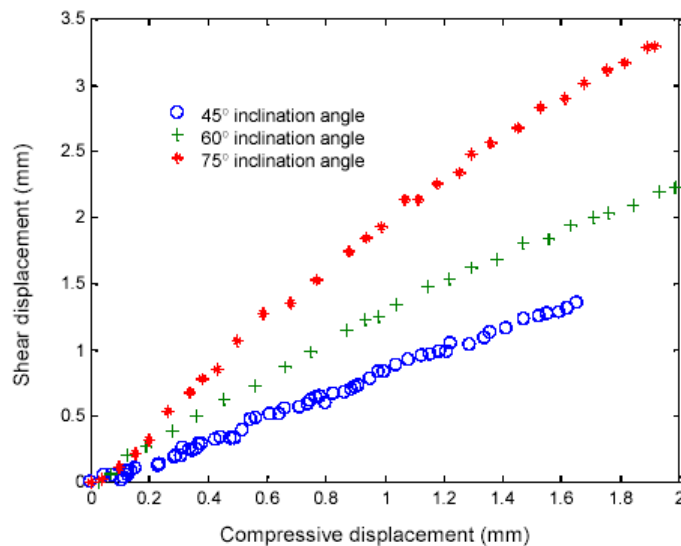


Figure A-10. The effect of inclination angle on the compressive-to-shear displacement behavior of a MAC (15-mm Z-machines).

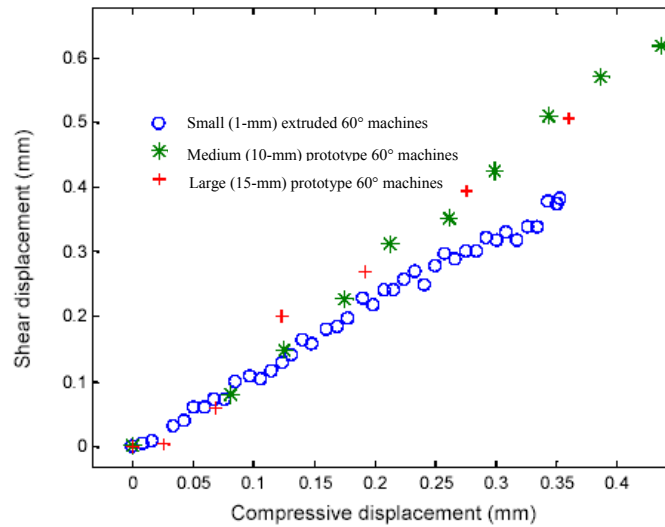


Figure A-11. Shear vs. compressive displacement for MACs with three different-sized machines.

Figure A-11 also shows that the samples containing the small, 1-mm extruded machines respond with a slightly lower slope than the larger, rapid-prototype machines. The difference is not significant considering that the size has changed over an order of magnitude and that the machines themselves were made of two different polymers. The predominant effect may be due to the substantial fillet present in the extruded machines. The extrusion process tends to round corners, which show up as fillets in this machine design. In any case, the large prototype machines adequately represent the response of the small extruded machines, allowing us to obtain the basic rules of the material using the large machines.

A-4. Conclusion

We have designed, manufactured, tested, and analyzed a new type of composite material that contains simple machines that act to modify the forces within the material. Using a Z-shaped prototype machine configuration, we have verified that our new composite material upon compression loads converts applied compressive displacement to shear displacement. From our investigation we have made the following conclusions:

1. As expected, under both small and large compressive loads, the machines translate the compressive displacement to shear displacement.
2. The presence or lack of matrix material does not seem to influence the overall displacement response of the MACs. However, at a local level, for large displacements, the matrix material applies loading on the walls of the machines, distorting their shape. This distortion in the shape of the machine walls is not present in the MACs without matrix material. The distortion in the shape of the walls seems to be a local phenomenon that does not affect the overall displacement behavior of the MACs.
3. The machine density has little influence on the displacement response of the MACs while undergoing small deformations. For large deformations and a fixed compressive deformation, the corresponding shear deformations of the MACs increase with increasing density. This effect is more significant in the case of the MACs with matrix material than in the case of MACs without matrix material.
4. Changes in the machine inclination angle have a strong influence on the compressive shear displacement conversion ratio. For a given compressive strain, the shear displacement will increase as the inclination angle is increased.
5. For small displacements, the machine size has little effect on the displacement response of the MACs, even with MACs that are made out of different constituent materials. For large displacements, the machine size also appears to have little effect of the displacement response of the MACS when considering different size MACs made with the same constituent materials.

Appendix B—The Load-Load Characteristics of Z-Shaped Machines

Prepared by

RAFAEL J. ZALDIVAR, MICHAEL J. O'BRIEN,
JULIET N. SCHURR, JAMES T. YAMASAKI,
and GARY F. HAWKINS
Space Materials Laboratory
Laboratory Operations

Abstract

Machine-augmented composite materials (MACterials) are composite materials that have tailored reinforcements that perform specific mechanical operations that are typically not available with other state-of-the-art systems. MACterials consisting of unidirectional Z-shaped machines embedded within a polyurethane matrix were fabricated. Larger (15-mm) Z-machines were fabricated through rapid prototyping, while small (1-mm) Z-machines were made of extruded nylon. These two MACterial systems were tested using a unique test fixture that was developed in our laboratory to measure the stress conversion behavior of the samples. This fixture allowed us to evaluate how the design and shape of the machines convert an applied load from one direction of the composite to another. Most constrained materials, when subjected to a load, apply a small portion, if any, of this load in a secondary direction. We have shown that MACterials can be designed to not only convert stress efficiently (1-to-1 ratio), but the stress conversion ratio can also be tailored depending on the lay-up of the MACterial. The effect of machine cell size, cell volume, wall inclination angle, lateral preload, and previous load-cycle behavior on the resultant stress conversion behavior was investigated, both experimentally and through finite element analysis. The results were also compared to traditional isotropic viscoelastic materials.

B-1. Introduction

Machine-augmented composite materials (MACterials) are composites that have tailored reinforcements to perform specific mechanical operations that are typically not available with other state-of-the-art systems. Recently, there has been an increased desire by researchers in the industry to tailor a material's properties to meet specific needs. The efforts in this field generally have involved using "smart materials," or the tailoring of the material's microstructure. The closest work from which we can gain insight into MACterial design and analysis is included in papers describing the analysis and construction of hierarchical composites. Hierarchical composites are defined as materials that contain structures of multiple-length scales with large but finite differences. Examples of hierarchical composites range from the Eiffel tower to materials with nanometer-sized microstructures. MACterials fit into this definition because they contain many small machines that combine for use in a material at a larger scale. Some of the references describe large arrays of interconnected micromechanisms that are studied both theoretically and, in some cases, experimentally. Lakes¹ gives a complete discussion of hierarchical composites. The theoretical treatment of hierarchical composites can be used as a basis for the development of the design rules for the MACterials.

Embedding simple machines in a matrix allows the material scientist to design a material with specific properties in mind. A full description of the fabrication of MACterials can be found in Zaldivar.² Depending on the shape and size of the machines, different resultant mechanical behaviors can be achieved. For example, when "Z-shaped" machines are employed, the MACterial distorts in shear when compressed as shown in Figure B-1. Converting compressive-to-shear load, and vice versa, is an ability that can be useful in applications where it is advantageous to change the size of a part when it is under an applied load. Most constrained materials, when subjected to a load, apply only a small portion, if any, of this load in a secondary direction. MACterials, however, can be designed to not only transfer the load efficiently, but the degree of the displacement and/or load can be tailored, depending on the lay-up of the MACterial.

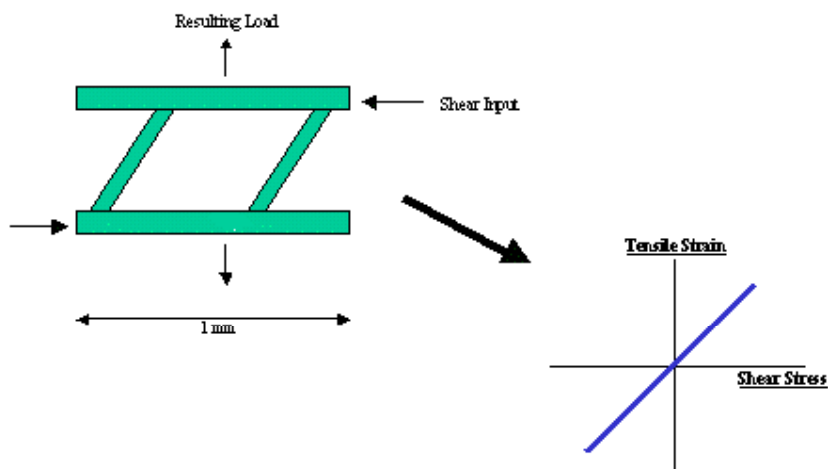


Figure B-1. Schematic showing shear-to-compression stress conversion.

Hawkins³ has described the concept of Stress Conversion Ratio as the percent utilization that the machine or material possesses when transferring stress from one direction or mode to another. For example, in the case of an isotropic viscoelastic material, an applied load is poorly transferred in the off-axis directions. Most of the stress conversion behavior is a result of the Poisson effect. In the case of MACterials, the machine shape can be optimized for the desired conversion behavior. Embedding Z-machines in a matrix allows the resulting composite to convert compressive to shear stresses, and vice-versa. This stress conversion could be used in the design of fasteners or clamping devices, where the shear load imposed on the MACterial could cause the MACterials to expand and wedge more tightly in position. In addition, seals or gaskets may be able to be made more effective if machines were incorporated into their design. As another, we have been exploring using these machines in adhesive joints to reduce peel forces.

We have designed and fabricated a unique test fixture in order to evaluate the stress conversion behavior of our composite systems. When subjected to a shear load, the unconstrained Z-shaped machines will distort and change size. When the material is constrained and the machines cannot change size, they will induce compressive or tensile loads on the constrained faces, depending on the direction of the shear load. Unfortunately, there is no ASTM test for measuring this conversion from shear to compressive load. Consequently, we have developed a unique experimental set-up (Figure B-2) to measure the compressive loads generated by a shear load. By applying an axial shear load on our machines, the lateral load can be measured with a separate load cell. This set up allows testing of numerous samples without many of the complexities typically associated with biaxial testing. Greater detail on the test procedure will be discussed in our experimental section. In this report, the effect of machine cell size, cell volume, wall inclination angle, lateral preload, and previous load-cycle behavior on the resultant stress conversion behavior was investigated.

Finite-element analysis (FEA) of the load-load behavior of the machine composites was also conducted to simulate and analyze the experiments. A parametric FEA study was performed to measure the stress-conversion response as a function of number of cells (that is, 3, 4 or 5 cells), material properties, cell aspect ratio, cell spacing, and load cell compliance.

B-2. Experimental

B-2.1 Fabrication

Both small (1-mm) Z-machines made of extruded nylon and large (15-mm) Z-machines fabricated through rapid prototyping were used to fabricate MACterial samples for testing in this study. A detailed overview of their processing is described in a previous technical report.² Besides material composition, an important difference to note is that the larger, rapid-prototype Z-machines are all connected to each other by a common base, whereas the smaller, extruded nylon Z-machines are completely separate, lacking a common base (see Figure B-2).

The rapid-prototype Z-machines and the nylon-extruded Z-machines were also tested without any matrix material. Rapid-prototype Z-machine composites containing 3, 4, and 5-celled volumes were utilized. Angle inclination for the 4-celled composites varied from 45° to 60°.

B-2.2 Mechanical Testing

A universal testing machine was used for all testing. A 2000-lb load cell was used. The testing rate was 0.05 in./min unless otherwise stated. Two acquisition systems were used to collect data from both lateral and vertical load cells using an IOTECH data converter. A unique experimental set-up was developed (Figure B-2) to measure the compressive loads generated by a shear load. In this experiment, two samples were prepared and bonded to the center plate of a double-lap shear test set-up. The samples were rotated 180° with respect to each other such that both samples tended to increase in thickness when the central plate was pulled down. The outer faces of the samples were bonded to the outer plates, completing the double-lap shear arrangement. The outer plates were attached to the mechanical testing machine in a pendulum-type manner (see Figure B-3).



Figure B-2. Z-machines used to fabricate MACterial samples. (a) 15-mm rapid prototype machines with a common base. (b) 1-mm extruded nylon machines without a common base (embedded within a polyurethane matrix).

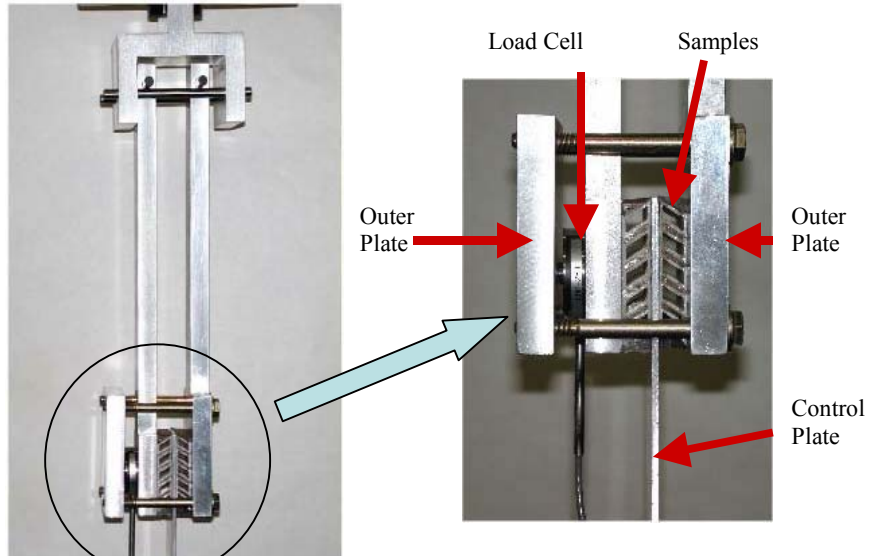


Figure B-3. Experimental set-up used to measure compressive load as a function of shear load.

This set-up allowed the outer plates to swing freely against the transverse load cell. The transverse load cell was mounted such that any forces attempting to separate the outer plates put the load cell into compression. Careful inspection of the experimental set-up of Figure B-3 shows that the load path coming in from the central plate was not co-linear with the pivot points at the top of the outer plates. This caused a small bending moment around the pivot points at the top of the pendulum, which was measured by the transverse load cell. This effect was small and was neglected for all our measurements.

B-3. Results

B-3.1 Rapid Prototype Z-Machine MACterial Testing

The results in Figure B-4 show a comparison of the stress conversion behavior of a neat polyurethane sample containing no machines in comparison to the stress conversion behavior of a machine-augmented composite material (MACterial). The MACterial consists of a 5-celled rapid-prototype Z-machine within a polyurethane matrix material. In the case of the neat polyurethane sample, there is virtually no relationship between the applied shear load and the measured compressive load. The slight slope in the line can be completely accounted for by the fact that the load input points are not co-linear and cause a bending moment around the pivot points of the pendulum arrangement (accounts for 7.5 lb lateral load per 100 lb shear load). The data was not normalized to take into consideration this effect. As expected, the stress conversion behavior of a non-reinforced viscoelastic material is minimal. In comparison, a rapid-prototype ZMACterial utilizing the same polyurethane material shows a substantially different effect. The stress conversion behavior is greatly affected and is more in line with a 1:1 stress conversion ratio.

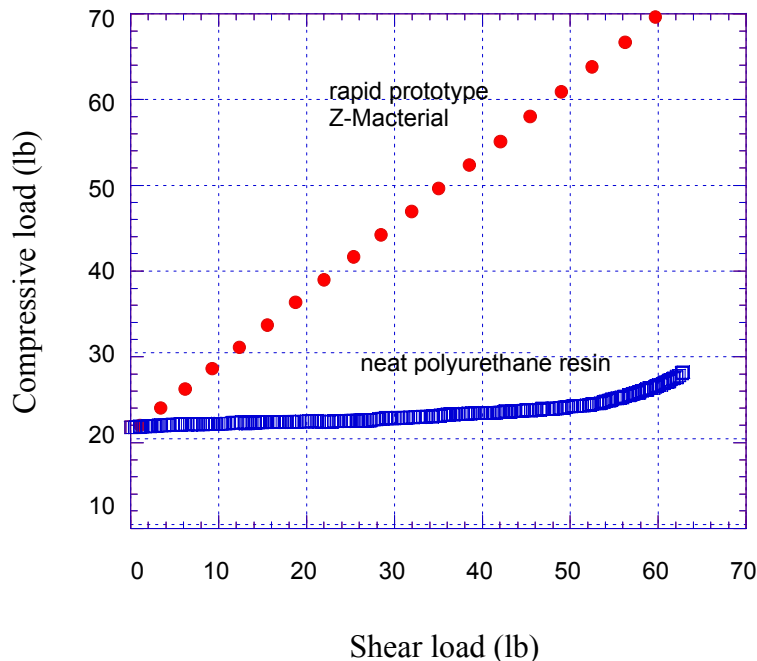


Figure B-4. Stress conversion behavior of an unreinforced polyurethane resin versus a 5 volume-celled rapid-prototype Z-machine augmented composite utilizing the same polyurethane material as the matrix.

Figure B-5 shows the relationship of the applied shear load to the resultant lateral compressive load for various machine cell volume MACterial specimens. The effect of 3, 4, and 5-celled MACterials on stress conversion behavior is shown. All of these samples had an original wall inclination angle of 60°. The stress conversion was measured to be the same for the three different specimens. Therefore, the effect of cell volume has little consequence on the slope of the line. A stress conversion factor of 1:1 was measured, which is quite pronounced.

The effect of the machine wall inclination angle on the stress conversion behavior of this system was also investigated. Figure B-6 shows a plot of applied shear load to measured lateral compressive load for two MACterials with different wall inclination angles. As shown, if the inclination angle is reduced, the stress conversion behavior is also reduced. As expected, this is in contrast to the displacement conversion ratio, which shows the converse, where the displacement conversion increases as the angle decreases.

The effect of lateral compressive preload was also investigated. The set clamps on our testing device were tightened by hand to apply various preloads. The resultant stress conversion was measured. Figure B-7 shows the results from this test on a 3-celled MACterial sample. The effects on 4- and 5-celled MACterial samples are similar. As shown, the lateral compressive preload has a negligible effect on the stress conversion behavior. All of our different preloads yield the same type of end result. However, at very low preloads, below 2.5 lb, there is a lag time before the lateral compressive load starts to build with respect to the applied shear load created by the Instron mechanical testing machine. We believe this may just have to do with a critical amount of frictional force that must be overcome to prevent slipping of the part prior to load translation.

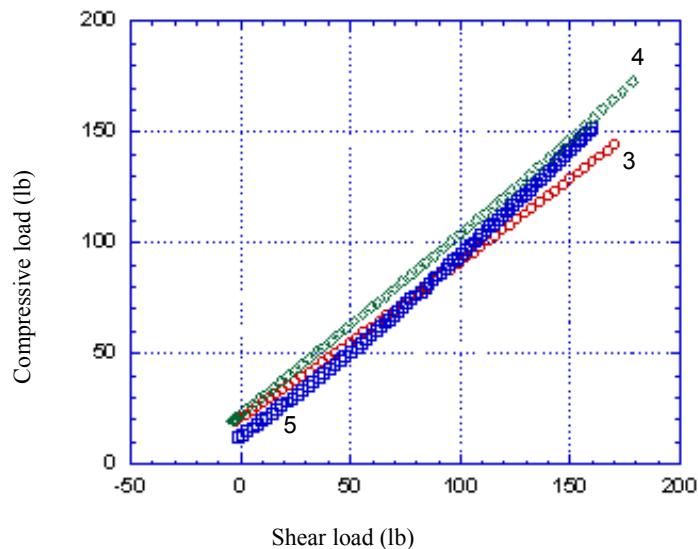


Figure B-5. Graph shows the effect of Instron vertical shear load on the resultant lateral compressive load of our prototype composite specimens. The effect of 3, 4, and 5-celled MACterials with a 60° inclination angle are shown.

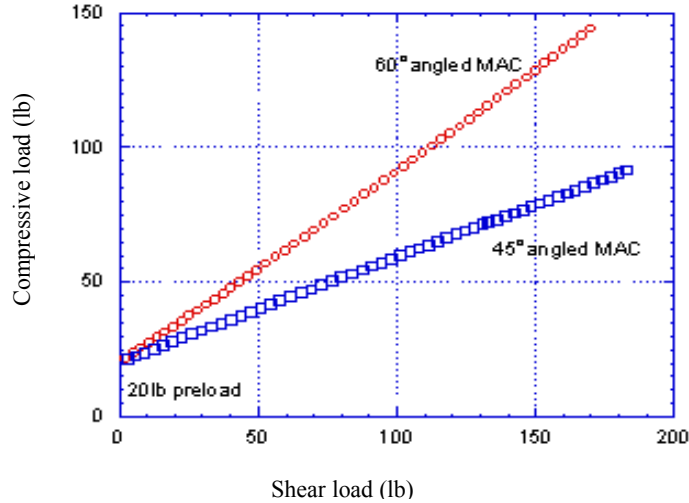


Figure B-6. The effect of wall inclination angle (45 and 60 degrees) on the resultant stress conversion behavior of a 4-celled rapid prototype MACterial (20-lb preload).

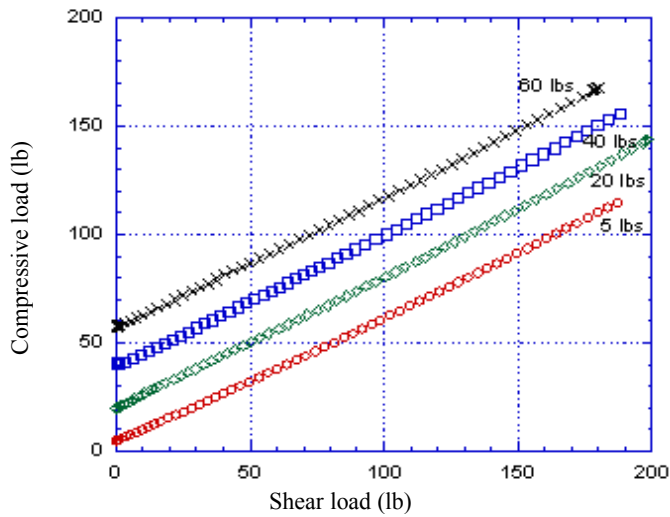


Figure B-7. The effect of lateral compressive preload on the stress conversion behavior of a 3-celled rapid prototype Z-MACterial.

The behavior of the rapid prototype Z-machines is quite consistent with analytical models and predictions. This data has enabled us to fabricate small-extruded Z-shaped machines (For more information on the extruded Z-machines refer to [Zaldivar 2]). The machines are approximately 1-mm in diameter and have an approximately 60-degree wall inclination angle. The primary difference between the small extruded Z-machines and the larger rapid prototype machines is that the rapid prototype machines are all connected to each other by a common base, unlike the completely separate and distinct extruded machines.

B-3.2 Finite-Element Analysis

Finite-element analysis (FEA) of the load-load behavior of the machine composites was conducted to simulate the experiments. The experimental sample shown in Figure B-2 was modeled. For this specimen, two layers of plastic machines were encapsulated by rubber matrix and sandwiched between a central steel platen and two outer steel platens. Also, as shown in Figure 2, a load cell contacted the outer steel platen.

The material properties of the rapid prototype material and the polyurethane resin were measured independently and used as inputs for the FEA. The polyurethane was modeled as non-linear elastic (hyperelastic), and the rapid prototype material was modeled as linear elastic. The steel platens were modeled as rigid plates because their compliance was expected to be much greater than the machine augmented composites.

As boundary conditions for the FEA model, the central steel platen was pulled in its long direction while the two outer platens were locked stationary (or, “cantilevered”) on their outer edges. In practice, the problem’s plane of symmetry was exploited so that only half the problem had to be modeled, which provided computational savings. Consequently, as shown in Figure B-8, the central steel platen was bonded to a single outer steel platen by one of the rapid prototype Z-MACterial samples, and a symmetry plane was enforced at the problem’s mid-plane. The load cell was modeled in the FEA as a simple one-dimensional spring in contact with the rigid platen, which is shown in Figure B-8. The spring’s compliance was set equal to the load cell’s stiffness. Quadratic elements with reduced-integration formulation were used in the FEA model.

Figure B-9 shows the comparison of the load-load behavior calculated using the FEA model with the load-load behavior measured experimentally. The FEA results were calculated for a 3-celled machine with 55, 60 and 60° angles in order to understand the influence of side wall angle on the stress conversion behavior of MACterial. The experimental sample was a 3-celled machine with a 60° side wall inclination angle.

As can be seen from the figure, the data for the experimental sample matches quite well with the FEA results, being bracketed by the FEA results for the 55° and 60° angle machines. Note that the stress conversion behavior increases as the side wall inclination angle increases. The slight discrepancy

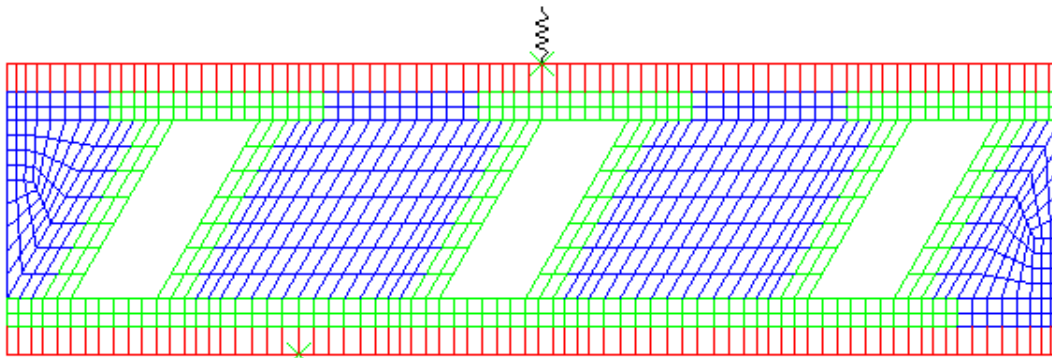


Figure B-8. Schematic of finite-element model of the rapid prototype Z-MACterial. (Rigid steel platens in red, rapid prototype machines in green, polyurethane matrix in blue, and spring-like representation of load cell’s compliance in black at top.)

between the experimental and FEA results may be attributed to the fact that the finite-element models idealize the side walls as perfectly formed and perfectly straight with a single-valued side wall angle. In contrast, the experimental samples naturally possess a manufacturing tolerance in the side wall angle and straightness. The finite-element model also idealizes the joint between side wall and top and bottom bases as perfectly sharp-edged, whereas the experimental sample actually possesses a small fillet at the joint. Any slight departures of the experimental sample from these ideals might be responsible for the observed slight discrepancy. Normal experimental variation may also be responsible for the discrepancy.

Thus, while there is some discrepancy between the experimental and FEA results, the stress conversion behavior of the rapid prototype Z-MACterials is quite consistent with the analytical model.

A parametric FEA study was also performed to measure the load-load response as functions of number of cells (that is, 3, 4 or 5 cells), material properties, cell aspect ratio, cell spacing, and load cell compliance. In all cases, the load-load response was identical as these parameters were varied. This finding reinforces the notion that the load-load response is determined solely by the geometry of the machine composites and not by the composite's material properties. Specifically, the side wall angle determines the response.

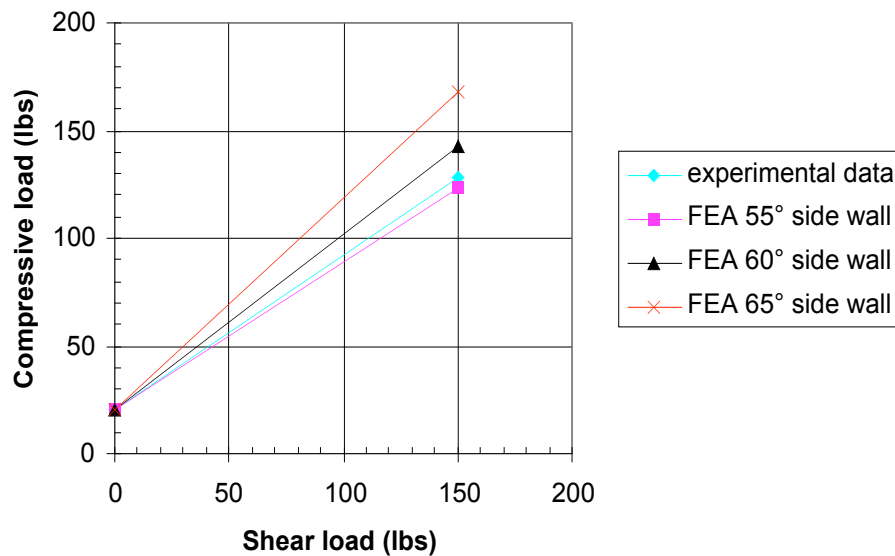


Figure B-9. Comparison of FEA results (side wall inclination angles of 55, 60 and 65) to experimental data (60 side wall angle) for 3-celled machine composites.

B-3.3 Small Extruded Nylon Z- Machine MACterial Testing

The same test set up was used to evaluate the stress conversion behavior of our small extruded nylon Z-machine augmented composites. Initially, tests were performed using the extruded nylon Z-machines without matrix material (unfilled). Figure B-10 shows the shear load to lateral compressive load graph for one of these samples. As shown, even with a 20-lb preload applied to prevent slipping, the stress conversion behavior was significantly lower than what would be expected for a machine with the suggested geometry, as verified using the rapid-prototype Z-machines. Upon unloading and reloading a second time, the slope, or stress conversion, became further depressed, as shown in Figure 10. Above 200 lb of axial shear load, the data became somewhat inconsistent, and other factors appeared to affect our testing.

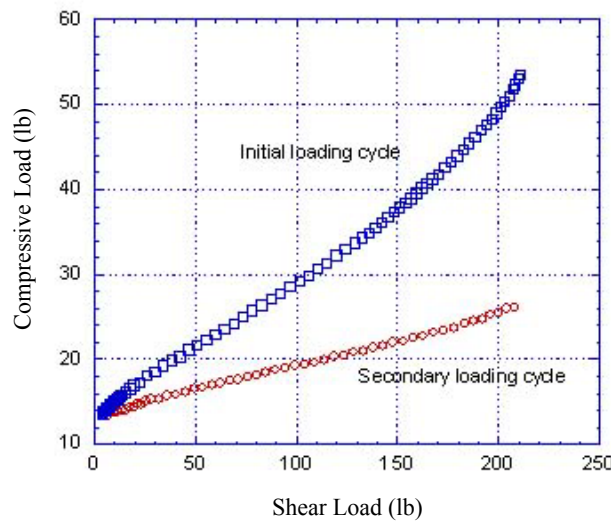


Figure B-10. Stress conversion behavior for unfilled extruded Z-machine sample during first and secondary loading-unloading cycle.

The decrease in stress conversion behavior with sequential loading and unloading is most likely a result of force relaxation and/or deformation of the machines. Since the Z-machines are fabricated out of a soft viscoelastic polymeric material, a constant load would be expected to cause creep and displacement to relieve applied forces. However, there may be a number of reasons the system has such a low initial stress conversion behavior from the start. The “actual” shape of the extruded machines may be considerably different than designed, and/or the motion of the machine may be different from what our model predicts. Increasing the loading rate, as shown in Figure B-11, also exhibited an apparent increase in the stress conversion behavior of these machines without matrix, as would be expected for a viscoelastic material. The sample tested at a lower loading rate was tested previous to the faster loading rate sample to overcome compression set effects that would cause a decrease in stress conversion.

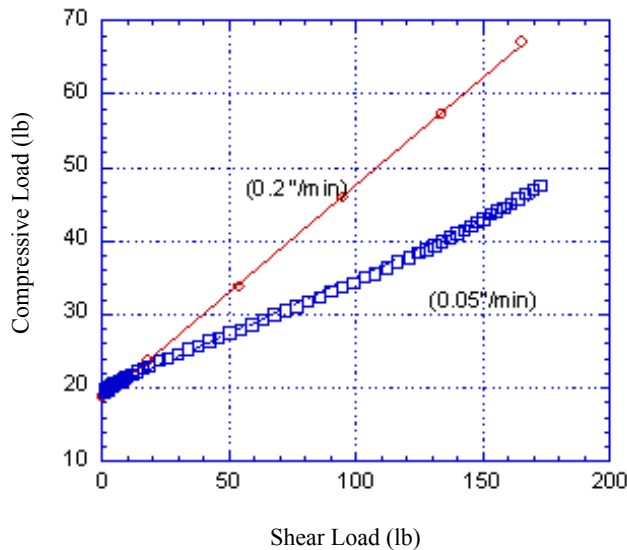


Figure B-11. Effect of loading rate on the stress conversion behavior of an unfilled small extruded Z-machine sample (0.05 in/min sample was performed first).

Figure B-12 shows sequential photographs of the small extruded nylon Z-machines as a function of applied load. As shown, the initial shape of the Z-machines is not as well defined as they were for the rapid prototype Z-machine system. In Figure 12, many of the extruded machines have side walls that are not inclined at the expected 60° inclination angle. In some cases, the walls appear bowed out or convex, like an inverted hourglass. In addition, unlike the rapid-prototype Z-machine samples that have one common base, these machines appear to be oriented in varied positions relative to the base. Figure B-13 shows how much of a variation can exist over a very small distance. Over a spacing of 6

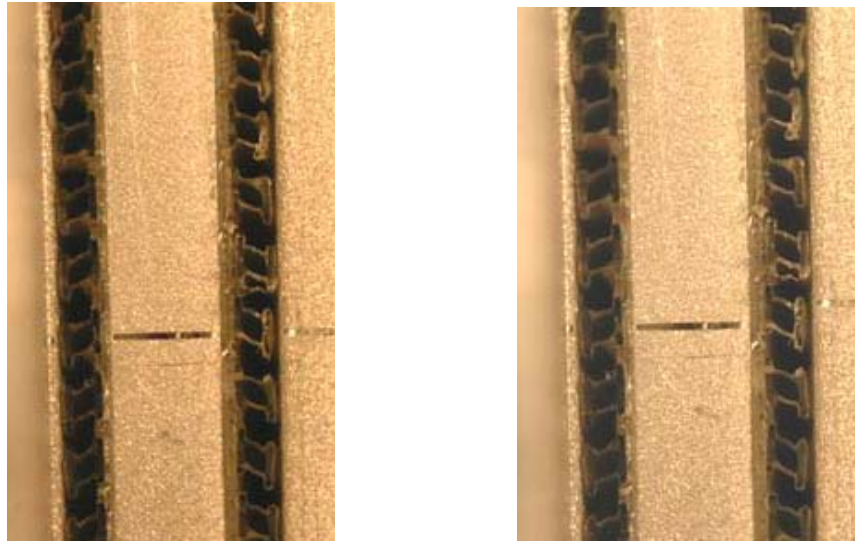


Figure B-12. Photographs showing sequential loading of small Z-machines.

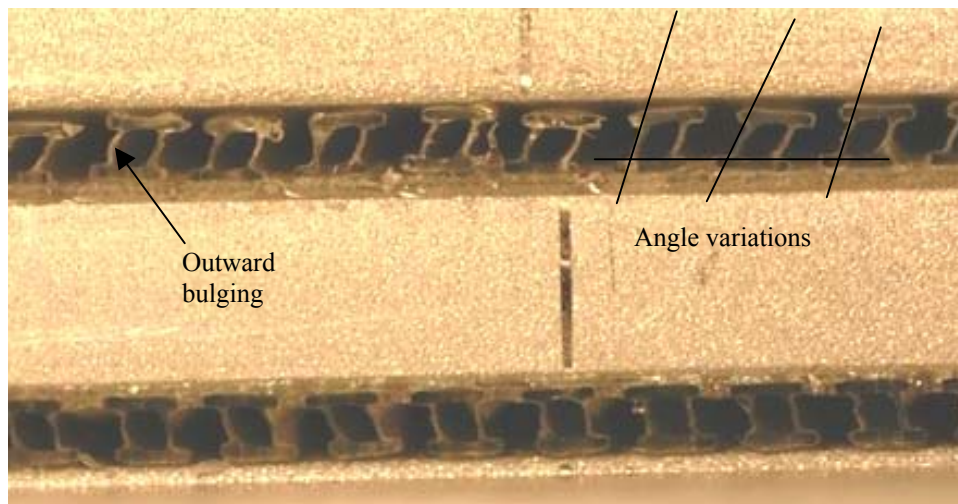


Figure B-13. High-magnification photograph showing variations in structure of small extruded Z-machines used in small composites.

to 7 machines, the inclination angle can vary by as much as 30°. In addition, many of the machines do not appear well bonded to the base, making it difficult to assess their behavior. The reduced stress conversion behavior with additional load and unload cycles may also be due to a debonding phenomena. All of these factors may contribute to the reduced stress conversion behavior.

The extruded nylon Z-MACterials with polyurethane matrix were then tested. Again, the behavior of these composites was not as well defined as that of the rapid-prototype Z-machine system, and the stress conversion behavior was significantly lower, as shown in Figure B-14. The stress conversion behavior was approximately half of what was obtained using the rapid-prototype system. The reasons for this behavior were expected to be the same as those for the unfilled system. As shown in Figure B-15, the shapes of the extruded Z-machines appeared to be highly compromised. The angles of the extruded machines, as well as the bonding to the base plate, varied greatly. As shown, the polyurethane matrix material compressed out from within the composite, which may account for some of the force relaxation during testing. Figure B-16 shows a plot of shear-to-compressive load curves for the filled extruded nylon Z-machines that were preloaded to different degrees. The samples were preloaded to 100, 75, 50, and 30 lb. As shown from the graph, each of the samples decreased from its initial preload once testing started. The highest four preloads were approximately 10 lb below their initial compressive load. The 30-lb preload exhibited no relaxation. As shown, the stress conversion behaviors for the samples preloaded above 50 lb were all similar. However, they were still much lower than expected for our intended design. The 30-lb preloaded sample showed absolutely no increase in stress conversion behavior until a shear load of over 100 lb was applied. This may have been due to slipping, which occurs during testing if the applied lateral compressive load is not great enough to overcome frictional forces.

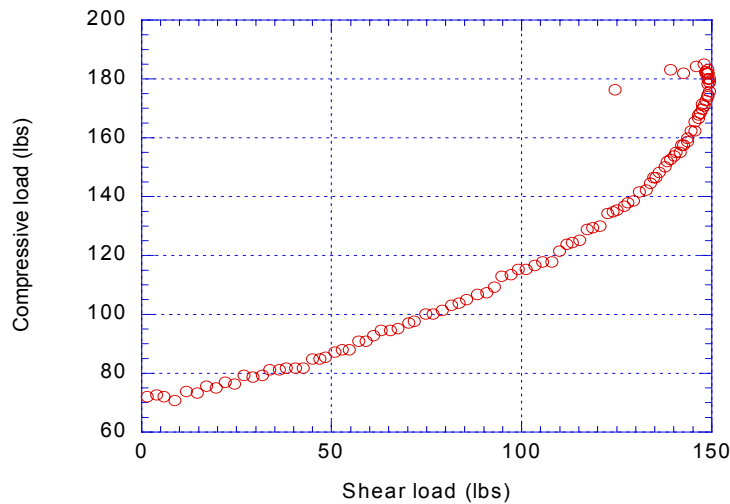


Figure B-14. Shear conversion behavior of polyurethane filled small extruded Z-machine composites tested in this study.

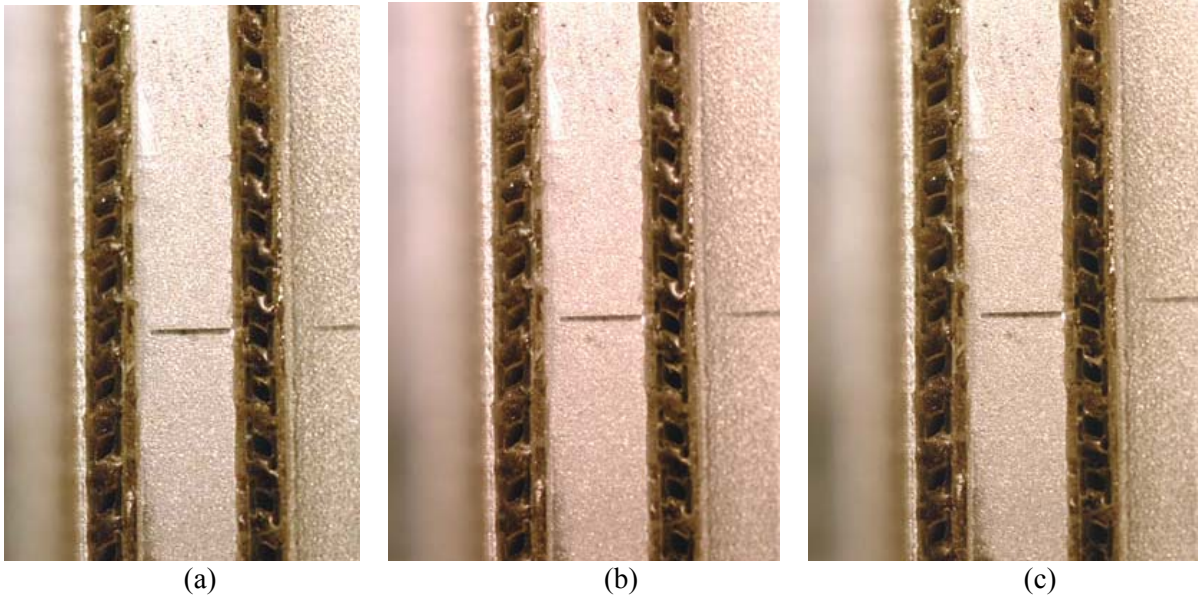


Figure B-15. Photographs showing sequential loading of filled small extruded Z-machine composites.

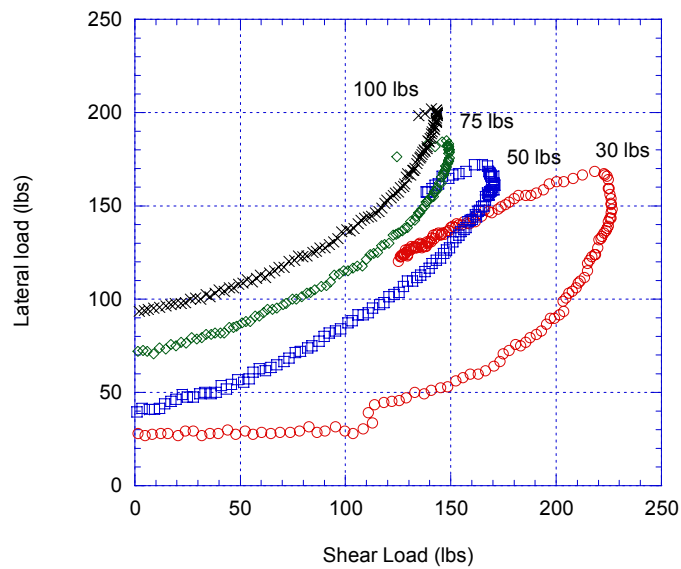


Figure B-16. A plot of shear-to-compressive load curves for the polyurethane filled small extruded nylon Z-machines that were preloaded to different degrees.

B-4. Conclusions

1. A simple testing apparatus was designed and manufactured to test the stress conversion behavior of a neat resin and machine-augmented composite materials (MACterials). The stress conversion behavior could be tailored depending on the inclination angle of the machines embedded within the MACterials. The smaller the inclination angle, the lower the stress conversion. Rapid prototype Z-MACterials were shown to have an excellent stress conversion behavior of nearly 1:1 for the 60° machines. In comparison, unreinforced neat resin materials exhibited no stress conversion capability.
2. The effect of machine cell volume was shown to have no effect on the resultant stress conversion behavior. 3-, 4-, and 5-celled, filled composites produced identical results when the inclination angle was kept constant. The effect of preload on initial compressive preload on the MACterials also had no effect on the resultant stress conversion behavior. However, if the preload approached zero, there appeared to be a lag before the compressive load increased with shear load. We believe this to be due to a necessary buildup in frictional force to prevent slipping.
3. Finite-element analysis (FEA) of the load-load behavior of the machine composites was conducted to simulate the experiments. The stress conversion behavior of the rapid prototype Z-MACterials closely matches the finite model. The discrepancy between the experimental and FEA results is attributed to small geometric differences between the experimental samples, which have small manufacturing “flaws”, and the finite element model, which is idealized and without flaws.
4. A parametric FEA study was also performed to measure the stress conversion response as a function of number of cells (that is, 3, 4 or 5 cells), material properties, cell aspect ratio, cell spacing, and load cell compliance. In all cases, the stress conversion response was identical as these parameters were varied. This finding reinforces the notion that the load-load response is determined solely by the side wall angle.
5. Unloading and loading of the small extruded machine-augmented composite materials produced a type of compression set, which reduced the stress conversion behavior. This effect was more pronounced for the unfilled MACterials. In contrast, the effect of higher loading rates versus lower rates also resulted in an increase in the stress conversion behavior. Both of these results are due to the viscoelastic behavior of the polymers used in the MACterials.
6. The stress conversion of our extruded nylon Z-MACterials was significantly lower than our rapid prototype Z-MACterials. This may be due to three factors: the small extruded nylon machines did not have as well defined a shape as our analysis required as verified by optical microscopy; debonding may have occurred; and/or the small extruded machines did not have a common base, as did the rapid prototype samples. Further studies are underway to better define our small extruded Z-machines.

7. We have manufactured and tested composites with embedded small machines that modify the internal forces within the material. In this manner, composites can be made that exhibit properties that cannot easily be obtained by other means.

B-5. REFERENCES

1. Lakes R. S., Lee T., Bersie A., and Wang Y. C., "Extreme damping in composite materials with negative-stiffness inclusions", *Nature*, vol. 410, pp. 565-567, 29 March 2001.
2. R. J. Zaldivar, J. Yamasaki, J. Schurr, and G. Hawkins, The Fabrication and Mechanical Behavior of Z-shaped Machine Composites, ATR-2002(881)-1, (3/2002).
3. G. F. Hawkins, M. O'Brien and R. J. Zaldivar, "Machine Augmented Composites", 43rd AIAA/ASME/ASCE/AHS/ASC Structures and Materials Conference, 22-25 April 2002, Denver, CO.

Appendix C—Theoretical and Finite Element Modeling of the Z-MACs

Prepared by

HUBERTUS F. VON BREMEN, MICHAEL J. O'BRIEN
CHING-YAO (TONY) TANG and GARY F. HAWKINS
Space Materials Laboratory
Laboratory Operations

Abstract

In this report we present a Finite-Element Analysis (FEA) model and an analytical model based on the theory of beam-on-elastic-foundation for the Z-shaped Machine-Augmented Composite (Z-MAC) that uses a special compliant mechanism as a constituent structure. The overall response of the Z-MAC was compared with results obtained from FEA, beam-on-elastic-foundation theory, and from experiments. A very close match was obtained between the analytical, the numerical, and the experimental response of the Z-MAC.

C-1. Introduction

There is a growing level of interest in microstructures, which is reflected by the large and increasing number of publications in this area over the last few decades. It is the importance and wide range of applications of microstructures that has fueled such interest. Noor et al. [1] discuss smart materials and structures, and multifunctional materials and structures in aerospace applications (among other topics) in which microstructures play a key role. Howell [2] focuses on compliant structural mechanisms from large-scale to the micro-scale. In his book, he presents a wide survey of recent activity in the field.

Composite materials have traditionally been manufactured out of fibers that reinforce a matrix material. The fibers add strength and stiffness to the structure. The matrix material serves to both hold the fibers in place and transfer the load among the fibers. The type of fiber used, as well as its orientation, ultimately controls the mechanical behavior of the composite structure. In the previous report (“The Fabrication and Mechanical Behavior of Z-shaped Machine-Augmented Composites” [3]), we discuss the fabrication and testing of a new type of composite material that possesses properties not otherwise easily attainable today (see also Hawkins G. F., “Augmenting the Mechanical Properties of Materials by Embedding Simple Machines” [4]). These Machine-Augmented Composites (MACs) contain simple machines that alter the stresses in the material. Tailoring the shape of the machines allows for a new method to control the properties of composite structures. The term machine is used to describe what the dictionary refers to as “an instrument designed to modify the application of power, force, or motion.” The machines used in the MAC are actually compliant mechanisms. The use of compliant mechanisms provides many advantages in the manufacturing of MACs. Mechanisms can be built using a single component (no assembly needed) that can be fabricated using extrusion, rapid prototyping, or other simple manufacturing methods. An additional advantage of using mechanisms is the fact that they can be easily scaled. In particular, for very small dimensions (in the scale of Micro-Electro-Mechanical Systems), no complicated components like hinges or bearings are used, simplifying the manufacturing process and avoiding complicated assembly. A wide scope of machine shapes can be designed, depending on the requirements of the application. Our MAC is a clear example where microstructures are used to manufacture a composite-like material that possesses special properties.

Researchers have shown that composite materials with unusual properties can be manufactured by introducing internal microstructures. For example, Sigmund and Torquato [5] designed three phase composites that have extremal values of the thermal expansion, both positive and negative. Sigmund [6] has also provided a class of two-phase composite materials with extremal bulk modulus. Lakes et al. [7] discuss composite materials with negative stiffness inclusions. Xu et al. [8] show how to manufacture a negative Poisson’s ratio microstructure using a soft lithography technique. Cederbaum et al. [9] present analytical tools to study poroelastic structures (porous structures consisting of an elastic matrix containing interconnected fluid-saturated pores). They also present an extensive list of references in the field.

Scale effects are important in the study of microstructures: Pecullan et al. [10] present results on the scale effects on the elastic behavior of two-dimensional composites, and Bendsoe and Triantafyllidis [11] studied the scale effects in the design of a microstructured medium against buckling. Neves et

al. [12] present a topology optimization-based method to design periodic microstructures with penalization of localized buckling modes.

In this report, we present a Finite-Element Analysis (FEA) model and an analytical model based on the theory of beam-on-elastic-foundation for a Machine-Augmented Composite (MAC) using what we call Z-machines as constituent structures. The manufacturing process and some experimental results of the Z-shaped-Machine-Augmented Composites (Z-MACs) were presented earlier in the report, “The Fabrication and Mechanical Behavior of Z-shaped Machine-Augmented Composites” [3]. The FEA model and some of the FEA results for Z-machines are presented in Section C-2. Section C-3 deals with a model based on the theory-of-beam-on-elastic-foundation. First, the general model is presented along with the special case of no foundation and a description of the vertical and horizontal displacement of the MAC. Next, a comparison of an analytical solution for the deformation pattern of the MACs with experimental and FEA results is presented. The section ends with a parametric study on the effect of modulus of the foundation and the flexural rigidity of the sidewalls on the deformation pattern of the sidewalls of the Z-MAC. Conclusions are presented in Section C-4 and references in Section C-5.

C-2. Finite-Element Model

C-2.1 FEA Background

Finite-Element Analysis solves the field equations of mechanical engineering in order to find the overall response of a structure. The physical structure, which is generally continuous, is represented mathematically as an assembly of discrete bodies (or “finite elements”) for each of which equilibrium is individually required. Equilibrium can be solved, for example, in response to a given set of forces or displacements applied to the outer surface of the structure (called “boundary conditions”). An important input to the FEA model is an accurate knowledge of the material’s constitutive response as a fundamental material property measured independently in the lab.

The attraction of FEA is that it is possible to predict through “virtual experiments” the response of a structure before it is fabricated physically. Of course, any analysis, whether numerical or closed-form, requires a model with simplifications and approximations in order to make the problem tractable. The calculation of the virtual response is only worthwhile if the model’s starting assumptions are validated at an early stage by comparison to an experimental result for a physical structure. Ideally, experiments and FEA calculations are actually complementary, not competitive, and proceed hand-in-hand to provide a problem’s solution as quickly as possible.

Once established, however, the validation provides confidence in calculations for structures too complicated or too expensive to be tested experimentally. The validated model can also be used to quickly iterate over a design space to find a structure with optimal properties, a process which is otherwise much more costly and time consuming if physical structures have to be built and tested at each iteration.

C-2.2 Description of the Finite-Element Model

The mesh was created using the mesh generating program TrueGrid. This program allows for the parameterization of the mesh in terms of geometry-dependent parameters such as machine inclination angle, distance between machines, and dimensions of the machines. The parameterized mesh was then used to easily and quickly generate meshes for any desired set of parameters.

The Finite-Element Analysis was performed using ABAQUS. Quadratic, reduced integration elements were used in the analysis, with a hybrid formulation used to model the polyurethane matrix material. These elements were chosen in order to prevent hourglassing and shear locking. For the constitutive formulation, the polymer machines were modeled as an elastic-plastic material, and the polyurethane matrix material was modeled as a non-linear elastic (hyperelastic) material. The material constants used in the formulation were obtained from experimental tests. A two-dimensional plane strain model was used in the calculations. A plane stress formulation was also considered, yielding results very close to the results from the plane strain formulation.

A full and a reduced model of the machines were used. Both models generated identical results. Exploiting the fact that there is a symmetry plane, the reduced model considered only the upper half of the MACs. Most of the simulations were thus performed on the more efficient reduced model. The experimental loading conditions were modeled using vertical displacement boundary conditions on the top nodes of the MACs model. The undeformed mesh of the model used is shown in Figure 1.

C-2.3 FEA results

Different MAC configurations were considered. Here we present some of the results for the 15-mm 4-celled MACs that were manufactured using rapid prototype with matrix material and a 60° inclination angle. The undeformed state of the experimental specimen and the corresponding full finite-element model are given in Figure C-2. The deformed state of the experimental specimen and the corresponding deformed FEA model are shown in Figure C-3. The finite-element model clearly captures the deformation response of the actual physical phenomenon. By contrasting the experimental pictures from Figures C-2 and C-3, one can observe that, as desired, vertical compression gives rise to transverse shearing.

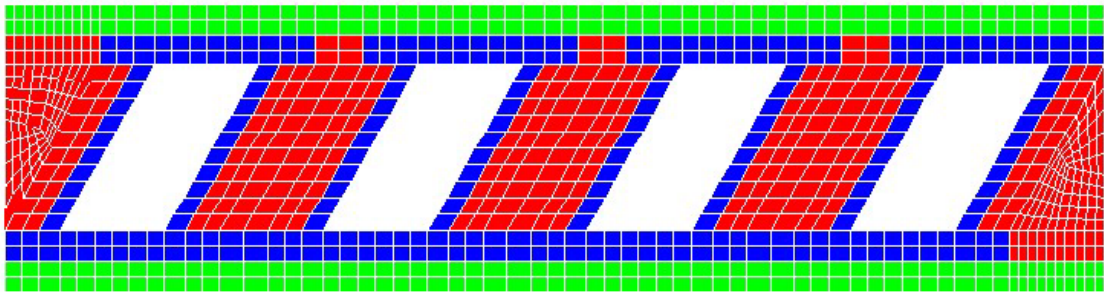


Figure C-1. Undeformed mesh of the physical model developed using TrueGrid.

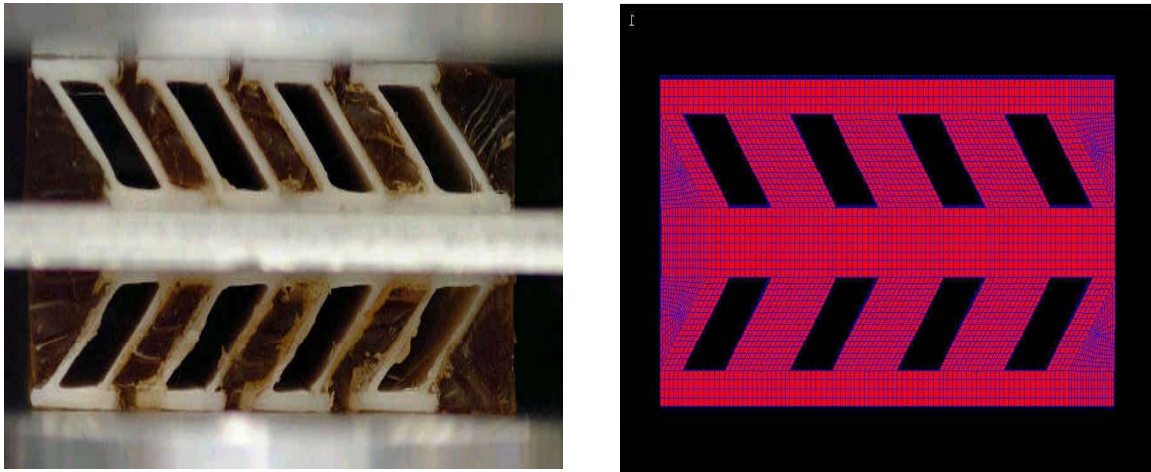


Figure C-2. Undeformed state of the experimental specimen and the corresponding undeformed finite-element model mesh.

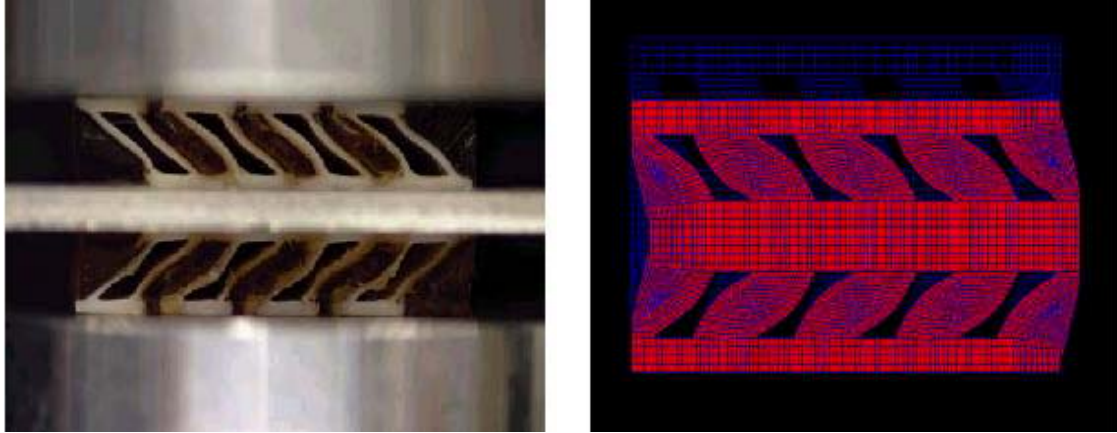


Figure C-3. Deformed state of the experimental specimen and the deformed finite-element model mesh at 10% vertical strain.

Figure C-4 shows the experimental and FEA compressive versus shear displacements for the same MAC configuration (15-mm 4-celled rapid-prototype MACs with matrix material and a 60° inclination angle). There is close agreement between FEA results and the experimental values, particularly for smaller displacements. The figure also shows the compressive versus shear displacements from FEA results for 50° and 70° machine inclination angles.

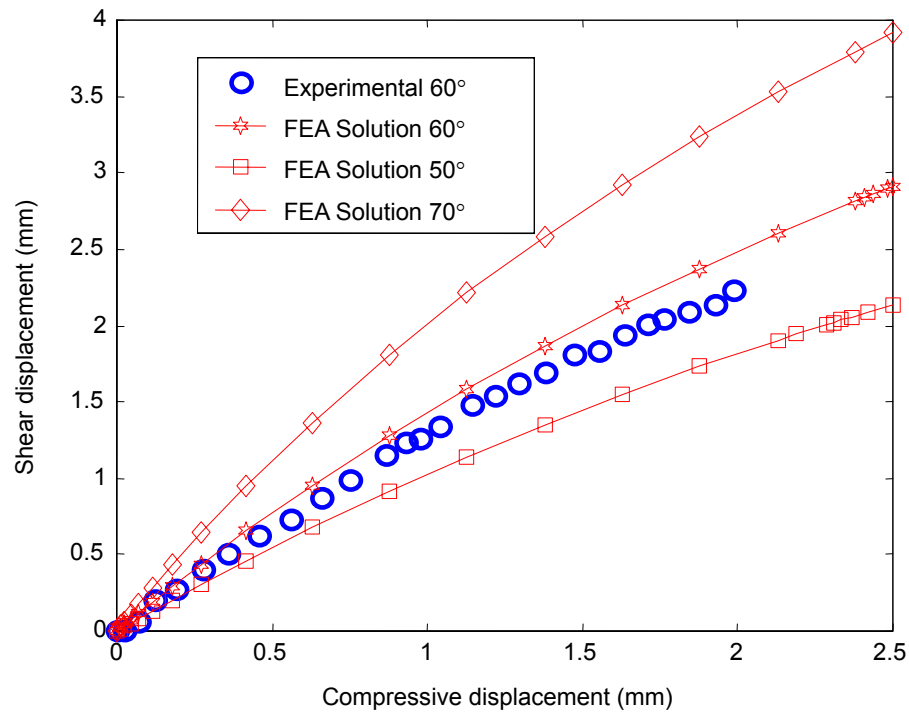


Figure C-4. Experimental and FEA compressive versus shear displacements for 15-mm 4-celled rapid-prototype MACs with matrix material for various machine inclination angles. The experimental results are for 15-mm 4-celled rapid-prototype MACs with matrix material and a 60° inclination angle, and the FEA solutions are for similar machines with 50°, 60° and 70° inclination angles.

C-3. Beam-on-Elastic-Foundation Model

C-3.1 Theory of Beam-on-Elastic-Foundation

The theory of beam-on-elastic-foundation (see Hetényi [13], or Boreši [14]) can be used to obtain an analytical solution for the deformation of the MACs under compressive loading. As can be seen in Figure C-5, the sidewalls of each machine act like a beam on an elastic foundation, which is provided by the matrix material. The closed-form solution allows us to understand the influence that the different parameters have on the deformation pattern. The closed-form solution will also permit us to easily optimize the MAC design.

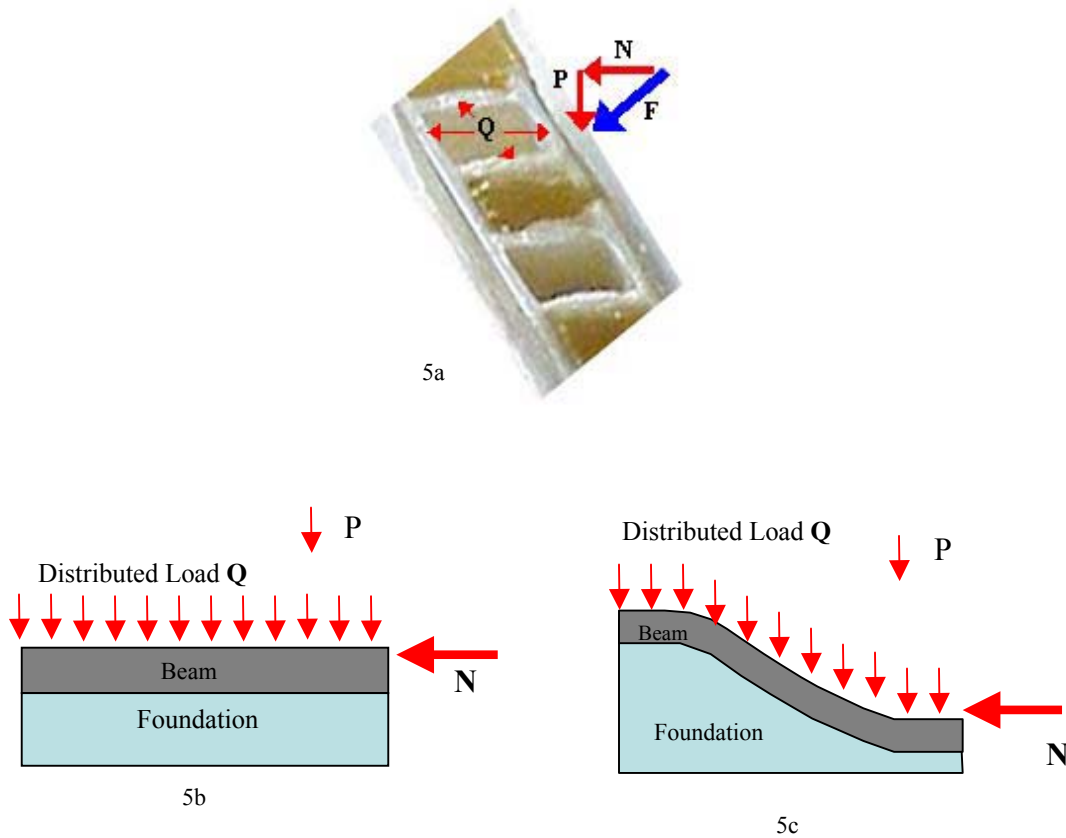


Figure C-5. Physical problem modeled as a beam-on-elastic foundation. The sidewall (beam) is supported by the compliant matrix material (foundation). The applied force (\mathbf{F}) on the material consists of 2 components perpendicular (\mathbf{P}) and parallel (\mathbf{N}) to the sidewall. Any internal pressure inside the machines is represented by a distributed load (\mathbf{Q}). Figure 5b is a model of the undeformed beam on foundation. Figure 5c is a model of the deformed beam on foundation.

C-3.2 Solution for the Beam Displacement Under Bending and Axial Loading

The sidewalls of the machines can be considered to be a beam, and the matrix material an elastic foundation. When the MACs are under compressive loading, the sidewalls experience axial and bending loads. By applying the theory of beam-on- elastic-foundation to the problem, one obtains a boundary value problem. The differential equation of the displacement of the sidewall under axial compression and a transverse load is given by

$$EI \frac{d^4 y}{dx^4} + N \frac{d^2 y}{dx^2} + ky(x) = 0, \quad (1a)$$

and the differential equation of the displacement of the sidewall under axial tension and a transverse load is given by

$$EI \frac{d^4 y}{dx^4} - N \frac{d^2 y}{dx^2} + ky(x) = 0, \quad (1b)$$

where $y(x)$ is the displacement of the beam (sidewall), x is the position along the beam, E is the beam's Young's modulus, I is the beam's moment of inertia, k is the foundation spring constant, and N is the axial load.

The boundary conditions used in the formulation are

$$y(0) = 0, \quad y'(0) = 0, \quad y'(L) = 0 \text{ and } y'''(L) = \frac{P}{EI}, \quad (2)$$

where L is the span of the beam, and P is the applied (transverse) bending load.

The solution of the boundary value problem for the case of axial compression given by Eqs. (1a) and (2) is

$$\begin{aligned} y(x) &= -P(A + B - C + D - E) / F, \text{ with} \\ A &= \alpha^2 \sinh(\beta L) \cos(\alpha L) \sinh(\beta x) \cos(\alpha x), \\ B &= \alpha \beta \cosh(\beta L) \sin(\alpha L) \sinh(\beta x) \cos(\alpha x), \\ C &= \alpha \beta \sinh(\beta L) \cos(\alpha L) \cosh(\beta x) \sin(\alpha x), \\ D &= (\alpha^2 + \beta^2) \sinh(\beta L) \sin(\alpha L) \sinh(\beta x) \sin(\alpha x), \\ E &= \beta^2 \cosh(\beta L) \sin(\alpha L) \cosh(\beta x) \sin(\alpha x), \\ F &= EI\alpha\beta((\beta^3 + \alpha^2\beta)\sin(2\alpha L) + (\alpha^3 + \alpha\beta^2)\sinh(2\beta L)), \end{aligned} \quad (3a).$$

The solution of the boundary value problem for the case of axial tension given by Eqs. (1b) and (2) is

$$\begin{aligned}
y(x) &= -P(A + B - C + D - E) / F, \text{ with} \\
A &= \beta^2 \sinh(\alpha L) \cos(\beta L) \sinh(\alpha x) \cos(\beta x), \\
B &= \alpha \beta \cosh(\alpha L) \sin(\beta L) \sinh(\alpha x) \cos(\beta x), \\
C &= \alpha \beta \sinh(\alpha L) \cos(\beta L) \cosh(\alpha x) \sin(\beta x), \\
D &= (\alpha^2 + \beta^2) \sinh(\alpha L) \sin(\beta L) \sinh(\alpha x) \sin(\beta x), \\
E &= \alpha^2 \cosh(\alpha L) \sin(\beta L) \cosh(\alpha x) \sin(\beta x), \\
F &= EI\alpha\beta((\alpha^3 + \beta^2\alpha)\sin(2\beta L) + (\beta^3 + \beta\alpha^2))\sinh(2\alpha L), \tag{3b}
\end{aligned}$$

$$\text{where } \alpha = \sqrt{\sqrt{\frac{k}{4EI}} + \frac{N}{4EI}} \text{ and } \beta = \sqrt{\sqrt{\frac{k}{4EI}} - \frac{N}{4EI}} \text{ in both Eqs. (3a) and (3b).}$$

The solution Eq. (3b) can be obtained from Eq. (3a) by simply exchanging α and β in Eq. (3a).

In the Subsection 3.4, we present a comparison of experimental results and the analytical solutions given by Eqs. (3a) and (3b). However, we will first consider the special case of formulation with an absent foundation.

As a special case, in the absence of a foundation ($k = 0$) we simply have a cantilever beam where the displacement $y(x)$ of the beam is given by the differential equation

$$EI \frac{d^4 y}{dx^4} + N \frac{d^2 y}{dx^2} = 0, \tag{4a}$$

in the case of axial compression, and

$$EI \frac{d^4 y}{dx^4} - N \frac{d^2 y}{dx^2} = 0, \tag{4b}$$

in the case of axial tension. The boundary conditions are the same as given in Eq. (2).

The solution of the boundary value problem for the axial compression case is given by

$$y(x) = \frac{P(-1 + \cos(\mu L) + \mu x \sin(\mu L) - \sin(\mu x) \sin(\mu L) + \cos(\mu x) - \cos(\mu x) \cos(\mu L))}{N\mu \sin(\mu L)}, \tag{5a}$$

and the solution for the axial tension case is given by

$$y(x) = \frac{-P(-1 + e^{-\mu L} + \mu x + \mu x e^{-\mu L} + e^{-\mu x} - e^{\mu(-L+x)})}{N\mu(1 + e^{-\mu L})}. \quad (5b)$$

In both Eqs. (5a) and (5b),

$$\mu = \sqrt{\frac{N}{EI}}.$$

C-3.3 Global Vertical and Horizontal Displacement of the MACs

The maximum y -displacement in Eqs. 5a and 5b occurs at $x = L$. For the case of axial compression, the largest displacement of the beam is given by

$$y_{\max} = -\frac{2P}{\mu N} \left(\tan\left(\frac{\mu L}{2}\right) - \frac{\mu L}{2} \right). \quad (6)$$

For the case of axial tension, the largest displacement of the beam is given by

$$y_{\max} = -\frac{2P}{\mu N} \left(\frac{\mu L}{2} - \tanh\left(\frac{\mu L}{2}\right) \right). \quad (7)$$

The above formulas of the maximum displacement of the beam can also be obtained from Roark's *Formulas for Stress & Strain* (Young, W.C.) [15] by using the formulas for beams under simultaneous axial compression and bending for a case of a beam that is fixed at the left and the right.

A simple relation between the horizontal and vertical displacement of the free end of the sidewall can be established by considering the sidewall as a rigid link pinned at one end. Figure C-6 shows a schematic of the pinned link depicting the vertical and horizontal displacements at a given inclination angle θ of the link (sidewall). The equation of the vertical position y of the link ("free end" of the sidewall) is given by

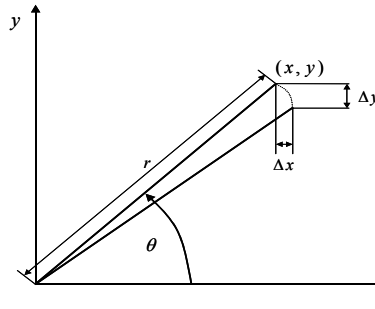


Figure C-6. Schematic of the pinned beam (link) depicting the vertical and horizontal displacements at a given inclination angle θ .

$$y = f(x) = \sqrt{r^2 - x^2}, \quad (8)$$

where x is the horizontal position of the “free end” of the sidewall, and r is the total length of the link.

From calculus we have that

$$\frac{\Delta y}{\Delta x} \approx f'(x) = -\frac{x}{\sqrt{r^2 - x^2}} = -\frac{x}{y} \quad (9)$$

for small values of the horizontal displacement Δx . Here Δy is the vertical displacement of the free end of the sidewall. From the geometric relations $x = r \cos(\theta)$ and $y = r \sin(\theta)$, it is clear that Eq. (9) becomes

$$\frac{\Delta y}{\Delta x} \approx -\frac{1}{\tan(\theta)}. \quad (10)$$

It should be noted that the ratio of the displacements in Eq. (10) depends solely on the inclination angle of the link and not on any material property of the link.

Figure C-7 shows the displacement of the “free end” of the sidewall, which corresponds to the overall compressive and shear displacement of the MAC structure. The thick line corresponds to the beam-on-elastic-foundation results. This curve includes several overlapping curves corresponding to different values of the modulus of the foundation for machines with an inclination angle of $\theta = 60^\circ$. In other words, the shape of the displacement trajectory of the “free end” of the sidewall of the MAC is independent of the foundation modulus (for the ranges of displacements and parameter values here considered). The thin lines with circles are the results from Eq. (10) (with a sign change). There is a very close match between the approximations using Eq. (10) and the beam-on-elastic-foundation results for the machine inclination angle of $\theta = 60^\circ$. See also Figure 4 for a similar plot showing experimental and FEA results.

C-3.4 Comparison of the Analytical Solution and Experimental Results

Using Eq. (3a), one can obtain the deformation pattern of the sidewalls of the MACs when undergoing compressive loads. Figure C-8 shows the experimental, FEA, and theoretical [based on Eq. (3a)] deformed state of the sidewall of a 15-mm 4-celled rapid-prototype MAC with matrix material and a 60° inclination angle. The theoretical deformation pattern obtained from the theory of beam-on-elastic-foundation captures very closely the actual deformation pattern obtained from the experiments and is in very close agreement with the FEA results.

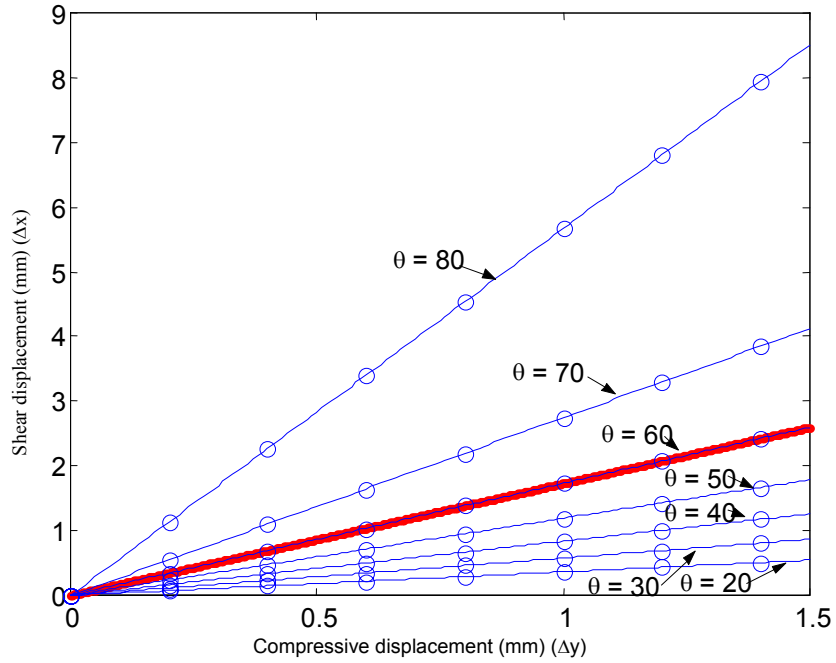


Figure C-7. Displacement of the “free end” of the sidewall, which corresponds to the compressive and shear displacement of the MAC structure. Thick line corresponds to beam-on-elastic-foundation results for an inclination angle of $\theta = 60^\circ$. The thin lines with circles are the results using Eq. (10) for various inclination angles, θ .

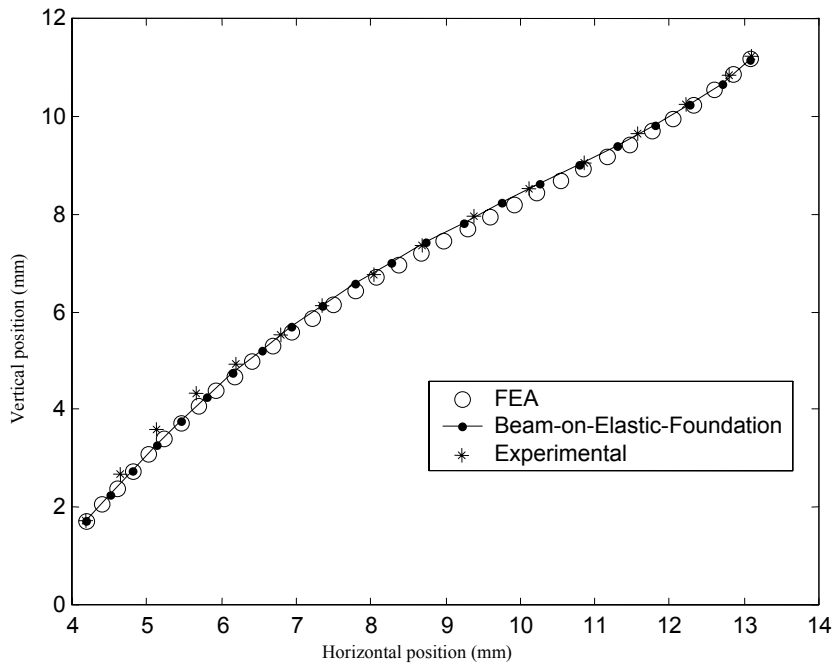


Figure C-8. Experimental (15-mm 4-celled rapid-prototype MACs with matrix material at a 60° inclination angle), FEA, and beam-on-elastic-foundation solution of the deformed state of the sidewall.

Note: the following nominal values are used throughout Subsections 3.4, 3.5 and 3.6:

flexural rigidity,	$EI = 9.24 \cdot 10^{-2}$	$\text{N} \cdot \text{m}^2$
foundation stiffness,	$k = 3.191 \cdot 10^8$	N/m^2
length (span) of the beam,	$L = 0.013$	m
(all units are in SI units)		

In Figure 8, a foundation stiffness of $5k$ was used (and all other values were taken as nominal).

C-3.5 Effect of the Modulus of the Foundation on the Deformation Pattern of the Beam

The effect of the modulus of the foundation on the deformation patterns of the beam is captured in Figure C-9. The deformation patterns corresponding to different values of the modulus of the foundation (k) with the nominal flexural rigidity value using Eq. (3a) are shown in the figure, together with an experimental deformation (see also Figure C-8) and the limiting case of $k = 0$ marked with '+' (using Eq. 5a). The sidewall inclination angle in this case is $\theta = 60^\circ$.

As the modulus of the foundation decreases and gets closer to $k = 0$, the deformation pattern of the sidewall approaches the deformation pattern of a beam in the absence of a foundation.

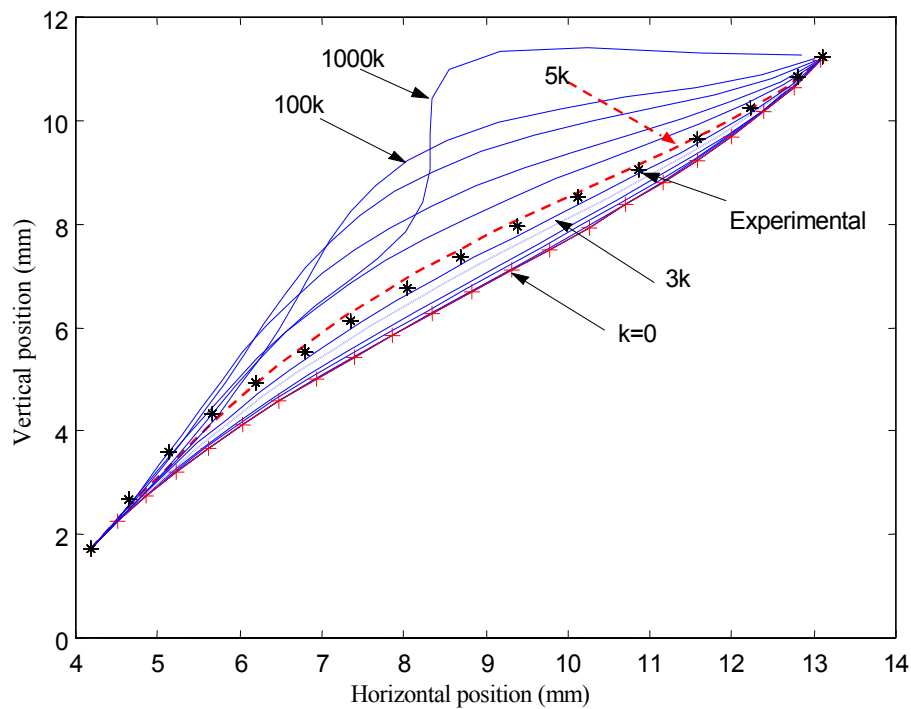


Figure C-9. Effect of foundation modulus (k) on the deformation pattern on the sidewalls of the MAC.

In all the cases presented, the displacement of the “free end” of the sidewall was kept to be constant; that is, in all cases the deformation patterns of the sidewall are taken at the same (constant) vertical displacement of the MAC. The required applied force needed to obtain the constant vertical displacement of the “free end” of the sidewall for different values of the modulus of the foundation is presented in Figure C-10.

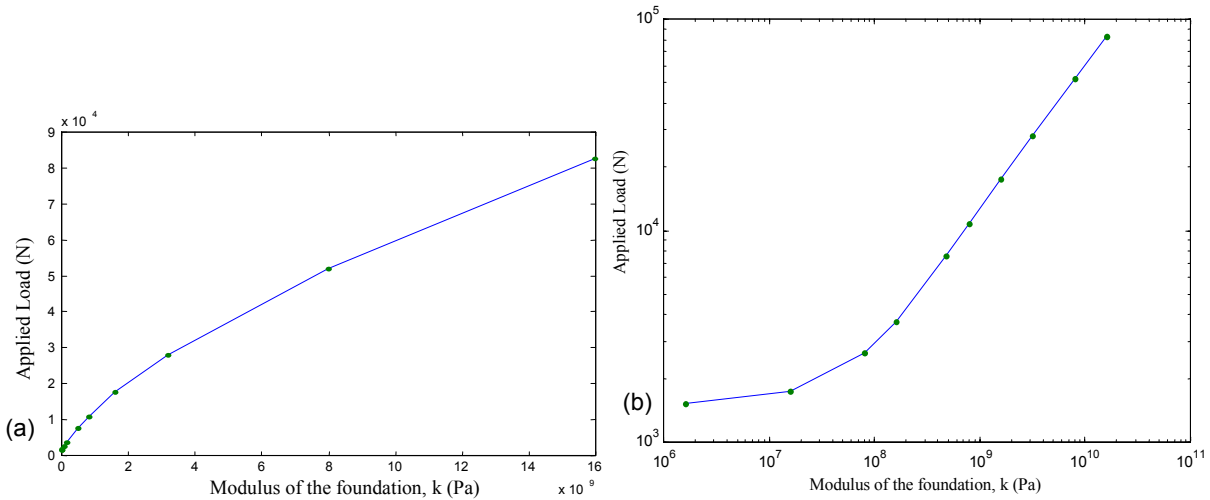


Figure C-10. Required applied load needed to obtain the constant vertical displacement of the “free end” of the sidewall for different values of the modulus of the foundation. (a) linear scale; (b) logarithmic scale.

Figure C-11 shows the applied load as a function of vertical (compressive) displacement of the “free end” of the sidewall for different values of the modulus of the foundation. As expected, as the modulus of the foundation increases, a larger load is needed in order to obtain a given vertical displacement of the MAC.

C-3.6 Effect of the Flexural Rigidity (EI) of the Beam on its Deformation Pattern

The effect of flexural rigidity (EI) of the beam (sidewall) on the deformation pattern of the beam is shown in Figure C-12. The deformation patterns corresponding to different values of the flexural rigidity using Eq. (3a) are shown in the figure, together with an experimental deformation. Here the nominal value of the stiffness of the foundation (k) is used and the flexural rigidity is varied.

As the flexural rigidity increases, the deformation pattern of the sidewall approaches the deformation pattern of the beam in the absence of a foundation. A large flexural rigidity of the beam makes the contributions of the foundation to the deformation pattern insignificant.

As before, in all the cases presented, the displacement of the “free end” of the sidewall was kept to be constant. The required applied force needed to obtain the constant vertical displacement of the “free end” of the sidewall for different values of the flexural rigidity is presented in Figure C-13.

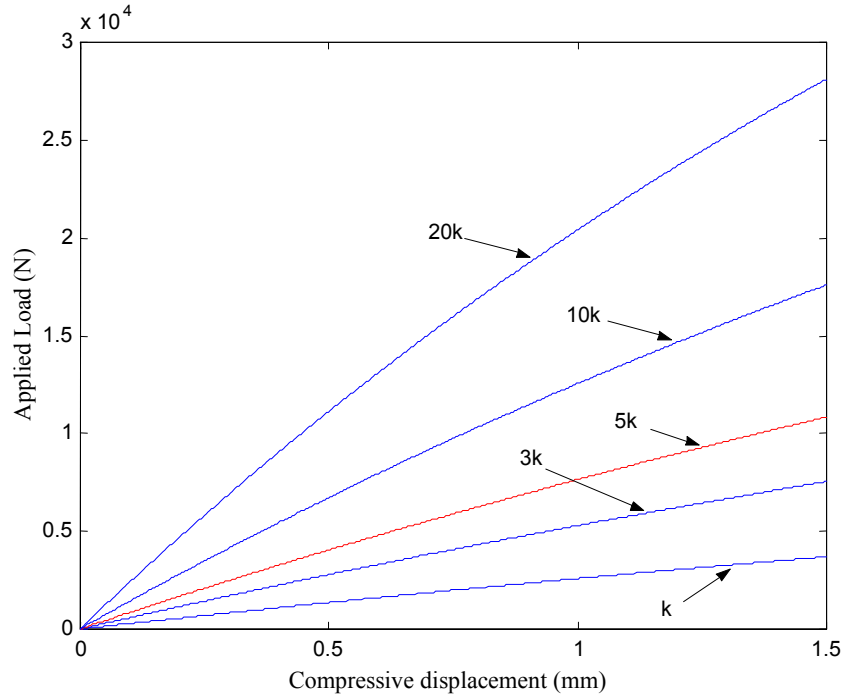


Figure C-11. Applied load as a function of compressive displacement of the MAC for different values of the modulus of the foundation.

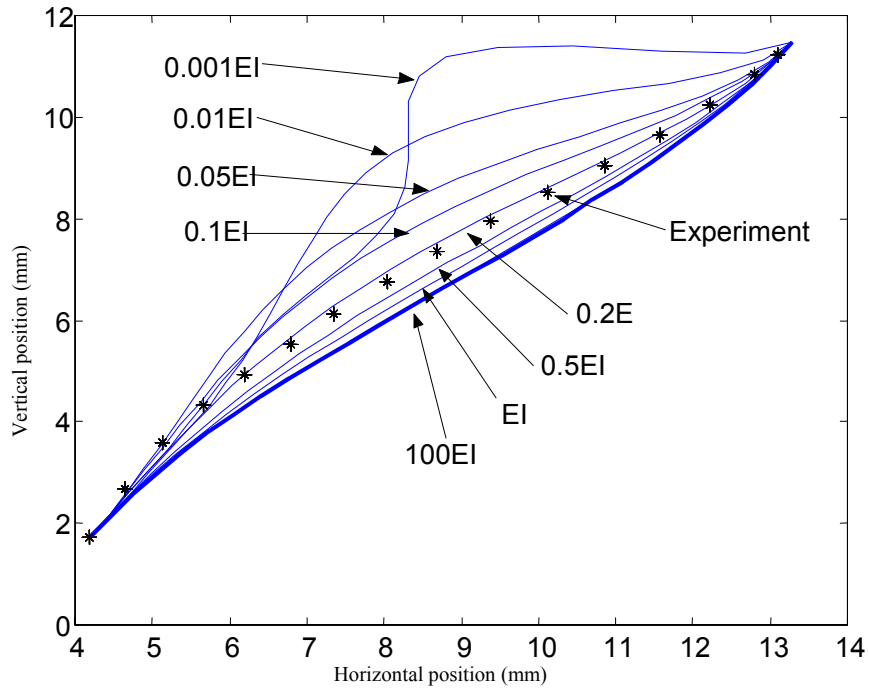


Figure C-12. Effect of the beam flexural rigidity (EI) on the deformation pattern of the sidewall of the MAC.

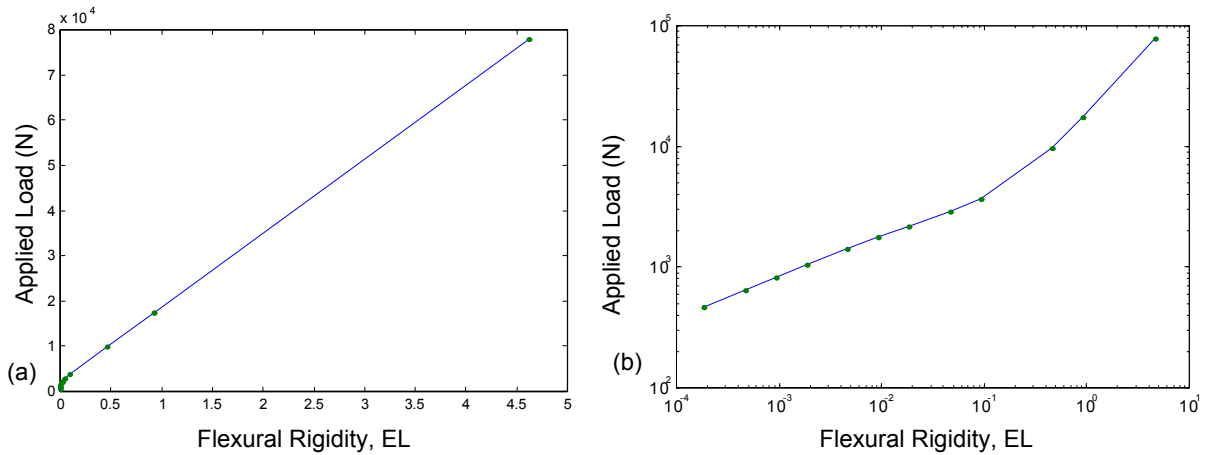


Figure C-13. Required applied load needed to obtain the constant vertical displacement of the “free end” of the sidewall for different values of the flexural rigidity. (a) linear scale; (b) logarithmic scale.

Figure C-14 is very similar to Figure C-7 and it shows the compressive versus the shear displacement of the “free end” of the sidewall as the system is loaded. As the load increases, the compressive displacement increases, and due to the “machine” action, the shear displacement increases. The results reflected on the figure were generated using the beam-on-elastic-foundation formulation (Eq. 3a). The same curve is generated when using different values of the flexural rigidity (while keeping the stiffness of the foundation fixed), and the curves overlap exactly. In this way, Figure C-14 shows that

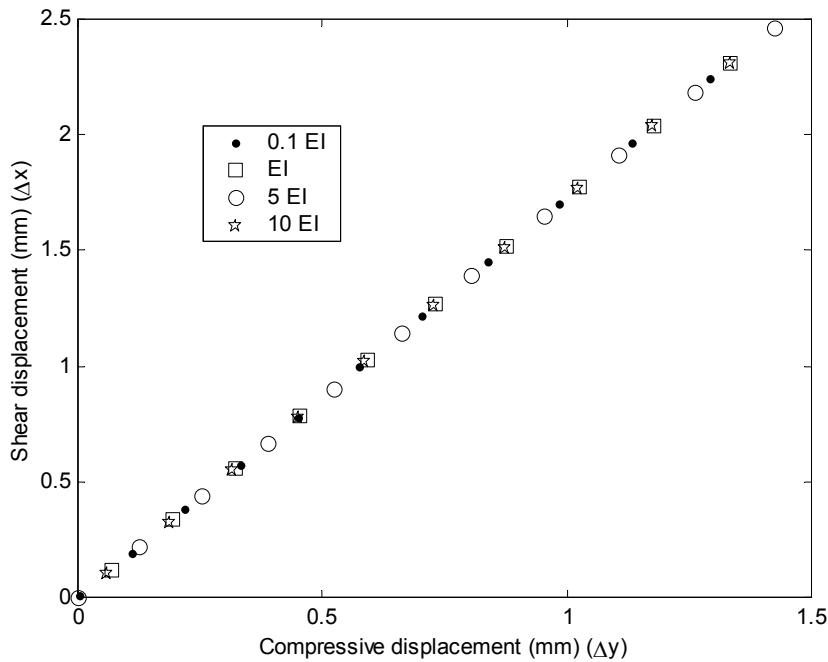


Figure C-14. Displacement of the “free end” of the sidewall, which corresponds to the compressive and shear displacement of the MAC structure.

the overall displacement of the MAC, i.e., the ratio of vertical versus horizontal displacement, is independent of the modulus of the foundation and the flexural rigidity of the beam (as suggested in Eq. (7)).

Figure C-15 shows the applied load as a function of vertical (compressive) displacement of the “free end” of the sidewall for different values of the beam flexural rigidity. As expected, as the flexural rigidity of beam increases, a larger load is needed in order to obtain a given displacement of the MAC.

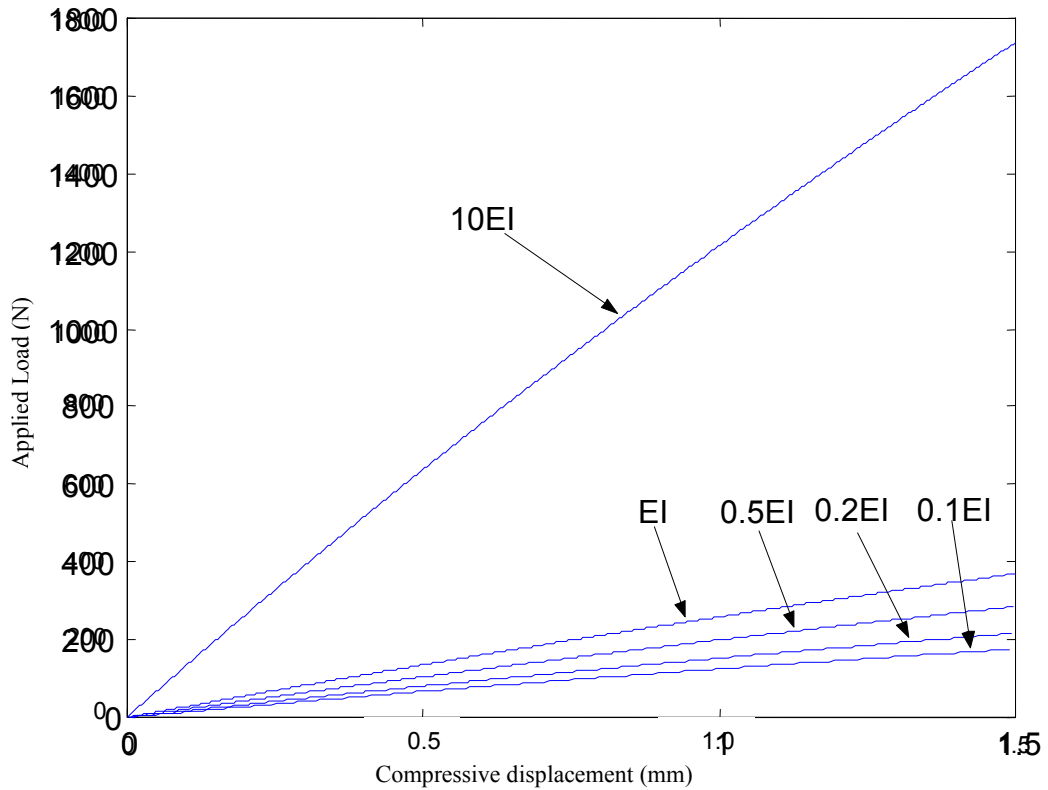


Figure C-15. Applied load as a function of compressive displacement of the MAC structure for different values of the sidewall flexural rigidity.

This page intentionally blank.

C-4. Conclusions

The overall response of Machine-Augmented Composites using a Z-machine structure was studied using FEA techniques and the theory of beam-on-elastic-foundation. Results from the FEA, the beam-on-elastic-foundation, and from experiments were compared. A very close match between the analytical, numerical, and experimental results was obtained. This gives us confidence in the FEA model used and in the analytical solution obtained from the theory of beam-on-elastic-foundation.

Based on the results reported in this report, the following conclusions can be drawn:

- There is a very close match between the FEA results and the experimental results (see Sections C-2 and C-3). The close match is observed in the global behavior of the MAC (shear versus compressive displacement of the whole MAC), as well as in the local behavior of the MAC (deformation pattern of the sidewalls of each individual machine embedded in the MAC).
- The deformation pattern of the sidewalls of the machines obtained from the theory of beam-on-elastic-foundation captures very closely the actual deformation pattern obtained from the experiments and FEA.
- A parametric study was performed by varying the modulus of the foundation (stiffness of the matrix material in the MAC) using the analytical results based on the beam-on-elastic-foundation theory. In all cases, the MAC was deformed so that the same vertical displacement of the “free end” of the sidewall was obtained. For large values of the foundation modulus, the deformation of the sidewall near the “free end” was large. As the modulus of the foundation was decreased, the overall deformation of the sidewall decreased, and in the limit case of a foundation with zero modulus, the sidewall acted as a simple cantilevered beam. It was also observed, as expected, that the larger the modulus of the foundation, the larger the applied load needs to be in order to obtain the same constant vertical displacement of the “free-end” of the sidewall.
- A similar parametric study was performed by varying the flexural rigidity of the sidewall (EI) using the analytical results based on the beam-on-elastic-foundation theory. In all cases, the MAC was deformed so that the same constant vertical displacement of the “free end” of the sidewall was obtained. For small values of the flexural rigidity the deformation of the sidewall near the “free end” was large. As the flexural rigidity was increased, the overall deformation of the sidewall decreased, and in the limit case of a “large” flexural rigidity, the sidewall acted as a simple cantilevered beam (with little effect from the foundation). It was also observed, as expected, that the larger the flexural rigidity, the larger the applied load needs to be in order to obtain the same vertical displacement of the “free-end” of the sidewall.

- The global response of the MAC appears to be independent of the modulus of the foundation and the flexural rigidity of the sidewall. It was observed that the compressive versus shear response of the MAC was identical for all the values of the foundation modulus and all values of the flexural rigidity of the sidewall considered. This suggests that the overall compressive versus shear response of the MAC depends more on the geometry of the constituent machines and less on the material properties of the constituent components of the MAC.

C-5. References

1. Noor, K. A., Venneri, S. L., and Torquato, S., "Structures technology for future aerospace systems," *Computers and Structures*, vol. 74, pp. 507–519, 2000.
2. Howell, Larry L., *Compliant Mechanisms*, John Wiley & Sons, 2001.
3. Zaldivar R. J., Yamasaki J. T., Schurr J. N. and Hawkins G. F., "The Fabrication and Mechanical Behavior of Z-shaped Machine-Augmented Composites," Aerospace Report No. ATR-2002 (8810)-1, March 5, 2002.
4. Hawkins G. F., "Augmenting the Mechanical Properties of Materials by Embedding Simple Machines", *Journal of Advanced Materials*, vol. 34 (3), pp. 16–20, July 2002.
5. Sigmund O., and Torquato S., "Composites with extremal thermal expansion coefficients," *Appl. Phys. Lett*, vol. 69 (21), pp. 3203–3205, 1996.
6. Sigmund O., "A new class of extremal composites", *Journal of Mechanics and Physics of Solids*, vol. 48, pp. 397–428, 2000.
7. Lakes, R. S., Lee T., Bersie, A., and Wang, Y. C., "Extreme damping in composite materials with negative-stiffness inclusions," *Nature*, vol. 410, pp. 565–567, 29 March 2001.
8. Xu, Bing, Arias, Francisco, Brittain, Scott T., Zhao, Xiao-Mei, Grzybowski, Bartosz, Torquato, Salvatore, and Whitesides, George M., "Making Negative Poisson's Ration Microstructures by Soft Lithography," *Advanced Materials*, vol. 11 (14), pp. 1186–1189, 1999.
9. Cederbaum Gabriel, Li Leping, and Schulgasser Kalman, *Poroelastic Structures*. Elsevier Science Ltd, Oxford, United Kingdom, 2000.
10. Pecullan, S., Gibiansky, L. V., and Torquato, S., "Scale effects on the elastic behavior of periodic and hierarchical two-dimensional composites," *Journal of Mechanics and Physics of Solids*, vol. 47. pp. 1509–1542, 1999.
11. Bendsoe, Martin P. and Triantafyllidis, Nicolas, "Scale effects in the optimal design of a microstructured medium against buckling," *International Journal of Solid Structures*, vol. 26 (7), pp. 725–741, 1990.
12. Neves, M. M., Sigmund, O., and Bendsoe, M. P., "Topology optimization of periodic microstructures with penalization of high localized buckling modes," *International Journal for Numerical Methods in Engineering*, vol. 54, pp. 809–834, 2002.
13. Hetényi, M., *Beams on Elastic Foundation*. The University of Michigan Press, Ann Arbor, 1961.

14. Boresi, A., Schmidt, R., and Sidebottom, O., *Advanced Mechanics of Materials*, John Wiley & sons, Inc, fifth edition, 1993.
15. Young, W. C., *Roark's Formulas for Stress & Strain*, 6th edition, McGraw-Hill, New York, 1989.

Appendix D—Damping Capabilities of Fluid-Filled Machine-Augmented Composites

Prepared by

CHING-YAO (TONY) TANG, MICHAEL J. O'BRIEN
and GARY F. HAWKINS
Space Materials Laboratory
Laboratory Operations

Abstract

The Machine-Augmented Composite (MAC) concept has been extended to develop a new type of structural damping material. Embedded within a composite are many fluid-filled machines that dissipate vibrational energy. The material can be designed for use in low frequency applications such as the structural damping of buildings or bridges, as well as in the damping of higher frequencies, such as those encountered by launch vehicles, airplanes, and automobiles.

This report focuses on the experimental results of MACs embedded with fluid-filled Z-Shaped machines (Z-machines) and the analyses that have led to the investigation of fluid-filled hour-glass machines, which are, in theory, more effective dampers than the studied Z-machines.

D-1. Introduction

The Machine-Augmented Composites concept has been extended to develop a new type of structural damping material. The main purpose for embedding fluid-filled machines in a matrix material is to dissipate vibrational energy. Any compression of the fluid-filled machines causes the top and bottom layers of the machines to collapse closer to each other. This motion decreases the machine's internal area, which causes the fluid inside the machine cells to flow. The greater the dissipation rate (i.e., the greater the fraction of fluid being forced out per unit time), the better the machines are for damping.

This material with embedded fluid-filled machines can be designed for use in low frequency applications such as in the structural damping of buildings or bridges. Alternatively, the material may also be designed to damp higher frequencies, such as those encountered by launch vehicles, airplanes, and automobiles.

The first half of this report will provide a brief description of the fabrication of Z-shaped Machine-Augmented Composites as well as the Dynamic Mechanical Analysis (DMA) experimental procedure involved in obtaining the damping characteristics of this material. Results of these data will be discussed. The second half of the report introduces the hourglass fluid-filled dampers, the theory in classifying their behavior, and Finite-Element Analysis results that further augment the appreciation of their unique properties.

D-2. Z-Machines as Fluid-Filled Dampers

D-2.1 Fabrication of Z-shaped MACs

The Z-machines used for damping are approximately 1.0 mm in cross-section and were extruded from nylon stock by Extrusioneering, Inc., located in Temecula, CA. The sizes of these machines can be varied, depending on the desired application. Figure D-1 shows the cross-section of one of these extruded Z-machines.

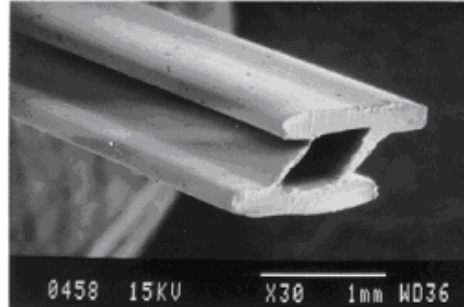


Figure D-1. SEM of extruded nylon Z-machines.

D-2.2 Experimental Procedure

The processing steps incorporating these Z-machine segments into a composite were patterned after current composite practices. The extruded Z-machine segments were laid down, side-by-side in a specially designed grooved Teflon mold, and adhesively bonded (3M Super 77 Spray Adhesive) to a polyester scrim cloth. This assembly represents one ply of machines. To produce a composite laminate, the single ply of machines was impregnated with a room-temperature-curing polyurethane resin matrix material (Smooth-On PMC-121/30) and placed in an evacuated bell jar to outgas the polyurethane as it polymerized and hardened. The ends of the machines were sealed beforehand with an adhesive (5-minute epoxy) to prevent polyurethane rubber matrix from infiltrating the cells. After the polyurethane cured, the sealed sample ends were trimmed off with sharp scissors so that the open machine ends were exposed as seen in Figure D-2.



Figure D-2. Z-shaped Machine-Augmented Composites.

Dynamic Mechanical Analysis (DMA) tests were done using an EnduraTEC ELeCTroForce® ELF® 3200 material testing system, as shown in Figure D-3, to determine the $\tan \delta$ (tan delta) values as functions of frequency and dynamic amplitude of our samples.

We tested samples that included the following: 1) machines embedded within a rubber matrix, 2) machines not embedded within a rubber matrix, 3) machines embedded within a rubber matrix and filled with water, 4) machines embedded within a rubber matrix and filled with 13,000 centipoise silicone oil, 5) machines embedded within a rubber matrix and filled with 30,000 centipoise silicone oil, and 6) polyurethane rubber (matrix alone). To fill samples, we used a syringe to inject fluid into each cell until the fluid came out the other end of the cell. Bubbles (or air gaps) were intentionally induced inside the cells to provide a lower pressure region for the fluid to flow.

Prior to the test, we specified the dimensions of our specimen and configured the setting inside the DMA control software of WinTest® (Figure D-4) such that the dynamic amplitude = 20 μm , mean level rate (rate the control system will use to ramp to the mean level) = 0.5 mm/s, mean level = -0.02 mm, dwell at mean = 5 s, load hold value (the value that the test system will use when temperature is changed and between test conditions) = -10 N, and pre-cycle = 20 s. There were typically 10 conditions that we ran, which ranged from 1 Hz to 100 Hz. The average dimensions of the specimen were usually 40 mm in length, 25 mm in width (\approx 14 cells), and 1.25 mm in thickness.

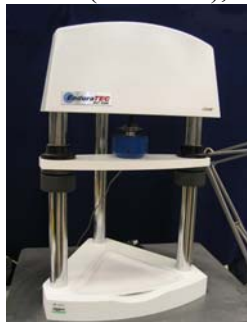


Figure D-3. EnduraTEC ELF® 3200.

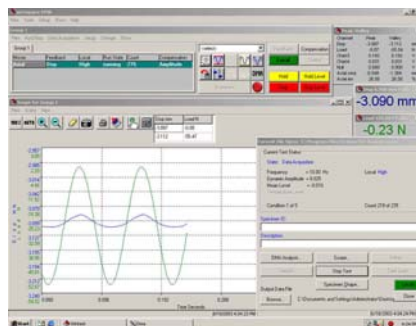


Figure D-4. Screenshot of WinTest® DMA.

During testing, the EnduraTEC ramps to the specified mean level, which is held for a specified time to allow for any creep or relaxation to occur prior to dynamic testing. It then calculates the start parameters (auto-tuning). Once the dynamic cycling has begun, the system pre-cycles the specimen a specified number of cycles to allow for amplitude control and specimen stabilization prior to actual data acquisition. Data is taken at an optimum acquisition rate for Fast Fourier Transform (FFT) analysis at that specific frequency of testing. The dynamic cycling is then stopped and the system again ramps to the original mean level. At the same time, data is stored to minimize dynamic cycling of the specimen and to prepare for the next test condition.

Using FFT analysis, the DMA software determines the fundamental frequency of data collected for each test condition and calculates the viscoelastic properties of the specimen. For materials, the analysis software calculates the tangent of the phase between the reference channel and feedback ($\tan \delta$) and uses the specimen shape to convert the stiffness and phase information to complex modulus (G^*), storage modulus (G'), and loss modulus (G'').

By analyzing results obtained from DMA tests and comparing them with the findings from theoretical analysis, we can explain and validate the behavior of $\tan \delta$ and load vs. displacement curves.

D-2.3 Experimental Results and Discussion

Various measurements of $\tan \delta$ were taken which allowed us to capture damping capabilities and characterize the damping behavior of the Z-machines. Each data curve depicts the frequency response of $\tan \delta$ for the samples and was plotted from the averages gathered from four separate runs in order to minimize any error associated with inconsistencies and fluctuations during the test.

Figure D-5 shows the curve of $\tan \delta$ vs. frequency for unfilled Z-machines and for polyurethane rubber, which is the material used as matrix inside the machines. As seen by the low $\tan \delta$ values, Z-machines alone (without filling or rubber matrix) demonstrate very little damping ability. However, when these unfilled Z-machines are embedded within the polyurethane rubber matrix, the $\tan \delta$ value increases significantly and the unfilled machines become fairly good dampers. On average, from the curves seen in Figure D-5, it seems that the $\tan \delta$ values of unfilled Z-machines with matrix are the results of the combined $\tan \delta$ values of rubber and unfilled Z-machines without matrix.

From the data seen in Figure D-5, it can be observed that damping decreases as frequency increases. This property is due to the fundamental relationship between loss modulus and storage modulus, which enables us to calculate $\tan \delta$. Loss modulus is directly proportional to the frequency while storage modulus is proportional to the square of the frequency. Since $\tan \delta$ is defined as loss modulus divided by storage modulus, we can infer that $\tan \delta$ is proportional to the inverse of the frequency (refer to Section D-3.2.3 for greater detail). In this way, no matter how effective a damping material may be, its damping ability will always drop off at higher frequencies.

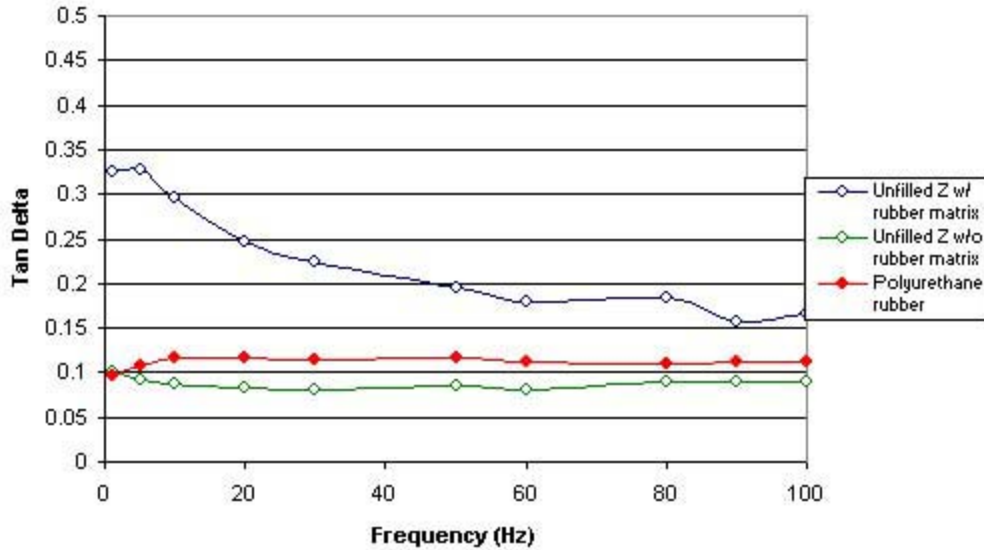


Figure D-5. Damping capabilities of unfilled Z-machines.

In Figure D-6, the Z-machines (both with and without matrix material) were tested after being filled with a fairly high viscosity fluid: 13,000-centipoise silicone oil. The silicone oil acts as a dissipative fluid that “drains out” energy during the constant cyclic deformation. In testing the Z-machines with matrix material, $\tan \delta$ values for filled Z-machines (i.e., filled with silicone oil) were roughly 30% higher than that of the unfilled Z-machines (i.e., no silicone oil).

In testing the machines not embedded within a matrix material, the percentage increase between filled and unfilled machines is even greater, with the filled machines also without matrix material having a $\tan \delta$ value ~50% greater than the unfilled machines without matrix material. The reason for the lower percentage increase for machines with matrix material might be attributed to the counteracting force the rubber had on the overall deformation of the system, where an equilibrium deformation may have been reached (note: still, it is not the percentage increase in damping that we are pursuing, but rather the absolute $\tan \delta$ value achievable).

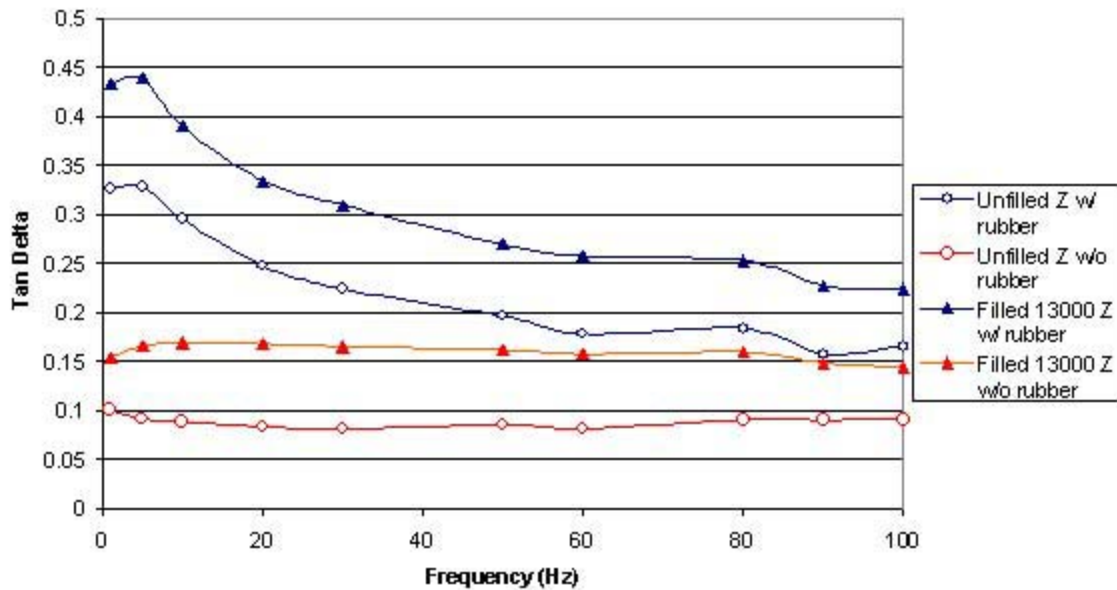


Figure D-6. Damping capabilities of Z-machines filled with 13,000 centipoise silicone oil, with and without rubber matrix.

Figure D-7 is a compilation of the curves from Figure D-5 and Figure D-6 with two additional cases: Z-machines with rubber matrix filled with 30,000 centipoise silicone oil and Z-machines with rubber matrix filled with water.

One of the most intriguing characteristics we have discovered from the DMA testing of Z-machines is that lower viscosity fluids provide higher damping capabilities. This is counterintuitive, especially when all the theoretical descriptions say otherwise. In various literature, energy dissipation increases as the viscosity of the fluid increases, and as cell size decreases. In addition, all equations and formulas used to calculate damping capacity and pressure profile within a cell have viscosity as the numerator, which would suggest that higher viscosity fluids result in more effective damping material. However, in Figure D-7, $\tan \delta$ results for water-filled Z-machines are the highest. This is unexpected, as water has the lowest viscosity among all the fluids used. The 30,000 centipoise silicone oil has the highest viscosity, but its damping capability is less than that of water-filled and 13,000 centipoise silicone oil filled machines. If the data is correct, then adding water into cell cavities significantly increases the energy dissipation of unfilled Z-machines by 67 – 130%.

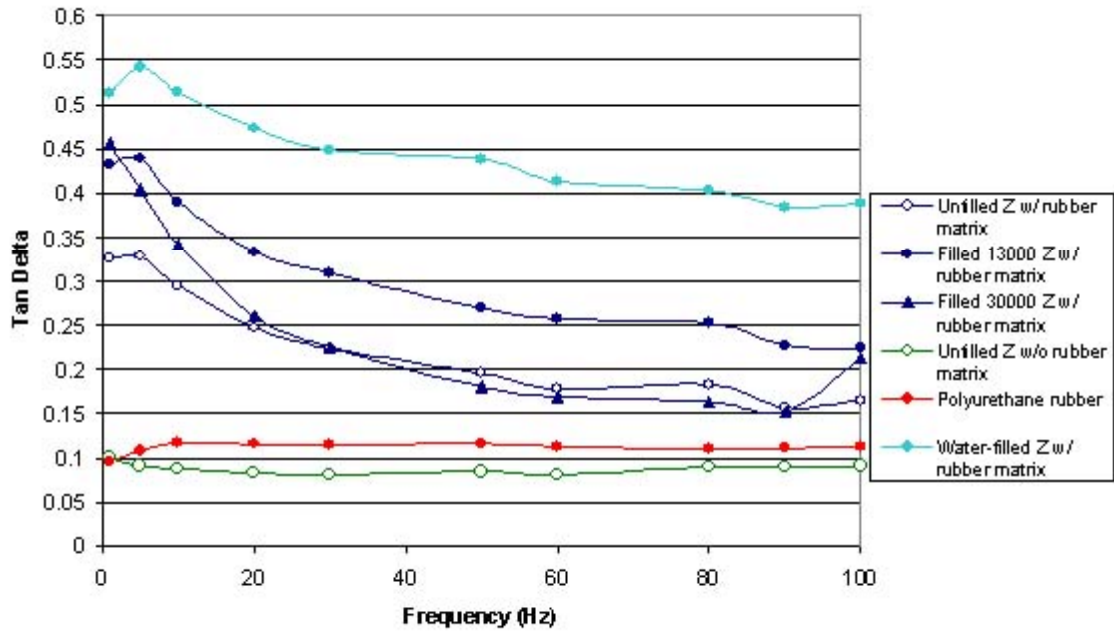


Figure D-7. Measurements of the damping as a function of the frequency.

D-3. Hourglass Machines as Fluid-Filled Dampers

D-3.1 Background

With an understanding of how machines behave when embedded in a matrix material, we were able to design and analytically explore a fluid-filled hourglass damping machine. Knowing that increasing fluid dissipation increases damping, we were able to analytically explore various tube designs which would be effective dampers. Engineering analysis showed that the most efficient tube design to force fluid through a medium was by way of an hourglass-shaped tube. Unlike Z-machines, which convert compressive force into shear force, resulting in small volumetric change, the hourglass machines change volume substantially under compression. Therefore, exploiting the behavior of this unique shape would result in a higher fluid dissipation rate. A cross-section of the machine is shown in Figure D-8. When this machine is put into compression the walls buckle towards each other and reduce the enclosed area. This results in a pressure increase of the fluid contained in that enclosed volume. In a machine made with this cross-section, the pressure increase will cause the fluid to flow to a lower pressure area. In our design, we intentionally induce bubbles in the fluid to provide a region for the fluid to flow.

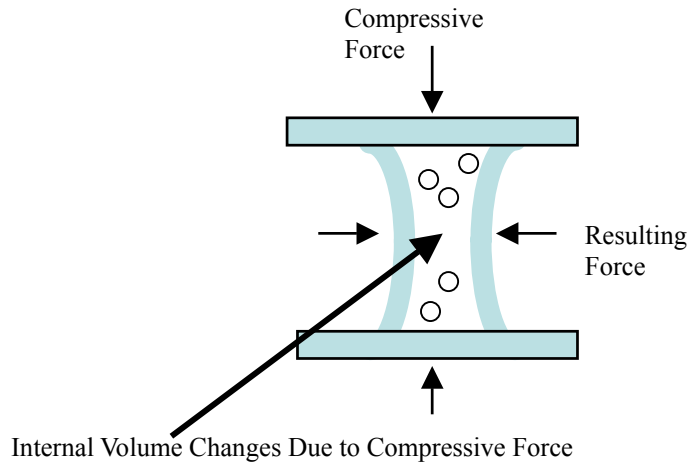


Figure D-8. When subjected to compression, the walls buckle inward and reduce the enclosed volume.

D-3.2 Theoretical Description

This section provides a theoretical approach for us to appreciate the behaviors of the hourglass machines. By analyzing the basic underlying physical properties and characteristics that govern hourglasses, we can optimize the design of the hourglass machines more easily and efficiently.

D-3.2.1 Determination of Flow Characteristics

To better understand the behavior inside fluid-filled machines in general, we would need to know the basic governing properties of flow within the “pipe.” One dimensionless quantity,

which is a characteristic of fluid flow, is the Reynolds number. The Reynolds number determines whether the flow is laminar or turbulent and is defined as the following:

$$\text{Re} = \frac{\rho_l u d}{\mu} \quad (1)$$

where, ρ_l is the density of the liquid, u is the fluid velocity, d is the diameter of the flow channel (cell size), and μ is the dynamic viscosity of the fluid. Experiments have shown that the critical value for transition from laminar to turbulent flow occurs at $\text{Re}_c = 2100$. Poiseuille or laminar flow ($\text{Re} < \text{Re}_c$) through a straight pipe is found to occur at approximately $\text{Re} < 30$.

For approximation purposes, suppose that the hourglass machines were filled with 13,000 centipoise silicone oil. Assume the opening of the cells is 2 mm (= 0.002 m) in height, which we will approximate as the diameter. The fluid inside the cell would have a low velocity when under compression, $u \leq 2$ mm/s (= 0.002 m/s), and a density of 948 kg/m³. Therefore, we are operating, at most, at a value of $\text{Re} = 2.9 \times 10^{-4}$. This value is well below the value required for a Poiseuille flow; therefore the fluid flow inside the cell would be laminar.

Work is done by forcing (squeezing) the fluid through the pipe. This means that the more fluid being forced out or the longer the force is applied, the more energy dissipation we get. If the flow is turbulent ($\text{Re} > \text{Re}_c$), work must be done to compensate for the loss of kinetic energy.

D-3.2.2 Pressure Profile Approximation

Assuming that the hourglass cells within the machines have constant volume, are round, and that only 2-D effects are considered, we can then approximate the fluid flow within the “pipe” as a simple Poiseuille flow. This is a simple and rough estimation.

For our approximation, we will assume steady, fully-developed flow. Therefore, from continuity we have

$$\frac{\partial u}{\partial x} + \frac{\partial v}{\partial y} = 0 \quad (2)$$

where, u is the velocity component in the x-direction and v is the velocity component in the y-direction. From these assumptions along with no slip condition near the wall, Equation (2) gives $v = 0$ everywhere. From the y-momentum equation, we have

$$\frac{\partial v}{\partial t} + u \frac{\partial v}{\partial x} + v \frac{\partial v}{\partial y} = \frac{1}{\rho} \frac{\partial p}{\partial y} - g + \frac{\mu}{\rho} \left(\frac{\partial^2 v}{\partial x^2} + \frac{\partial^2 v}{\partial y^2} \right)$$

where, ρ is the density of the fluid, μ is the dynamic viscosity, p is the pressure of the flow, and g is the acceleration due to gravity. Using the consequence of Equation (2) and integrating the above equation to get the total pressure of the flow in the y-direction, we have the following equation:

$$p = -\rho g y + p(x) \quad (3)$$

Differentiating Equation (3) with respect to x , we see that the pressure only varies in the x -direction.

From the x -momentum equation, we have

$$\frac{\partial u}{\partial t} + u \frac{\partial u}{\partial x} + v \frac{\partial u}{\partial y} = -\frac{1}{\rho} \frac{\partial p}{\partial x} + \frac{\mu}{\rho} \left(\frac{\partial^2 u}{\partial x^2} + \frac{\partial^2 u}{\partial y^2} \right)$$

Using the same result obtained from Equation (2) and integrating the x -momentum equation twice to obtain u , we have the following:

$$u(y) = \frac{1}{2\mu} \frac{dp}{dx} y^2 + c_1 y + c_2 \quad (4)$$

Applying the boundary conditions for no slip condition, we find that $c_2 = 0$ and $c_1 = -(1/2)(h/\mu) dp/dx$. Substituting the value of c_1 and c_2 into Equation (4), rearranging, and then substituting $y = h/2$ (along centerline), we get

$$\frac{dp}{dx} = \left| -\frac{8\mu}{h^2} u \right| \quad (5)$$

where, h is the height of the cell or “pipe.” Equation (5) represents the total change in pressure along x .

Integrating Equation (5) gives us the total pressure of the flow in the x -direction for a given tube length.

$$p(x) - p_0 = \left| -\frac{8\mu}{h^2} ux \right| \quad (6)$$

If we assume that $u \leq 2$ mm/s (= 0.002 m/s), the silicone oil has a dynamic viscosity of 13,000 centipoise (= 13 Pa*s), the height of the cell is about 1.9 mm (0.0019 m) after compression, and the length of our sample is 50 mm (0.05 m), then $p(x)-p(0) = 0.42$ psi above gauge pressure for each cell. Because the fluid flow inside the hourglass cell was initiated due to compression or change in area of tube, the value of $p(x)-p(0)$ gives the equivalent value of pressure difference had the flow been instigated by a pressure gradient.

D-3.2.3 Measures of Damping

Damping is a measure of the rate of energy dissipation by a structure that takes place during its cyclic deformation. A useful dimensional parameter that has no physical magnitude is the $\tan \delta$, which gives a measure of the ratio of energy lost to energy stored in a cyclic deformation.

$$\tan \delta = \frac{G''}{G'} \quad (7)$$

where, G'' is defined as the loss modulus and G' is the storage modulus. The loss modulus (G'') is the stress 90° out of phase with the strain divided by the strain, and it is a measure of the energy dissipated or lost per cycle of sinusoidal deformation. The storage modulus (G') is the stress in phase with the strain in a sinusoidal shear deformation divided by the strain, and it is a measure of energy stored and recovered per cycle.

The $\tan \delta$ parameter determines material properties such as the damping of free vibrations, the attenuation of propagated waves, and the frequency width of a resonance response. It is often measured more readily and is of considerable interest compared to any other viscoelastic function in that a high $\tan \delta$ value corresponds to an effective damping material.

A good damping material has a higher $\tan \delta$ value than a stiffer material. The typical value of $\tan \delta$ for a steel bar is roughly 0.001. If we take our Machine-Augmented Composites to be a simple mass-spring-dashpot system, the matrix (polyurethane rubber) and the machine itself are the “spring” of the system and the fluid within the cells is the “dashpot.” As seen from Equation (7), in order to increase $\tan \delta$, we could either decrease the storage modulus or increase the loss modulus. Generally, it is easier to increase the loss modulus by increasing the volume fraction of “dashpot” in our system. From literature, G' is proportional to the square of the frequency (ω^2) while G'' is directly proportional to the frequency (ω) (Ferry¹). Therefore, one may deduce from these approximations the behavior of $\tan \delta$, when plotted against frequency, to be the inverse of the frequency (ω^{-1}).

Perhaps the most commonly used measure of damping seen in literature is the loss factor (coefficient), η , which represents the ratio of the energy removed per radian to the stored vibrational energy (Ungar^{4,5}). In this way, loss factor is *equivalent* to $\tan \delta$. One may encounter one or the other in various literature, but in this report they may be used interchangeably.

$$\eta = \frac{\Psi}{2\pi} = \frac{D}{2\pi W} \quad (8)$$

where, Ψ is the damping capacity, D is the energy that is removed from the system per cycle, and W denotes the vibrational energy stored in the system (can usually be approximated as kinetic energy plus potential energy). For approximation purpose, take D as the energy dissipated for a square tube using Equation (33) in “Viscous Dissipation in Machine-Augmented Composites” (Karion³) and multiply that by a factor of $1/f$ for energy dissipated per cycle.

$$D = \frac{K\mu \dot{A}^2}{3A^2 f} L^3 \quad (9)$$

where, $K = 28.4616$ is the shape factor for a square, f is the frequency (cycles/second), μ is the dynamic viscosity of fluid inside the cell, \dot{A} is the rate of change in area, and L is the half-length of the tube. Since the dynamic viscosity for silicone oil is 13,000 centipoise

(= 13 Pa*s), let $A/A = 0.25$, $f = 1$ Hz, and the half-length is 25 mm (= 0.025 m), then D equals to $1.2 \cdot 10^{-4}$ kg m²/s². W is the sum of kinetic and potential energy. Therefore,

$$W = \frac{1}{2}(mv^2 + kx^2) \quad (10)$$

where, m is the mass of fluid within the cell, v is the velocity of the fluid as a result of an applied force, and k is the “spring” constant of rubber and machines. Approximating $m = 0.05$ g, $v = 0.5$ mm/s, $k = 2.0 \cdot 10^6$ N/m, and $x = 0.02$ mm (= $2.0 \cdot 10^{-5}$ m), we have $W = 4.0 \cdot 10^{-4}$ kg*m²/s².

Substituting the corresponding values of D from Equation (9) and W from Equation (10) into Equation (8), we obtain a loss factor, η , of approximately $0.3 = \tan \delta$ for hourglass machines with rubber matrix filled with 13,000 centipoise silicone oil. This is a reasonable value that lies in the higher region of loss factors for plastics and rubbers, as seen from Figure D-9.

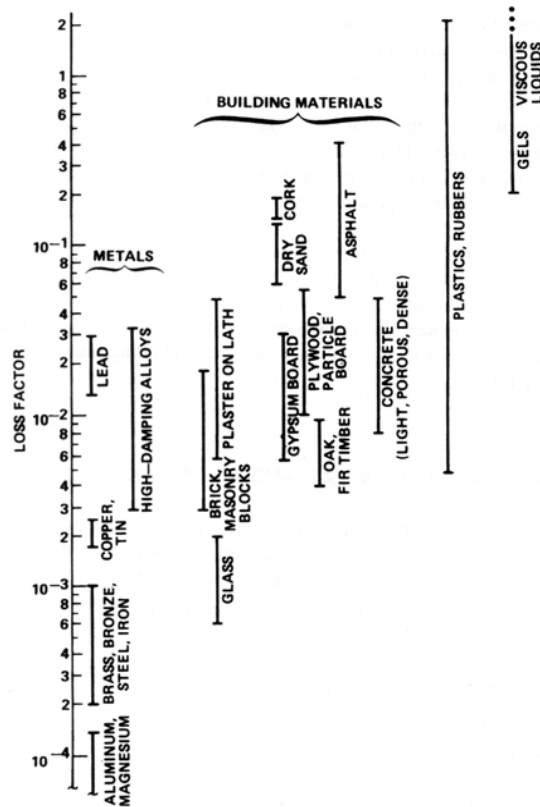


Figure D-9. Typical ranges of loss factors for some common materials.^{4,5}

Equation (6) and Equation (9) show that the energy dissipated increases as the viscosity of the fluid increases, and as the cell size decreases. This is in agreement with viscous dissipation in open-cell foams containing a fluid (Gibson and Ashby²). When the hourglass machines are compressed, the fluid the cells contain is squeezed out; when extended, fluid is drawn back in. Work is done by forcing the fluid through the cells. The faster the cell is deformed, the more work is done.

To further increase the damping capability of our machines, we need to devise a way to increase the pressure inside the cells. As a secondary means, we could also increase the length of our test samples, since $D \propto L^3$ (from Equation 9).

Future research includes conducting experimental tests to validate this theoretical result.

D-3.3 Finite-Element Analysis (FEA)

This hourglass fluid-filled machine design was modeled using the finite-element method for the solid portion and an analytical expression for the fluid. The solid was a composite of two materials consisting of hourglass-shaped plastic sidewalls embedded in a matrix of rubber. The plastic was modeled as linear elastic and the rubber as nonlinear elastic (“hyperelastic”) with constitutive properties measured independently. The constitutive response for the fluid was given by the following analytical expression:

$$\frac{P(L) - P_0}{\rho L^2} = -\frac{1}{2} \frac{\ddot{A}}{A} - N \frac{\dot{A}^2}{A^2} + \frac{K\nu}{2} \frac{\dot{A}}{A^2} \quad (11)$$

where, K is the shape factor for the cross-sectional area, ν is the kinematic viscosity, A is the cross-sectional area, \dot{A} is the rate of change in area, ρ is the fluid density, P is the pressure at the outlet of the fluid-filled cavity, and $P(L)$ is the pressure at a distance of L from the outlet.

Equation (11) relates the pressure change in the fluid, P , to the change in cross-sectional area, A , of the fluid-filled cavity caused by deformation of the sidewalls. The pressure change calculated from Equation (11) was implemented in the finite-element model as hydrostatic pressure boundary condition acting at the interface between the fluid-filled cavity and the plastic sidewalls. Equilibrium between the solid and fluid was established by iteratively varying the pressure boundary condition supplied to the finite-element model. The iteration continued until the change in cross-sectional area provided by the deformation of the solid matched the change in area calculated from Equation (11), at which time the iteration was halted and the finite-element calculation proceeded to the next time step.

Figure 10 shows the undeformed and deformed shapes for the fluid-filled device. The vertical strain applied to the top external boundary causes the hourglass-shaped fluid cavity to shrink. (As an explanatory note, the finite-element problem has two planes of symmetry, which allows one quarter of the problem to be solved in Figure D-10.)

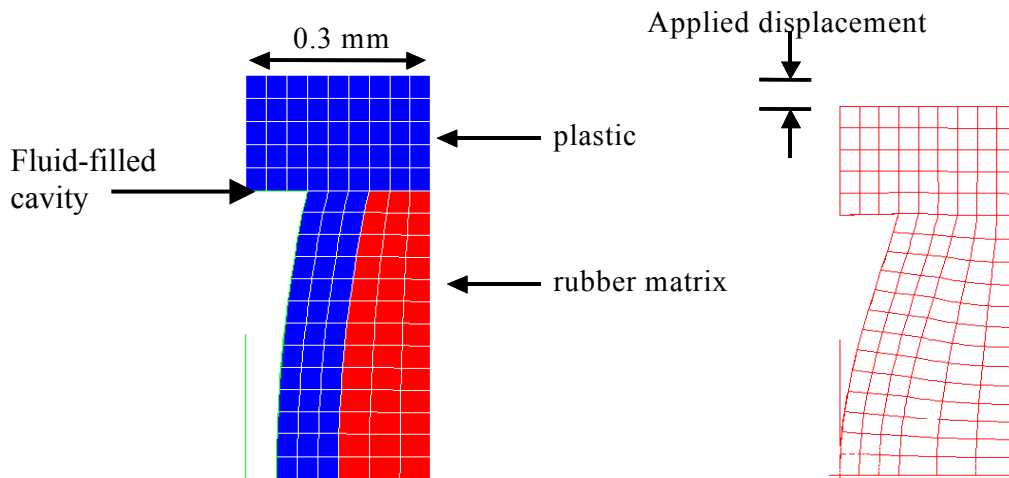


Figure D-10. Undeformed (left) and deformed (right) meshes for the fluid-filled device. The plastic sidewall is shown in blue on the left and the rubber matrix is shown in red on the left. (The FEA problem has a vertical and a horizontal symmetry plane, which allows one quarter of the problem to be solved.)

Physically, the hourglass shape of the fluid-filled cavity provides a dramatic machine action that “amplifies” the strain applied to the external boundary. Figure D-11 shows that a 3% applied strain causes a 50% drop in the cross sectional area of the hourglass-shaped fluid cavity. This amplification allows a relatively small applied strain to move a large volume of fluid.

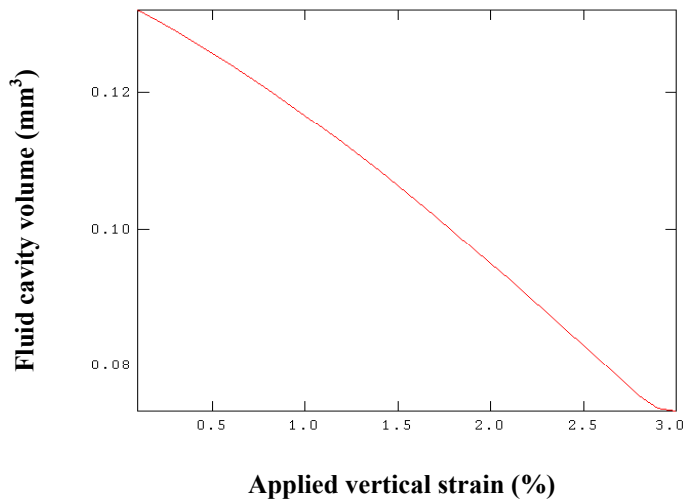


Figure D-11. Decrease in volume of fluid cavity due to applied strain.

The finite-element model was used to calculate the work done by external forces upon the external boundary of the solid. The energy stored in the solid (consisting of plastic sidewalls and polyurethane rubber matrix) was also calculated. From conservation of energy, any difference between these two energy quantities was attributed to energy dissipated by the fluid. Physically, the energy can be dissipated either as heat due to viscous losses or as kinetic energy exiting the control volume of the fluid-filled cavity.

The dissipated energy was calculated as a function of fluid viscosity. Three viscosities representative of silicone oil were used in the calculations: 13,000; 30,000; and 100,000 centipoise. As shown in Figure D-12, the maximum dissipation occurs at an intermediate viscosity. Physically, the energy dissipated is a balance between the work done by the fluid and the energy stored in the solid structure. At a higher viscosity, the fluid-filled cavity does not deform significantly, providing little opportunity for fluid motion and consequent viscous dissipation. At a lower viscosity, there is little resistance to the forces exerted by the external environment, and a significant force between the fluid-filled cavity and the solid does not develop. Therefore, for both low and high viscosities, the fluid does little work and dissipates little energy.

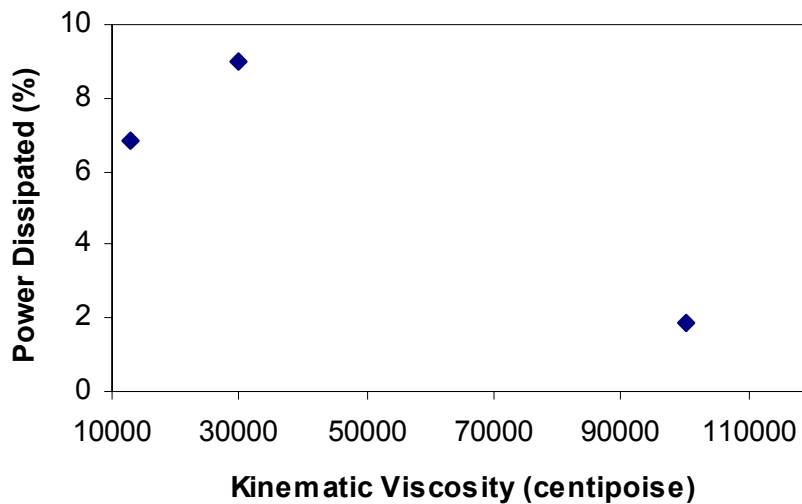


Figure D-12. Power dissipated by the fluid-filled device as a function of fluid viscosity.

D-4. Conclusion

We have designed, tested, and analyzed the damping capability of Z-machines that contain fluids of various viscosities. Further analysis conveyed to us that machines with hourglass-shaped design are more efficient in damping than Z-machines, simply because they are capable of a greater volumetric change. From our research, we can make the follow conclusions:

1. As expected, the presence of fluid inside machines increases the damping capability of a system substantially. For Z-machines, low viscosity fluids (e.g. water) displayed the greatest damping capacity.
2. Hourglass machines have been shown, both geometrically and theoretically, to be the best dampers. Forces coming in from the top and bottom compress the machines. The hourglass shape causes the machines to bend inward, decreasing the internal volume. Since the structure is filled with fluid, the decrease in volume causes the fluid to flow. The volume decrease is enhanced by the Poisson's effect in the matrix between the machines.
3. A simple, yet reasonable, theoretical approximation of $\tan \delta$ for hourglass machines filled with 13,000 centipoise silicone oil puts the material in the higher region of loss factors for plastics and rubbers (or in the lower region for gels and viscous liquids). Increasing the pressure inside the cells, the viscosity of fluid, the rate of change in area, or the half-length of the specimen would increase the loss factor of hourglass machines.
4. Finite-Element Analysis showed that a 3% applied vertical strain causes a 50% drop in the cross-sectional area of the hourglass-shaped fluid cavity and the maximum dissipation occurs for fluid at an intermediate viscosity, e.g. at 13,000 centipoise silicone oil.

Additional analysis through experiments will be conducted to validate our findings. Furthermore, we will devise a way to increase the pressure inside the hourglass cells to increase loss factor.

D-5. References

1. Ferry, J. D., *Viscoelastic Properties of Polymers*, 3rd ed., Wiley, New York, 1980.
2. Gibson, L. J. and Ashby, M. F., *Cellular Solids: Structure and Properties*, 2nd ed., Cambridge University Press, Cambridge, 1999.
3. Karion, A., "Viscous Dissipation in Machine-Augmented Composites," Aerospace Technical Memorandum ATM 2001(1720-40)-1, The Aerospace Corporation, 2001.
4. Ungar, E. E., "Structural Damping," in Beranek, L. L. and Ver, I. L. (Eds.), *Noise and Vibration Control Engineering*, Chapter 12, Wiley, New York, 1992.
5. Ungar, E. E., "Vibration Isolation and Damping," in Crocker, M. J. (Ed.), *Handbook of Acoustics*, Chapter 55, Wiley, New York, 1998.

Appendix E—Potential Infrastructure Applications of Machine Augmented Composites

Prepared by

GARY F. HAWKINS
Space Materials Laboratory
Lab Operations

Abstract

This document describes a simple and economical method for the pre-stressing of carbon fiber-reinforced polymers (CFRP). This method uses a mechanism based upon simple machines that are compressed. The machine action converts the compressive force into shear force, which displaces the CFRP strip and tensions it in a way that is simple, easy and economical to use. Tests on a prototype version of our stress-conversion mechanism have been performed that demonstrate the pre-stressing technique. A cost-effective method to pre-stress carbon fiber reinforced polymer materials will optimize the retrofit and repair of concrete structures used in the nation's transportation infrastructure.

E-1. Introduction

Carbon Fiber Reinforced Polymer (CFRP) materials are a cost-effective alternative to traditional methods for the retrofit and repair of concrete structure. Pre-stressing the CFRP results in a significantly stronger concrete structure than when applying un-stressed CFRP. In applications where the CFRP strips are pre-stressed, current methods use a large reaction frame with two tensioning rollers or a system of elaborate end-anchors to generate the large pre-stressing loads that are needed. In these cases, adhesive is applied to the concrete, after which the pre-stressed CFRP strip is mounted onto the concrete.

Unfortunately, the current pre-stressing methods are so complicated, hard to use and expensive that, in general, CFRP strips are generally applied without pre-stressing. Instead, adhesive is applied to the strip and the strip is simply placed onto the concrete to be reinforced. Anchors are often bolted near the ends of the strip as a precaution against peeling. Because the CFRP strips are currently not pre-stressed in general, the concrete structures are not efficiently strengthened. There is, therefore, a great need to develop a simple, robust and inexpensive method to pre-stress the CFRP strips used to retrofit and repair concrete structures.

E-2. Z-MACs

We have recently demonstrated that composites with unique properties can be manufactured by embedding many small simple machines in a matrix material. We have been referring to these as Machine-Augmented Composites (MACs). In particular, embedding Z-shaped machines within a matrix material results in a composite material which distorts in shear when placed under compression and vice versa (see ATR-2002(8810)-1, “The Fabrication and Mechanical Behavior of Z-Shaped Machine-Augmented Composites, and ATR-2003(8810)-2, “Theoretical and Finite-Element Modeling of the Z-MACs” for a more detailed description). This property allows design engineers a new method to solve mechanical issues.

E-3. Clamping Forces in Anchor Applications

Figure E-1 shows a device that contains two layers of 15-mm 4-celled rapid prototype machines at a 60° inclination angle. Each layer of machines is adhesively bonded to the outer plate on one side and a rubber sheet on the other. A slider is placed between the layers of machines. When the slider is pulled to the left, it slides quite easily. Conversely, when the slider is pulled in the other direction, it will not move at all, as the shear forces created by the slider are converted into compressive forces by the embedded Z-shaped machines. In this way, the device in Figure 1 acts effectively as a clamp.

This effect can be explained using Figure E-2. Normally, movement commences when a force is applied to the slider (resulting in a shear force at the interface) that exceeds the force of static friction. The force of static friction is a constant value (μ) times the normal force (N). In this device, the normal force is set by adjusting the four bolts. In a device without machines, the normal force is a constant and sliding would begin as indicated.

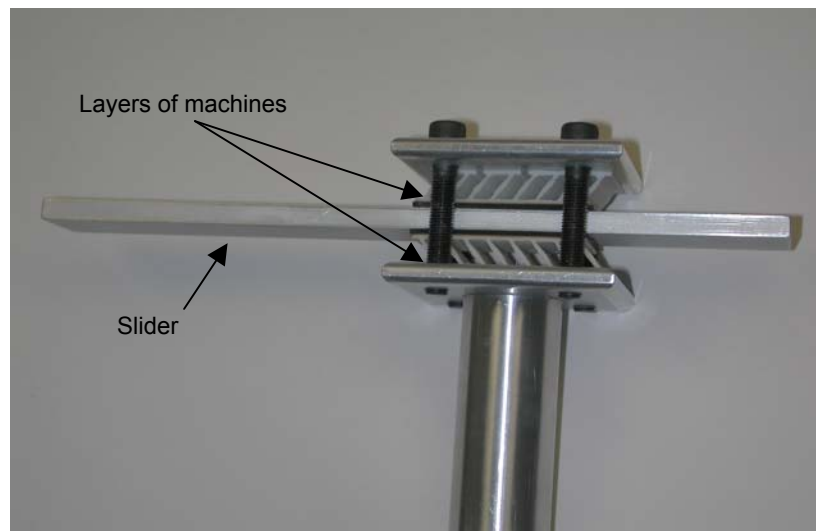


Figure E-1. Device containing two layers of the 15-mm 4-celled rapid prototype machines at a 60° inclination angle. When the slider is pulled to the left, it will pass through the device easily. When the slider is pulled to the right, the device acts like a clamp, locking the slider in place.

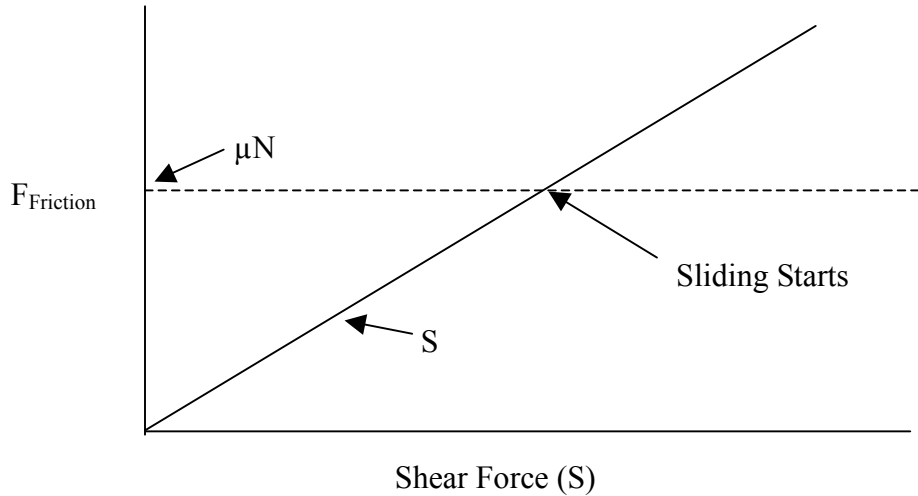


Figure E-2. Friction force versus shear force for slider device.

In the device shown in Figure E-1, the normal force is a function of the shear force due to the influence of the machines. More specifically, when you pull on the slider, the machines convert the shear forces so they either add to, or subtract from, the normal force depending on the direction of the shear force. This is shown graphically in the Figure E-3.

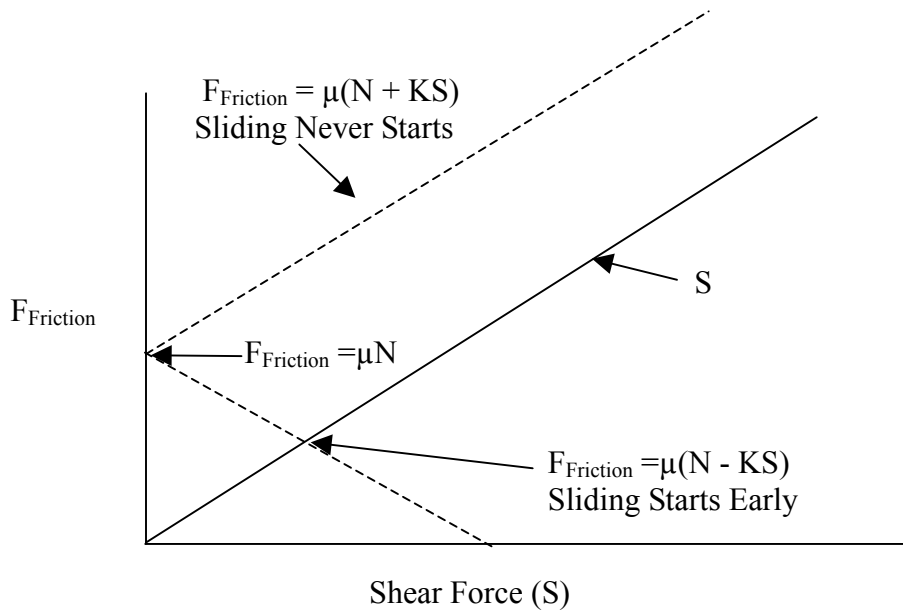


Figure E-3. Friction force versus shear force for slider device illustrating the effect of pulling the slider in one direction versus the opposite direction.

The machines convert shear to compressive force with an efficiency that is indicated by the constant “K” in the figure above. In the easy sliding direction, the normal force decreases as the slider is pulled until breaks free. In the opposite, or hard, direction the normal force increases as you pull. If K times μ is greater than one, the slider cannot break free and clamping occurs. We have put a layer of rubber with quite a high μ in between the slider and the machines to dramatically show this effect.

E-4. Pre-stressing Carbon Fiber Reinforced Polymer

A possible application for this stress-conversion material is for pre-stressing Carbon Fiber-Reinforced Polymer (CFRP) in infrastructure applications. By inserting our Machine Augmented Composite between the anchor plates and the CFRP, we create a clamping system that will hold the CFRP in place (see Figure E-4). Furthermore, when the anchor bolts are tightened onto the concrete beam, the MAC becomes compressed. The resulting machine action within the composite converts the compressive force into a shear force that displaces and pre-stresses the CFRP strip into tension (i.e., pre-stresses the CFRP strip). The MACs are fastened to the concrete beam by the same anchors that are placed near the ends of the CFRP strips to prevent peeling. This procedure to pre-stress CFRP uses the same adhesive, CFRP strip, and anchors as in the current non-pre-stressed method.

Unlike other current pre-stressing devices, our proposed mechanism would not require large amounts of extra machinery or use an elaborate end-anchorage system but would still be capable of generating the same forces as these devices. We have already successfully performed a test on a prototype version of our stress-conversion mechanism that demonstrates the pre-stressing technique. Thus, our method is simple, inexpensive, and easy to use. These benefits will make it possible to use pre-stressed CFRP routinely in all applications.

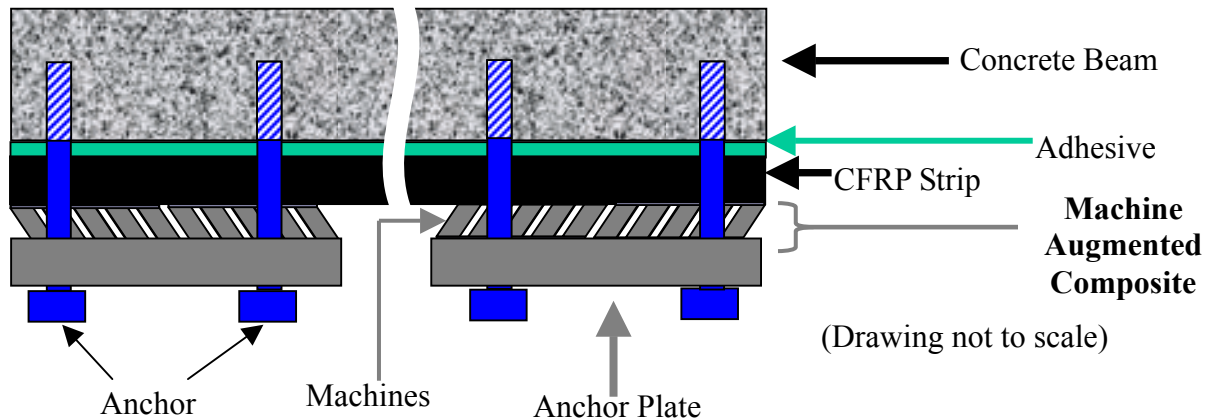


Figure E-4. CFRP is Stressed in Tension when Anchor Bolts are Tightened.

E-5. Proof of Concept

We have already performed a test on a prototype version of our stress-conversion mechanism, which is shown in Figure E-5.

During the testing of this prototype stress-conversion mechanism, the four bolts were tightened, causing compressive forces on the angled shim stocks. The shims force the grip up and to the right. For this test, we adhesively bonded the grip to the lower plate, which simulated a CFRP strip. Grease simulating uncured adhesive was placed between the lower and upper plates, allowing them to slide with respect to each other.

During this test, a tensile load of 450 lbs per square inch of grip was generated in the plates before the angled shims buckled. We feel that 1,000-lb/sq. inch will be necessary for the proposed device and that these results would be easily achieved simply by using thicker shim stock. The first series of tests will use a universal testing machine to evaluate the proposed mechanism designs and to select the best design.

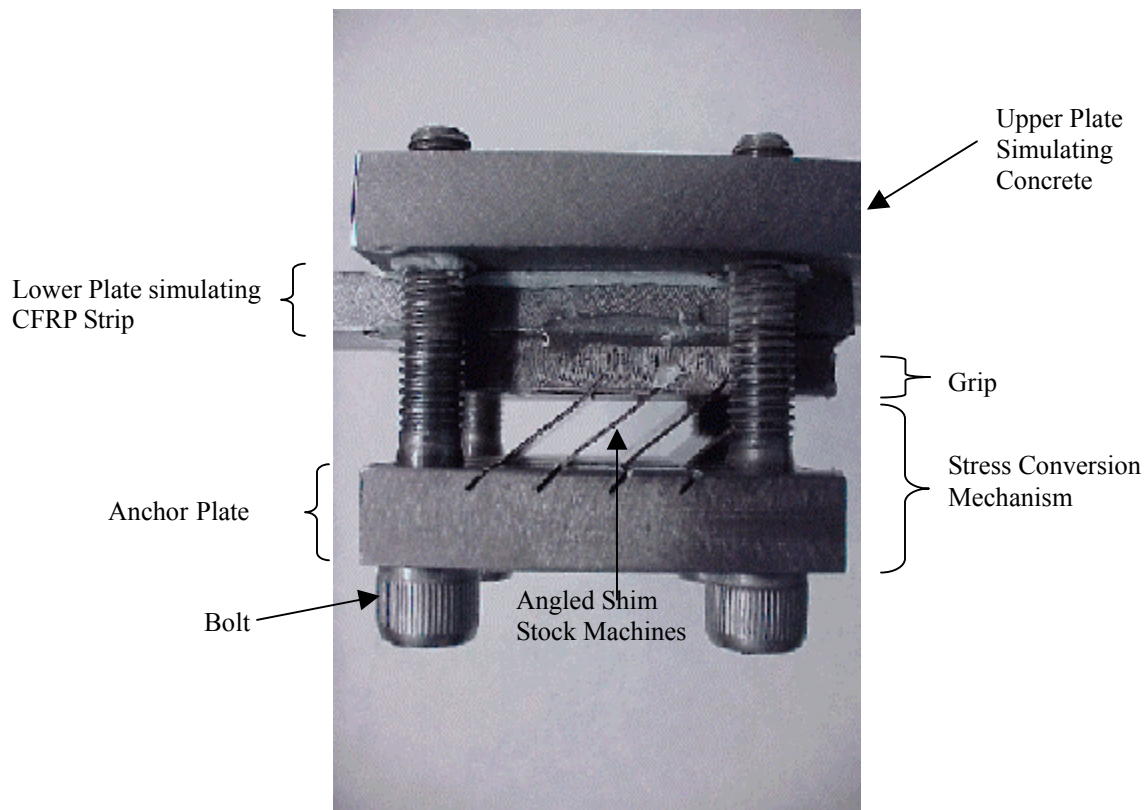


Figure E-5. Prototype Stress-Conversion Mechanism.

E-6. Potential Impact and Payoff for Practice

Urs Meier et.al. and Deuring at EMPA in Switzerland have convincingly demonstrated that pre-stressing CFRP strips before they are bonded to the concrete results in a significantly stronger concrete structure by more efficiently using the strength of the composite. The infrastructure applications include seismic retrofitting, improving design margins, and increasing the service life of existing structures.

The main technical factor obstructing the widespread use of pre-stressed CFRP in concrete structural reinforcement is the difficulty in tensioning the composite before it is bonded to the concrete. Because of this level of difficulty, the cost of pre-stressing CFRP is prohibitively high for most applications. This application directly addresses this issue and would create a simple and economical method for the pre-stressing of CFRP. A cost-effective method to pre-stress fiber-reinforced composite materials will optimize the retrofit and repair of concrete structures.

E-7. References

1. Zaldivar R. J., Yamasaki J. T., Schurr J. N. and Hawkins G. F., “The Fabrication and Mechanical Behavior of Z-shaped Machine-Augmented Composites” Aerospace Report No. ATR-2002 (8810)-1, 2002.
2. Zaldivar R. J., O’Brien M., Schurr J. N., Yamasaki J. T., and Hawkins G. F., “The Load-Load Characteristics of Z-shaped Machines” Aerospace Report No. ATR-2003(8810)-2, 2003.
3. Meier, U. et al. (2001), “Making Better Use of the Strength of Advanced Materials in Structural Engineering” FRP Composites in Civil Engineering, Vol. I, J.-G. Teng (Ed.), 2001 Elsevier Ltd.